REDUCING THE NOISE GENERATED BY CAR ROOF RACKS

by

Oliver Charles Graham Hill BE(hons)(mechanical)

A thesis submitted in fulfilment of the
requirements for the degree of

Masters of Engineering (Mechanical)

University of Canterbury

Chairperson of the Supervisory Committee: Dr John R. Pearse
Department of Mechanical Engineering

March 2000

Acknowledgments

I would like to sincerely thank all those people who played a part in the completion of this thesis. Special thanks to my supervisor, Dr John Pearse for his help and consistent encouragement and to Mr Peter Hubbard for his time, facilities and steady supply of roof racks through whom this Masters thesis has been made possible. I am also very grateful to Professor D. C. Stevenson for sharing his understanding and insight in the field of aeroacoustics.

I would like to thank the departmental technicians and workshop staff for their input, in particular Graeme Harris who showed great enthusiasm toward the project and helped immensely with the wind tunnel noise work.

I am grateful to the department's secretarial staff, for their help with the formalities associated with this submission, the library staff, for assistance in the location of reference material, and the computer technicians who helped facilitate the publishing of this thesis.

I acknowledge gratefully the financial support provided by the Foundation for Research Science and Technology and the Institute of Professional Engineers NZ.

Lastly and most importantly, I wish to thank my parents, friends and extended family for their emotional support during the time of writing and Deborah Jackson for her help with the admin.

Abstract

The aerodynamic mechanisms responsible for the production of noise present in the flow field around the Hubco A-bar roof rack have been investigated experimentally. The frequency spectra of sound emissions were determined using sound measurement equipment in the field and in a specially designed low noise wind tunnel. Flow visualisation and hotwire anemometry techniques were also used to establish a model of the flow around the roof rack. Correlation was drawn between flow phenomena and sound emissions. The source of the annoying tonal emission was established to be a periodic vortex shedding from the trailing edge of the aerofoil shaped profile.

Treatments to reduce or eliminate this sound emission were developed, based upon changing the flow pattern across the surface of the roof rack. The generation of chordwise trailing vortices near the leading edge of the A-bar was found to be effective in noise abatement by disturbing the formation of the regular vortex street. These chordwise vortices may also break up the spanwise correlation of the periodic wake reducing the strength of the noise emission.

Chordwise vortices are generated by installation of cross flow inducing obstructions such as cylinders, hemispheres, serrations and diagonal steps near the leading edge.

The treatments have been developed to meet the design requirements for robustness, durability and aesthetic appeal without sacrificing the strength or life of the roof rack itself. The noise treatment techniques chosen for the A-bar were trialled successfully on competitor roof racks.

TABLE OF CONTENTS

LIST OF FIGURES

NOMENCLATURE

Symbol	Meaning	Units
a	Speed of Sound	m/s
A.P	Atmospheric pressure (head)	mm_{Hg}
c	Chord	mm
d	Distance (relevant dimension)	mm
f	Frequency	Hz
g	Gravitational Constant	ms^{-2} value 9.81
h_V	Velocity Head	mm_{H2O}
l	Length	m
OASPL	Overall Sound Pressure Level	dB (or dBA)
Re	Reynolds Number	dimensionless
RH	Relative Humidity	%
S	Strouhal number	dimensionless
SPL	Sound Pressure Level	dB (or dBA)
T	Temperature	^{o}C (Degrees Celsius)
t	Thickness	mm
TI	Turbulence intensity	% (of velocity)
U	Velocity	ms^{-1}
ρ	Density	kgm^{-3}
θ	Angle (of incidence)	^{o} (Degrees)
λ	Wavelength	m
μ	Viscosity	kg/ms

Chapter 1

INTRODUCTION

roof rack *n.* a rack attached to the roof of a motor vehicle for carrying luggage, skis, etc[1].

1.1 General

Automotive roof carrier systems commonly known as roof racks have traditionally been designed for functionality only, with little thought for aerodynamics, aesthetics or, as the primary concern in the case of this thesis, the production of noise. This has not been much of a problem in the past, as cars themselves were rather noisy. But as the focus of car manufacturers has moved toward driver and passenger comfort, the need for focused effort in the removal of sources of discomfort has increased. The primary sources of annoyance for the human occupant of a car as in many other situations are vibration and sound, this has led to the rise in success of the NVH (noise, vibration, and harshness) industry.

Aerodynamic noise not only has the characteristic of being a source of annoyance, but also in many cases cannot simply be eliminated by following principles set out in easily obtainable texts and references. The best solution to date, for many automotive manufacturers, has been to try to prevent the entry of noise into cabin rather than combat the sources of noise. This is typically done by sealing the openings around doors and windows and placement of noise attenuating foams in the head linings of the roofs. Even in these cases, there is still noise intrusion. Ironically, in order to remove the lower more intrusive frequencies, the amount of sound abatement material needed would reduce useable space in the passenger compartment to the extent of leaving no room for occupants! Rather than follow this path (which ultimately leads to "the city of bankrupt automotive companies") automotive manufacturers place the onus on the manufacturers of their automotive accessories to produce silent (or nearly silent) products.

One local manufacturer of automotive accessories, Hubco Industries, under the direction of Peter Hubbard, has responded to the demand for reduced levels of annoying sound produced by its roof racks and embarked upon a development program to meet this demand. With the support of Technology New Zealand through a TBG[2] grant, Hubco industries employed IRL[3] to mathematically model and simulate the flow around various cross sections that would be suitable for employment as roof racks (taking design requirements into consideration). The purpose of this study was to establish guidelines by which quiet roof racks could be produced without the necessity for an extensive experimental programme. Unfortunately, owing to the complexity of model needed, and software limitations, this could not be achieved. The work does however indicate the need for a streamlined shape[4].

The product resulting from the above work, called the A-bar in this work, was producing high levels of tonal noise, too high for Ford Australia to include them as standard accessories on their range of cars. The upshot for Hubco was more research. This time Hubco approached the University of Canterbury's Mechanical Engineering Department for a solution. A small amount of preliminary field-testing jointly undertaken by Hubco and the University was completed at the Ruapuna racetrack, which indicated the need for a more in depth investigation. This time an experimental program was decided upon. Technology New Zealand supported once again with funding, this time through their Graduate Research in Industry Fellowship program.

---

[1] Collins *English Dictionary and Thesaurus*
[2] Technology for Business Growth
[3] Industrial Research Ltd
[4] Donohue, B. *Prediction of Aerodynamic Noise from Automotive Roof Carrier Systems – Final Report*

This project has provided techniques for solutions based on experimental data. The project itself is primarily an experimental study with interpretations and explanations based on observations and theory as presented in reference material. Noise reducing treatments for Hubco's existing products have been identified and guidelines for the design of subsequent roof carrier systems have been produced.

1.2 Sound and Noise

It is not within the scope of this thesis to describe what sound is in depth, the basics are summarised as follows… Physically speaking, sound is pressure fluctuations that travel at a speed governed by the medium within which they occur. These fluctuations are of infinitesimal size and can be periodic, random, impulsive or any combination of these. When a study of sound is concerned with human response this definition is incomplete. Pressure fluctuations stimulate the ear, but it is our brains that interpret this experience as sound. Psychologically speaking, sound is much more. Sound plays an integral part in our lives, the ear cannot be turned off and thus hearing is a passive sense, and a sense that is inundated with stimulus.

We can, however be very selective as to what sounds we actually listen to, having the ability to shut out or ignore those we would rather not perceive. Too much sound can be unpleasant and damaging to the ear, but absence of sound can also cause problems, from disorientation through to psychological sickness. Sound can cause us to feel various emotions, lifting or lowering our state of mind. It can motivate and drive us or create apathy, generate tension or relaxation. Hirsh[5] described the way sound does this through consonance, described as the "quality of harmony, smoothness or unity of a combination of tones often experienced as agreeable", and dissonance, described as the "quality of disharmony, ill-fittingness and lack of unity of combinations of tones often experienced as disagreeable".

Disagreeable or unwanted sound is often described as noise. Noise, like sound, has a physical definition. This is, "Complex sound that has little or no periodicity"[6], which may be understood as sound without a specific frequency but containing all frequencies to varying degrees. A more fitting name for this kind of sound would be broadband or white-noise, as the essential characteristic of "noise" is its undesirability[7], Rodda[8] defined noise as "any annoying or unwanted sound".

Interestingly enough, the sound of flowing water, waves and falling rain, all forms of white-noise, can be very pleasant.

A more irritable sound is an unyielding tone (single frequency sound) of around 1000 – 4000 Hz, the range in which the ear is most sensitive. It is interesting to note that the average human ear can distinguish 1,400 discrete frequencies or tones from 16 to 16 000 Hz the average hearing range[9]. A typical source of "noise" often has a dominant tone or tones superimposed on white-noise, for example, an electric drill, in which the dominant tones equate to the speed of revolution of the motor and the gear meshing frequencies.

The type of "noise" that is dealt with in this thesis is of this type.

1.3 Aeroacoustic Theory

Aeroacoustics is the science of aerodynamically generated sound. It is primarily concerned with sound sources as opposed to the propagation, attenuation and reception of sound, the first comprehensive theory was published by Lighthill[10]. In it, he set out to create a model by which the intensity of the sound can be related to the actual flow conditions. It deals with the mechanism in the fluid by which the kinetic energy of fluctuating shearing motions present is converted to the acoustic energy of fluctuating longitudinal motions. It was a fundamental understanding that the frequencies present in a flow are identical with those of the sound produced, but until Lighthill's paper, a general procedure for estimating the intensity of the various frequencies had never been attempted.

Lighthill explained that there are three fundamental ways in which energy is converted from kinetic to acoustic - three source types. Each has a unique sound field and differ in efficiency.

1) Monopole – Sound is generated by a net fluctuating mass flux in a region. This can be represented as $\int \rho d\tau$, where τ = volume. Practical examples include, a siren in which a jet of air is chopped rapidly and a loud speaker embedded in a large baffle.

2) Dipole – Sound is generated by a net fluctuating force on a region. This is represented as $\int \rho u_i d\tau$,

---

[5] Kretch, B. and Crutchfield, R. S. *Elements of psychology*
[6] Hirsh, I. J. *The measurement of Hearing*
[7] Glorig, A. *Noise and Your Ear*
[8] Rodda, M. *Noise and Society*
[9] Olson, H. F. *Music, Physics and Engineering*
[10] Lighthill, M. J. *On Sound Generated Aerodynamically*

where u_i = velocity component in x_i direction. Examples of dipoles include any solid object that vibrates after being struck such as the oscillating string of a string instrument.

3) Quadrupole – Sound is generated by a net fluctuating momentum in a region ie. momentum in the x_i direction is transferred in the x_j. This is represented as $\int \rho u_i u_j d\tau$, where u_j is the velocity component in the x_j direction. Examples of this are sound generated by free air jets, wakes or shear layers.

All complex sound generators can be analysed as a combination of monopole, dipole and quadrupole sources.

The sound fields of these three source types vary also:

1) The monopole sound field is analogous to the pressure field that would be created by a spherical ball submerged in a fluid expanding and contracting radially with changing volume. The strength of the signal varies with the inverse square of the distance from the source.

2) The dipole source sound field is equivalent to the sound field that would be generated by two monopole sources separated by a small distance exactly 180º out of phase. This is analogous to the hydrostatic pressure field that would be created by a rigid sphere oscillating in a linear motion. It can be represented by the following diagram figure 1.1[11].

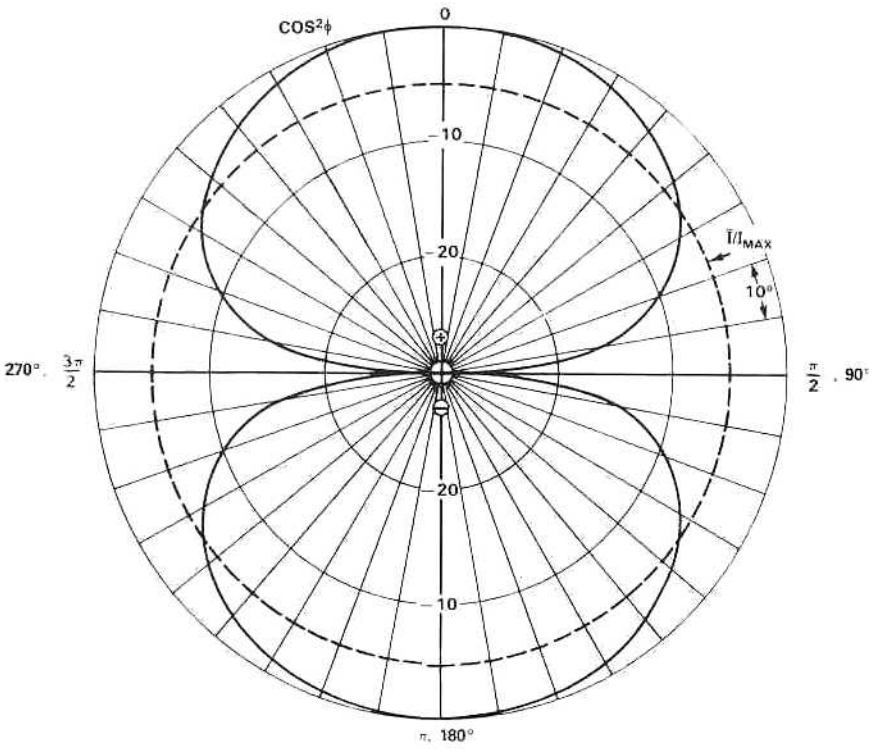

Figure 1-1 Directivity pattern in far field of a compact dipole

3) The quadrupole source (or more specifically, the lateral quadrupole source) sound field is equivalent to the sound field that would exist if two dipoles of equal strength but opposite phase were brought close together. This is analogous to the hydrostatic pressure field that would be generated by a sphere that oscillates so that at one point in its cycle the poles are pushed in and the equator is enlarged and at the opposite point in its cycle the poles are pushed out and the equator is reduced. This field is represented in the following diagram fig. 1.2[12].

[11] Figure from Blake W. K. *Mechanics of Flow-Induced Sound and Vibration*

[12] Figure from Blake W. K. *Mechanics of Flow-Induced Sound and Vibration*

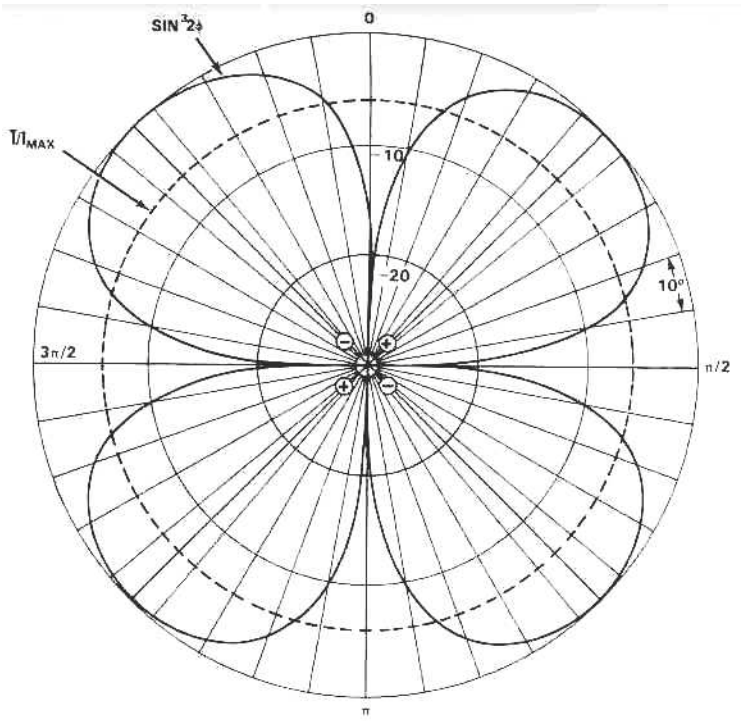

Figure 1-2 Directivity pattern for lateral quadrupole source

As this is an experimental study, it was decided that the detailed mathematics, that describes the model, by which predictions of sound fields for particular flows may be predicted, would be omitted. It is however helpful to note that, the relative efficiency of the source types is generally

Monopole > Dipole > Quadrupole.

1.4 Scope of the Present Investigation

In this work, the noise generated by the Hubco A-bar Roof-Rack will be investigated, relating the noise to the flow structure around the profile. This will be compared to other aerofoil noise investigation and common factors identified.

In the past, much work has been done on the noise produced by aerofoils and many mechanisms have been identified. (See chapter 2). Whilst researching these, the author noticed that there is blurring between the two mechanisms responsible for the vortex street type patterns often present in the wake of aerofoils. These will be distinguished from one another and treatments for each sought.

This is predominantly an experimental study and tests have been carried out in the Mechanical Engineering Department's low noise wind tunnel. This required acoustic treatment prior to sound level testing and this is described in chapter 3.

Lastly, because the roof racks must be marketable, the treatments chosen for the reduction of noise have to be easily and economically manufactured as well as aesthetic.

Chapter 2

AN EXAMINATION OF PREVIOUS WORK ON RELATED SUBJECTS

2.1 Introduction to this chapter

The noise generated by prominent additions and irregularities on cars has long been an issue for automotive manufacturers, but it is not only in the automotive industry that one finds reference to solutions and techniques for removing these annoying occurrences. The developers of most products exposed to wind or air flow will have to combat noise and the vibration associated with it to some extent. In this project, the ultimate goal is to remove the features and/or flow patterns that are the cause of noise. In *Mechanics of Flow-Induced Sound and Vibration*, Blake[1] makes the statement, "Sound is potentially produced whenever there is a disturbance-filled fluid region", he goes on to explain that flow disturbances occur mainly in unstable flow situations for example jets, wakes and flow over cavities. As will be seen in the following chapter, it *is* the unstable regions of a fluid flow that account for the major sources of noise.

2.2 Aerofoil noise

The design of the roof rack was based around the aerofoil Clark Y[2]. It is for this reason that papers were sought that dealt with general aerofoil noise. An obvious avenue was the aerospace industry, where aerofoil profiles are used extensively. In Crighton's report Airframe Noise[3], several different noise-generating mechanisms are identified that are present on aircraft. These are summarised as follows: Trailing edge noise, blunt trailing edge vortex shedding noise, cavity resonances and noise produced by sharp protrusions and edges.

[1] Blake W. K. *Mechanics of Flow-Induced Sound and Vibration*.
[2] Ref. Donohue, B. *Prediction of Aerodynamic Noise from Automotive Roof Carrier Systems – Final Report*
[3] Crighton, D. G. *Airframe Noise*.

2.2.1 Trailing edge noise

This noise is produced when a flow moving adjacent and parallel to a solid boundary passes over the arrestment of that boundary. See fig. 2.1[1]

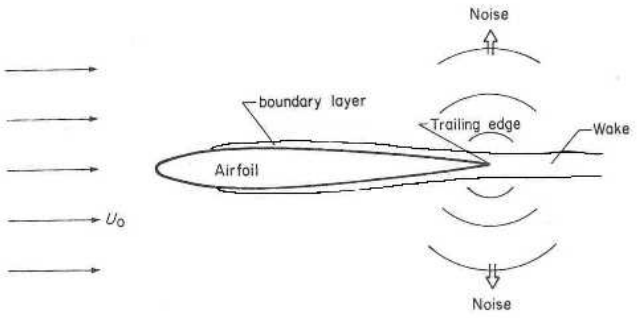

Figure 2-1 Emission of noise from a trailing edge

The pressure fluctuations that are present in the boundary layer of the flow are diffracted by this trailing edge. This occurs for both laminar and turbulent boundary layers. Inside a laminar boundary layer, the pressure fluctuations are Tollmien – Schlichting type instabilities[2], in the case of a turbulent one, the pressure fluctuations are caused by mixing of the fluid and are larger scale and much more frequent. This noise is present and significant in the case of a sharp trailing edged aerofoil. Brooks and Hodgson[3] accurately predicted the trailing edge noise from turbulent flow over a sharp trailing edged aerofoil by measuring the surface pressures on the aerofoil upstream of the trailing edge, confirming that the acoustic noise is a direct manifestation of the hydrodynamic noise. In cases where the laminar boundary layer extends the whole length of the aerofoil, the acoustic signal from the trailing edge travelling upstream may trigger hydrostatic disturbances (Tollmien – Schlichting) that grow and in turn, are diffracted at the trailing edge producing noise.

This feedback loop between the acoustic waves and the hydrodynamic waves produces a tone at a frequency governed by the velocity of the flow and the geometry of the aerofoil (or boundary). In resonance, the amplitude of the hydrodynamic disturbances can become large to the extent of causing the wake to become a periodic pattern of vortices sometimes described as a vortex street. Tone producing systems of this kind were first proposed by Tam[4] and Fink[5] and summarised by Arbey and Bataille[6]. It must be noted that this phenomenon is dependent on two factors being present: 1) a sharp trailing edge and 2) a laminar boundary layer on the pressure surface of the aerofoil. The work that really laid a foundation for the establishment of a theory for this mechanism was an experimental study by Paterson et al[7] in 1973. They established that there is a 'ladder-type' variation that relates the velocity of the main flow to the discrete acoustic frequency. i.e. "a piecewise continuous function of the flow velocity U which increases locally according to an $f \sim U^{0.8}$ power law and under*goes* a number of jumps… the average evolution of the

[1] Figure from Brooks T. F. and Hodgson T. H. *Trailing Edge Noise Prediction from Measured Surface Pressures*

[2] These disturbances exist mainly in unstable regions of flow i.e. the transition region of a boundary layer. They are very sensitive events and usually precede the onset of turbulence. In Betchov and Criminale's '*Stability of Parallel Flows'* they make the point that Tollmien – Schlichting type waves strictly correspond to those waves where *friction is critical* and do not exist in the absence of viscosity. The mathematical derivation of these disturbances can be found in Schlichting. *Boundary Layer Theory*.

[3] Brooks T. F. and Hodgson T. H. *Trailing Edge Noise Prediction from Measured Surface Pressures*

[4] Tam C. K. W. *Discrete tones of isolated airfoils*

[5] Fink M. R. *Prediction of Airfoil tone frequencies*

[6] Arbey, H. and Bataille, J. *Noise generated by Aerofoil profiles Placed in a Uniform Laminar Flow*

[7] Paterson, Robert W. Vogt, Paul G. Fink, Martin R. and Munch, C. Lee. *Vortex Noise of Isolated Airfoils*

frequency – smoothing out all jumps – proves to follow an $f \sim U^{1.5}$ law".[1] The original result by Paterson et al. can be seen in fig. 2.2.

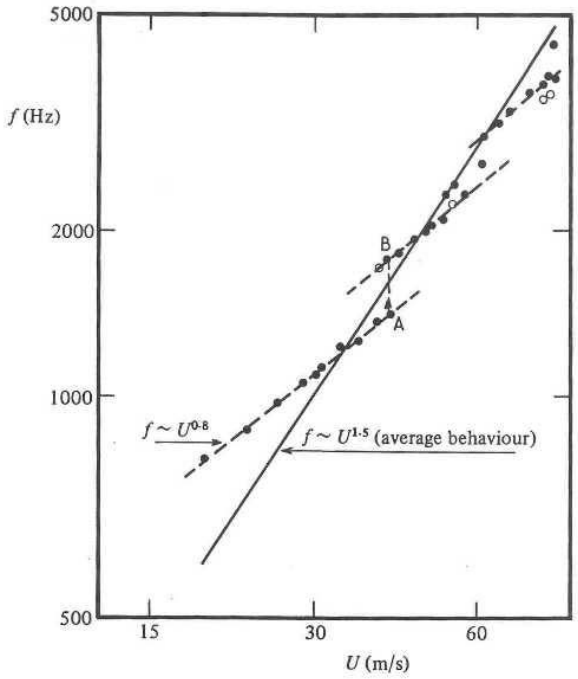

Figure 2-2 Emitted trailing edge frequency variation with velocity

[1] ref. Arbey and Bataille

When the trailing edge is blunt another noise production regime comes in to play that generally overshadows the trailing edge noise (summarised in the next section) and when the boundary layer is turbulent on the pressure surface of the aerofoil, the frequencies of the disturbances which exist in the laminar region do not propagate efficiently through to the trailing edge.

2.2.2 Blunt trailing edge vortex-shedding noise

In the case of a fully developed turbulent boundary layer flow, the discrete frequencies associated with a sharp trailing edge cannot be heard. However, there is a mechanism associated with bodies with blunt trailing edges that also displays discrete frequencies. In Brooks and Hodgson's work[1] with aerofoils with fully developed turbulent boundary layers, they identified that the far-field sound pressure level differs between those aerofoils with a sharp trailing edge and those with a blunt edge. With the blunt case being typically louder. The frequency spectrums of the aerofoils showed the growth of an additional peak as the trailing edge bluntness was increased. The mechanism that caused this peak is understood to be the same mechanism responsible for Aeolian tones, present when air moves across bluff bodies e.g. circular and square cross sectioned cylinders. A common occurrence of this phenomenon is the singing of telephone wires often heard in strong winds. Strouhal[2] was one of the first to investigate these tones, noting that the frequency of the tone emitted was proportional to the velocity U of the flow and inversely proportional to the diameter of the cylinder. The dimensionless constant of proportionality of the relationship is called the Strouhal number:

$$S = fd/U$$

In the case of a cylinder of circular or square cross section the value of $S \approx 0.2$. Von Karman and Rubach[3] observed the cause of the tones to be eddies shed in the wake of an object alternately from each side of the cylinder. This mechanism is often called vortex shedding as the eddies migrate downstream at the flow velocity in the form of two rows of discrete vortices with typical dimensions h and l, a configuration described as a Karman vortex street. (See fig 2.3[4]).

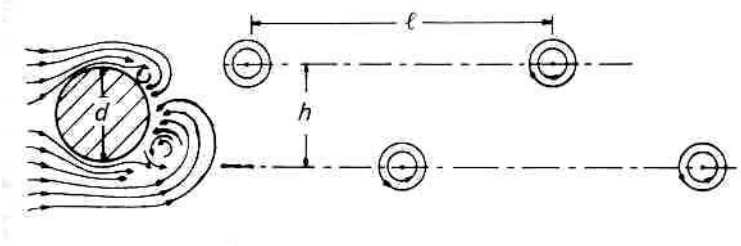

Figure 2-3 Vortex Shedding in the Wake of a Cylinder

The street slowly diverges and deteriorates due to the effects of viscosity. It is a dipole type source of sound. In the past this mechanism has been responsible for more than noise production, both suspension bridges and chimneys have failed catastrophically in the past on occasions of high wind and as a result, now generally have features designed into them to combat the vibration induced by vortex shedding. A necessary characteristic of the flow around a body, in order for vortex shedding to take place, is separated flow. This explains why in the case of sharp trailing edged aerofoils, at low incidence angle, this type of vortex shedding is often not present. At high incidence, when the aerofoil is in a stalled condition, (or if it is a poorly designed aerofoil) a Karman vortex street may be observed. Koobus, B. et al, modelled this computationally on an NACA 0012 aerofoil[5]. See fig. 2.4

[1] Brooks T. F. and Hodgson T. H. *Trailing Edge Noise Prediction from Measured Surface Pressures*
[2] Strouhal, V. *Uber eine besondere ort der Tonne regung*
[3] Von Karman, T. and Rubach, H. *Uber den Mechqnismus des Flussigkeits und Luft-widerstandes.*
[4] Figure from Massey, B. S. *Mechanics of Fluids*
[5] Koobus, B. Tran, H. and Farhat, C. "Turbulence Models for Computational Aeroelasticity" Internet site: http://caswww.colorado.edu/~charbel/turb.html

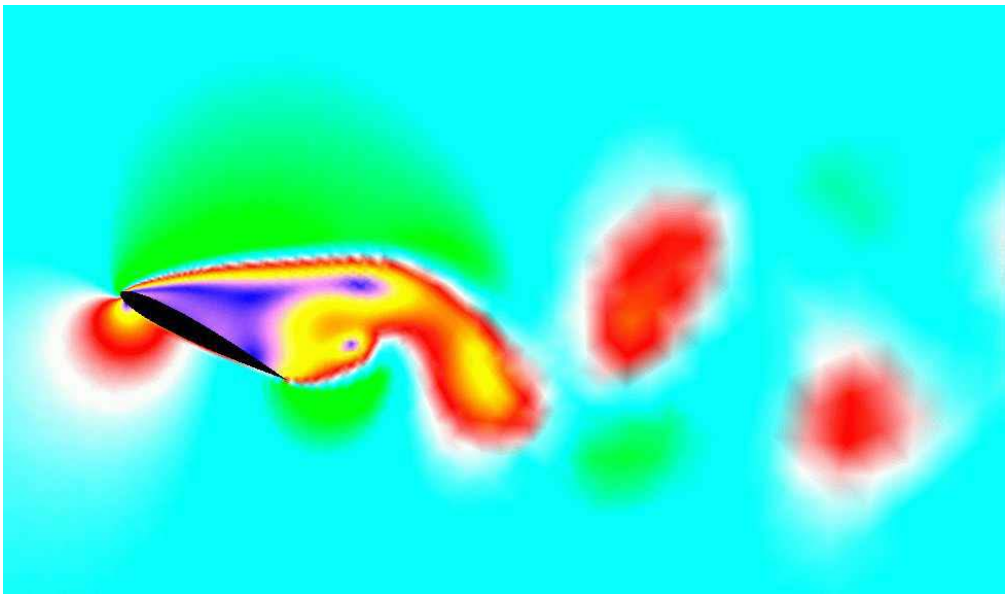

Figure 2-4 CFD Modelling of the Vortex Shedding behind NACA0012 Aerofoil

Bernathy et al[1] explained that the cause of vortex shedding of this kind was the interaction of the two layers or sheets of vorticity[2] cast off the bluff body at the upper and lower separation points. Disturbances in these unstable regions lead to concentrations of vorticity that grow and interact to form the stable Karman vortex street pattern. This theory is supported by Kovasznay's experiments[3] in which he observed the vortices forming some distance downstream of the body.

2.2.3 Cavity Resonances

Whenever a fluctuating airflow, such as that found in a boundary layer or a separation region, encounters a cavity it is possible for tones to be emitted. There are three tone-producing mechanisms that have been identified as being relevant to this project.

If the cavity "encloses a volume of air coupled to the outside free air by means of an aperture"[4] it has a resonant frequency and is described as a Helmholtz resonator. The tones emitted are typically the fundamental frequency and sub-harmonics. The resonant frequency is dependant on the volume of the cavity and the flow resistance through the aperture, very much analogous to the resonance of an electrical circuit containing a resistor, capacitor and an inductor. In these systems energy is transferred from one storage element to another. For the Helmholtz resonator, energy is stored in the acoustical capacitance of the cavity and the inertiance of the aperture.

The second type of resonance that can occur is that demonstrated by columns of fluid inside cylindrical tubes. Analogous to the longitudinal vibration of a solid bar, the fundamental resonant frequency is:

$$f = a/\lambda = a/2l$$

where l is the distance between the antinodes corresponding to the length of an open-ended cylinder or cavity. This resonance if excited could exist inside the roof-rack.

The third type of cavity resonance that occurs can take place whether or not the cavity itself is a resonant entity. This is exhibited when the flow over a boundary passes across a slot or gap in the boundary. The laminar boundary layer becomes a free shear layer. As it moves across the opening its profile changes and it eventually impinges on the downstream edge. This results in "alternate inward and outward motions"[5] of of the flow. Small vortices are cast off the downstream edge generating acoustic disturbances. In a similar way to the feedback mechanism present in trailing edge noise the acoustic waves can trigger instabilities in the free shear layer that grow and convect (propagate) downstream. These hydrodynamic disturbances generate noise as they encounter the downstream edge reinforcing the cycle. The overall effect is the production of a tonal resonance that depends on the geometry of the cavity and the flow velocity and properties.

2.2.4 Edge Noise

Sometimes a protrusion or sharp edge projecting into a flow can generate distinct tones, this type of sound production can be complex depending on the geometry of the projection and its material properties. The following is a simple summary of the basic mechanism present in most cases.

The noise produced by turbulence in a fluid flow, away from solid boundaries, is low efficiency quadrupole emission, this is because there is only momentum transfer within the fluid. If the turbulent flow encounters a solid body (or surface), there will be a fluctuating reaction force between the body and fluid. According to acoustic theory, when a fluctuating force acts on a fluid, the emission of sound is dipolar. This is a much more efficient emitter and the sound radiated will overshadow the quadrupole noise from the free turbulent flow. If the body is made to vibrate with the pressure fluctuations inherent in the flow, noise will be emitted due to this mechanical vibration as well. This also will be dipolar emission.

If the body has a natural frequency in the region of the turbulence frequency this may be excited and a tone heard.

---

[1] Abernathy, F. H. and Kronauer, R. E. *The formation of Vortex Streets.*

[2] These exist when parallel adjacent layers of fluid move at differing velocities in a fluid of not-insignificant viscosity.

[3] Kovasznay, L. S. G. *Hotwire Investigation of the Wake Behind Cylinders at Low Reynolds Numbers.*

[4] Ref. Olson, H. F. *Music, Physics and Engineering*

[5] Ref. Blake W. K. *Mechanics of Flow-Induced Sound and Vibration*. Applied

2.2.5 Miscellaneous Noise Sources

Certainly the aforementioned list of aeroacoustical sources is not exhaustive. Even in the case of airflow over an aerofoil, there are secondary sources which depending on the conditions present and the actual aerofoil under investigation may be of significant importance. For example if the aerofoil surface has grooves running along the chord, channeling of the airflow may result. If small jets are expelled at the downstream end of these channels, then a significant sound source may be created.
We will assume at this stage however, that there are no extraordinary features like this.
One feature however, that distinguishes roof rack noise from those of other aerofoils is the close proximity of the roof of the car. This may affect the noise production in three ways.

1. It may alter the flow regime by causing the streamlines to converge, increasing the velocity on the under surface of the roof rack. The likelihood of early flow separation on this surface of the roof rack is therefore reduced.
2. It may cause the flow onto the roof rack to be at some angle of attack due to the camber of the roof and the wind being swept off the windscreen. The higher the angle of attack, the higher the probability that the roof rack is stalled.
3. The presence of the roof may enable a resonance to be set up in the air gap between the roof and the roof rack.

2.3 Preventative techniques

In many studies, the understanding of the mechanism by which a noise is produced is an end, in this project however, understanding is only a means, a tool by which the culprit mechanism may be suppressed or eliminated. There are various references that do address techniques in noise suppression. Crighton[1] outlines those used in the aircraft industry. Also, summary of the noise mechanisms present on wind turbines and efforts in their attenuation is made by Lowson[2]. The following is a description of their findings and the findings of others as applied to the mechanisms described in the previous section.

2.3.1 Trailing edge noise

It is a rather difficult thing to remove the broadband noise generated by this mechanism. Howe[3] discusses the effect of having either sinusoidal or sawtooth serrations on the trailing edge of a flat plate. It is stated that both of these modifications reduce the intensity of the radiated sound. The attenuation of the sound increases as the serrations sharpen. Howe also mentions the effect of a serrated leading edge, stating that these generate chordwise trailing vortices that modify the character of the wake flow from the trailing edge. Crighton[4] states that swept trailing edges will have reduced trailing edge noise, this is similar in principle to the way serrations work.

The removal of tonal trailing edge noise seems to be a lot simpler to achieve. In Paterson et al[5]. they noticed in trailing edge noise experiments with turbulent boundary layers, the usual tones present when the boundary layers were laminar could not be heard. Hersh et al[6]. confirmed this result showing that a leading leading edge serration removed trailing edge tonal noise by tripping the boundary layer on the pressure surface from laminar to turbulent.

---

[1] Crighton, D. G. *Airframe Noise*
[2] Lowson, Martin V. *Applications of Aero-Acoustic Analysis to Wind Turbine Noise Control*
[3] Howe, M. S. *Noise produced by a Sawtooth Trailing Edge*
[4] Crighton, D. G. *Airframe Noise*
[5] Paterson, Robert W. Vogt, Paul G. Fink, Martin R. and Munch, C. Lee. *Vortex Noise of Isolated Airfoils*
[6] Hersh, A. S. Soderman, P. T. Hayden, R. E. *Investigation of Acoustic Effects of Leading Edge Serrations on Airfoils*

2.3.2 Blunt trailing edge vortex-shedding noise

The suppression of blunt trailing edge vortex shedding has long been an area of great interest[1]. The mechanical vibration that it can induce on cylinders of large diameter, for example, suspension bridge structures and chimneys, has been a problem requiring focused efforts to solve. The treatments used to combat this phenomenon have included the use of perforated shrouds, helically wound cables and fences, varying diameter sleeves and trailing splitter plates. Blunt trailing edge vortex shedding is a much more stable flow regime than the periodic wake that can be induced in the case of a sharp trailing edge. It exists even when the boundary layer over a body is turbulent and the treatments are rather more complicated than a simple tripping of the boundary layer. They are generally one of the following 3 types or a combination of:

1. Treatments that focus on preventing the interaction of the pair of vorticity sheets cast off the rear of the body as in the case of the trailing splitter plate or base bleed in the case of a blunt trailing edge aerofoil[2].
2. Treatments that seek to introduce spanwise motion into the flow over the body, causing the flow to become 3-dimensional and prevent the vortex street from forming in a regular fashion. Examples of this type of treatment are the use of perforated shrouds, varying diameter sleeves or even the use of helically wound cables.
3. Treatments that split the body spanwise into smaller sections upsetting correlation along the span. Although each section may induce vortex shedding, the sections are unlikely to be in phase and thus the overall strength of the sound emission is reduced. Helically wound fences or strakes may do this, depending on the height of the strake. See fig 2.5[3]

[1] Steinman, D. B. *Pipeline Bridge Stabilized with Diagonal Rope Stays*, Baird, R. C. *Wind-Induced Vibration of a Pipe-Line Suspension Bridge and its Cure*, Price, P. *Suppression of the fluid-induced vibration of circular cylinders*

[2] Ref. Wood, C. J. *The effect of base bleed on a periodic wake*

[3] Figure from *New Zealand Engineering.* IPENZ publication. Vol 54/3 April 1999

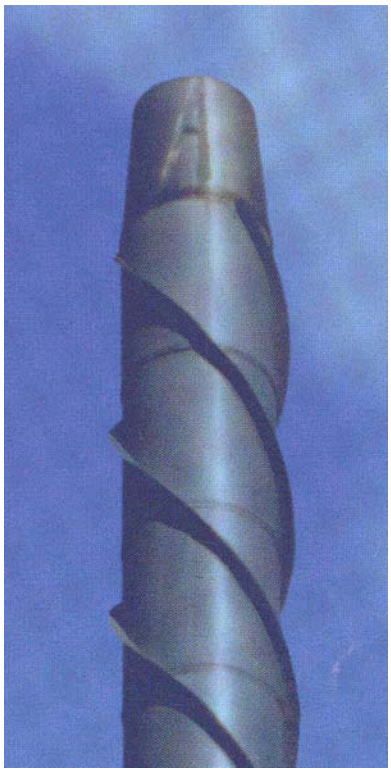

Figure 2-5 Helical Strake around Chimney

The leading edge serrations used by Hersh et al[1] on an NACA0012 were shown to reduce the vortex shedding noise generated, even when the flow over the aerofoil was turbulent. The use of these followed from studies on the wings of owls that typically exhibit quiet flight. This is an example of a device that induces a 3-dimensional flow through the production of chordwise vortices. These interfere with the spanwise vortices being cast off the trailing edge.

2.3.3 Cavity Resonances

Probably the best solution for combating the noise generated by a cavity exposed to a fluctuating fluid flow is to seal off the cavity. If the source of excitement is removed then the system will not resonate.
In the case of resonance due to feedback in a free shear layer, tripping the laminar boundary layer upstream of the cavity to a turbulent boundary layer may eliminate this[2].

[1] Hersh, A. S. Soderman, P. T. Hayden, R. E. *Investigation of Acoustic Effects of Leading Edge Serrations on Airfoils*
[2] Ref. Blake W. K. *Mechanics of Flow-Induced Sound and Vibration*.

2.3.4 Edge Noise

Crighton[1] describes changing the surface impedance to reduce edge noise. For example, the use of porous leading edges can reduce the level of noise perceived by minimising the discontinuity experienced by a convected eddy passing the edge. It seems that modifying protrusions or edges to shift their natural frequencies away from the frequencies encountered in the turbulent air stream can be useful in reducing noise emitted. In practise, this means either stiffening or dramatically increasing their flexibility.

[1] Crighton, D. G. *Airframe Noise*

Chapter 3

WIND TUNNEL MODIFICATION

3.1 Introduction to Chapter

Wind tunnels are in use for many aerodynamics applications where a controlled flow velocity and quality is needed. Field experiments, generally cannot avoid the large-scale turbulence and variability present in the natural wind environment. In contrast, it is possible to generate flows in the wind tunnel that have a much lower degree of turbulence and are very repeatable. The particular wind tunnel that was used in this study, was one designed originally for aeroacoustic work, with a low noise working section. In aeroacoustics, this is necessary for acquiring good results. The standard term used to describe the quality of an aeroacoustic test facility is the *signal to noise ratio* (SNR). This describes the level of the sound generated by the experimental subject compared to the background level and should be sufficiently large in the frequency range of interest that the subject noise can be identified above the ambient. In fact, it is almost always necessary, that the subject noise be measurably higher than the wind tunnel noise, a curious fact being that the ear can distinguish a pure tone of lower sound pressure level (SPL) than the surrounding background noise level. This is something that sound level meter manufacturers have not yet emulated. This chapter outlines the modifications that were needed to bring the signal to noise level of the open circuit wind tunnel in the aeronautics lab of the Mechanical Engineering Department at the University of Canterbury, up to an acceptable level for the current project.

3.2 History

The wind tunnel in the Mechanical Engineering Department was built in 1970 and had originally been designed to be quiet in operation for investigations with aeroacoustic content. Professor Cliff Stevenson, a specialist in the field of aeroacoustics, oversaw the design and construction. The configuration was a horizontal non-recirculating blower wind tunnel that had a maximum speed of 31.4m/s in a 0.76m square working section. This was located in the Mechanical Engineering Department aeronautics lab on the ground floor. See fig. 3.1[1]

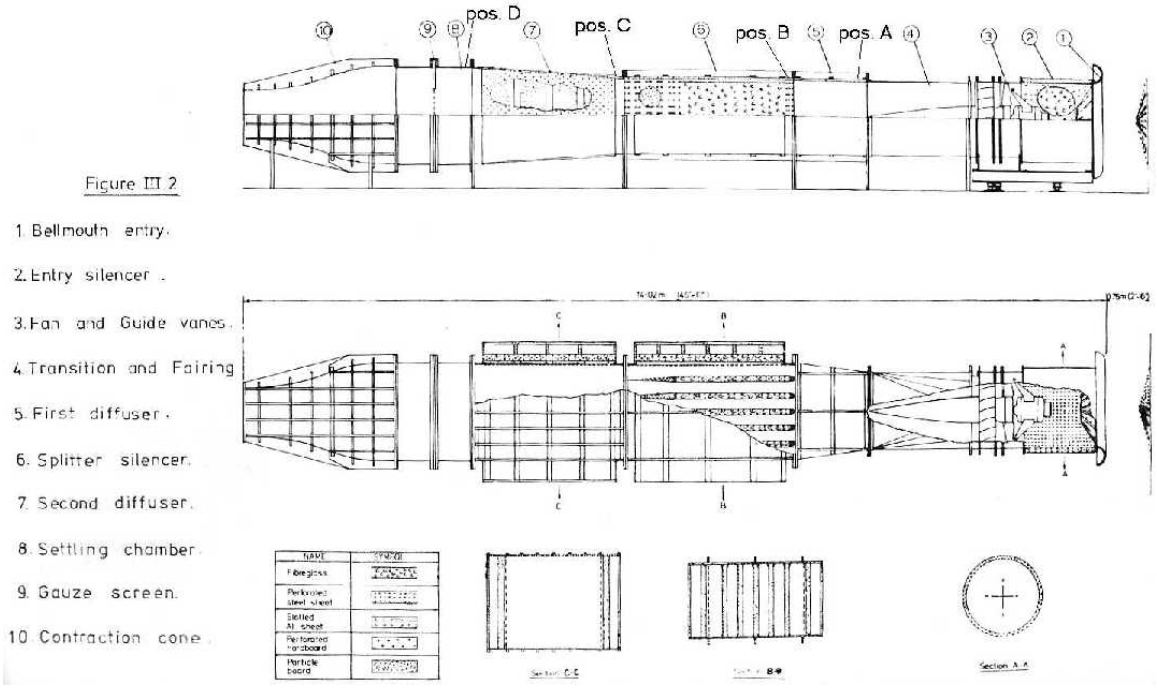

Figure 3-1 The original blower wind tunnel.

The tunnel was acoustically treated in a number of ways: an entry silencer, splitter-silencer, attenuating diffuser and an acoustic termination positioned downstream of the working section. It was constructed of timber, particle-board and plywood. The first two experiments, completed in 1971, were the investigation of the noise of tube banks systems[2] and separation bubble noise around bends[3]. As the years passed, the amount of work done in this field reduced, especially following Professor Stevenson's retirement from the Mechanical Engineering Department. A result of this was, when modifications were done to the wind tunnel, they were done with little regard for the aeroacoustic requirement of low noise. The most significant modification to the wind tunnel was the extension and inclusion of a 1.2m square boundary layer working section for the investigation of wind phenomena in 1974[4]. (See fig. 3.2[5])

[1] Figure from Tang, T. T. *Aerodynamic Noise in Tube-Bank Systems*
[2] Tang, T. T. *Aerodynamic Noise in Tube-Bank Systems*
[3] Nguyen, H. B. *Aerodynamic Noise in Separated Flow*
[4] Raine, J. K. *Modeling the Natural Wind Protection by Fences*
[5] Figure from Raine, J. K. *Modeling the Natural Wind Protection by Fences*

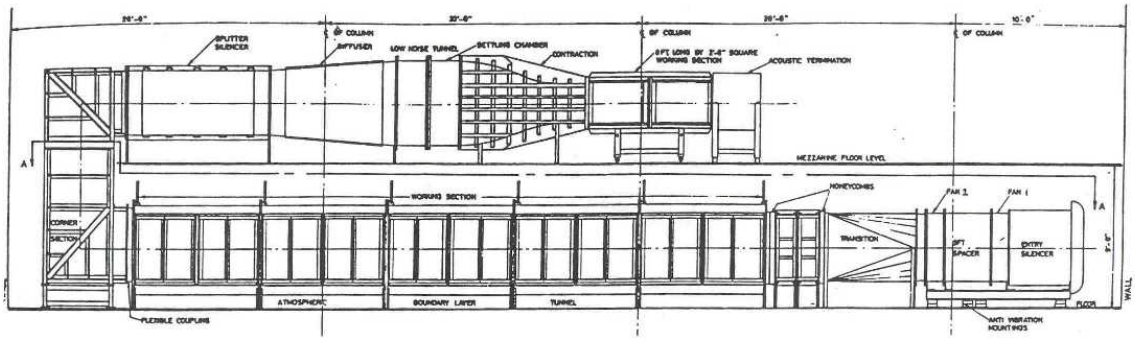

Figure 3-2 The open circuit wind tunnel after 1974 modifications.

In this development, the original wind tunnel was placed on a new mezzanine level and extended upstream through two 90-degree elbow bends and a 12.2m long working section that was positioned directly beneath the original section on the ground floor. An extra identical fan unit was added to increase the volume flow and these were placed upstream of the new boundary layer working section. These operated off the single speed controller.

Later in 1976, these were placed in between the two working sections on the mezzanine floor and a new intake placed at the upstream end of the boundary layer tunnel. This was to allow a settling chamber and honeycomb section to be placed prior to the boundary layer working section, to give better quality airflow. (See fig 3.3[6])

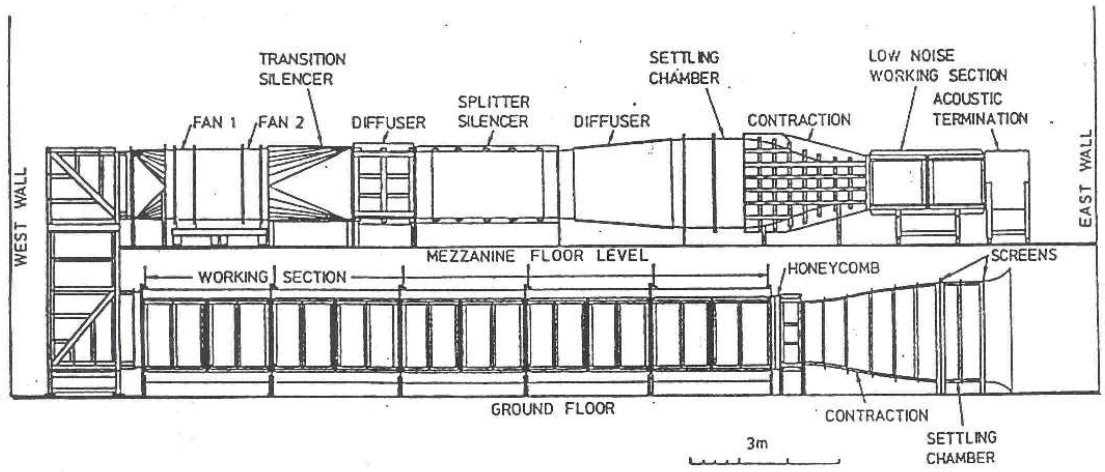

Figure 3-3 The open circuit wind tunnel after 1976 modifications.

The maximum flow velocity achievable in the low noise working section after the modification was 38.7m/s. The intended use for the extension was investigations in atmospheric and boundary layer aerodynamics. It had no acoustic treatment applied to it except for sound absorbent material being placed in the underside of the mezzanine floor.

3.3 Description of General Arrangement

The wind tunnel is an open circuit type with two working sections, powered by a Woods 1.2m dia. 50kW two stage, contra rotating fan unit with pneumatic blade pitch control. This is driven by two three-phase

[6] Figure from Stevenson, D.C. and Raine, J. K. *Dual Working Section Wind Tunnel at the University of Canterbury.*

electric motors that operate at the constant velocity of 1475rpm. The complete wind tunnel circuit is as follows:

i) Bell mouth entry with 2.45m by 1.85m rectangular cross section with cloth filters for the removal of impurities in air supply, protecting hotwire probes.
ii) Settling chamber with screens for removal of large-scale turbulence.
iii) Contraction to 1.2m square cross section.
iv) Honeycomb for flow straightening and boundary layer initiation.
v) 12.2m working section for boundary layer and atmospheric aerodynamics investigations. This is equipped with a traverser for computer controlled positioning of DISA and TSI hotwire probes and is accessible anywhere along its length from both sides via hinged doors.
vi) 90˚ horizontal to vertical elbow bend with guide vanes.
vii) 90˚ vertical to horizontal elbow bend with guide vanes.
viii) Square to 1.2m diameter round transition.
ix) Two stage fan unit. Each fan has six pneumatic pitch controlled blades. The speed is adjusted by altering the pitch of the fan blades. This is pneumatically actuated and controlled via a portable air regulator unit
x) Round to 1.2m square cross-section transition with sound absorbent panels to stop the transmission of noise.
xi) Diffuser with expansion ratio of 1.25:1 in vertical direction.
xii) Splitter silencer.
xiii) Diffuser with expansion ratio of 1.25:1 in transverse horizontal direction.
xiv) Wire Gauze to remove large-scale turbulence.
xv) Settling chamber.
xvi) Contraction to 0.76m square cross-section.
xvii) Working section for aeroacoustical investigations.

When the author encountered the wind tunnel in 1999, the original acoustic termination was not present nor the acoustic jet deflector.

3.3.1 Description of Acoustic Condition

The modifications caused problems, in terms of the acoustic condition of the tunnel, as they produced a significant increase in the overall noise level. This came about by the addition of the second fan unit and the positioning of the non acoustically treated section below the aeroacoustic test area with little to stop the propagation of the noise from one to the other. A grill was placed into the mezzanine floor between the outlet and intake of the wind tunnel, this was intended to allow a smoother passage of air from the one to the other and thus an increase in efficiency. Unfortunately this also allowed the passage of noise from the intake to the low noise working section and there was a considerable amount of noise being transmitted. Described as intake roar, it was typically low frequency broadband. Because of the lack of acoustic treatment applied to the modifications from 1974 onward, much of the sound generated in the system upstream of the fan unit is propagated freely to the intake, this includes noise generated in the fan unit itself.
As a result, much work had to be done to improve the acoustic condition of the test area. The signal to noise ratio was originally very low and it was rather difficult, even with the ear, to hear the (usually) telltale roof rack noise.

3.4 Requirements

The A-bar sound spectrums, from the preliminary field tests carried out at the Ruapuna track, showed a dominant sound peak in the 1/3rd octave frequency band of 500Hz. This was attributed to a pure tone. This tone was identified as that one most likely to be annoying for vehicle occupants.
The sound pressure level of the empty wind tunnel in the bands around 500Hz was going to need to be low, to allow easy recognition of this sound when measured with a sound level meter. It was conceivable that this peak was mobile, ie. the dominant frequency altered as the flow conditions, velocity etc changed. For this reason the empty tunnel noise levels in the frequency range from 200 to 1000Hz were required to be at a minimum.

3.5 Measurement of Sound Level

The noise throughout and around the wind tunnel needed to be measured. Treatments would be based upon the frequencies present and the strengths and locations of the sources. When a sound spectrum is measured, the frequencies are divided into 1/3rd or 1/1st octave bands[7]

3.5.1 Acoustic Equipment

There were two pieces of equipment used for determining the noise levels around the wind tunnel, these were both Brüel & Kjær instruments. The 2260 Investigator, for basic 1/3rd octave sound pressure level spectrums, and the 4433 intensity meter, for determining the direction of emitted noise and the location of sources.

2260 Investigator

The 2260 Investigator is a versatile, hand-held, battery operated, 2-channel sound analyzer. (See fig. 3.4[8])

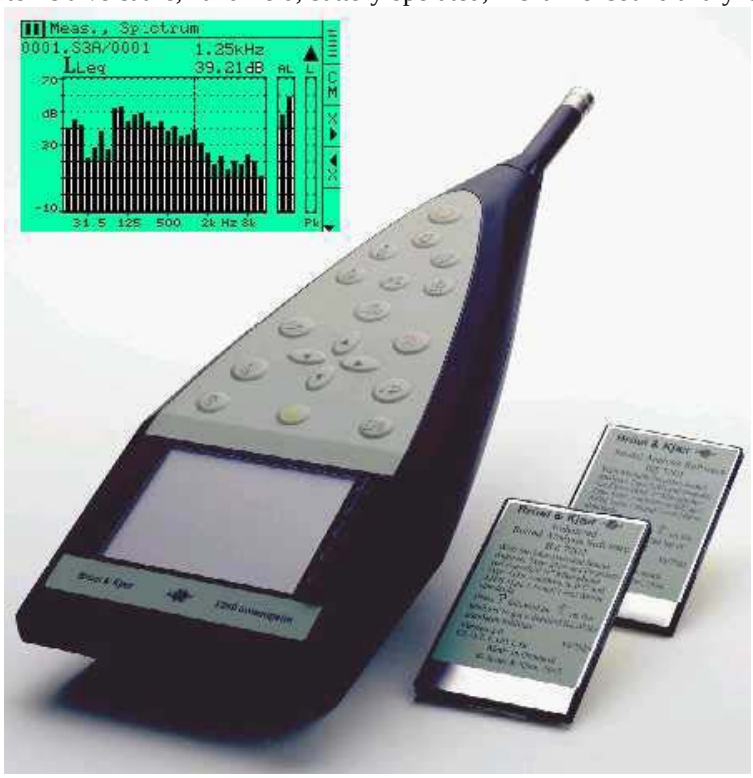

Figure 3-4 The 2260 Investigator with upgrade modules. (Inset) The Investigator display.

It is a microprocessor-based platform that supports a range of applications, from a building acoustics analysis system to a noise profile analyzer. In this project the Enhanced Sound Analysis Software BZ7202 was used. It automated the measurement of sound spectra. Although the 2260 has the capability to apply weighting networks[9] (A and C) to measurements, in the tests in this project, the linear levels were taken and A-weighted manually during the processing of results. For most tests in the course of the work the sound pressure level (SPL) was averaged over 10s to give a linear equivalent level or L_{Leq} spectrum. Figure 3.4 inset shows a typical L_{Leq} spectrum on the 2260 display.

---

[7] Table of 1/1st and 1/3rd octaves and their ranges in Appendix A

[8] Figure from Brüel & Kjær Product Data catalogue BP1583 –13.

[9] Weighting networks seek to emulate the sound response of the human ear. The ear is more sensitive to some frequencies of sound than others. It is most sensitive to the frequency range 1000-4000Hz. The A, B and C weighting networks can be found in Appendix A

The ½" microphone, which is characteristically attached to the top of the 2260, can be mounted on a variety of accessories from telescopic booms to goose necks. In low or no airflow, foam windscreens are used to reduce psuedo sound, the noise produced by wind impinging on the microphone itself. In high unidirectional airflows the normal protection grid of the microphone can be replaced with an aerodynamic nose cone. See fig. 3.5[10]

Figure 3-5 A typical aerodynamic nose cone.

This has a streamlined shape with a polished surface to reduce air friction and thus turbulence noise. The fine wire mesh around the nose cone permits sound pressure transmission to the microphone diaphragm. This was used whenever the microphone was submerged in the moving airstream of the wind tunnel. Before commencing each experiment, the 2260 Investigator was calibrated with a Brüel & Kjær calibrator type 4231 to an accuracy of ±0.2dB.

4433 Sound Intensity Analyser

The 4433 is a portable battery operated serial analyser used for measuring sound intensity and sound power levels. (See fig. 3.6) It is a digital instrument that has the capability to automate measurements. The measurements taken in the following section were an average intensity over 8s. The 4433 can be used to measure individual octave bands with center frequencies ranging from 63Hz to 8kHz. It can apply the A-weighting network to measurements and can be operated remotely from the probe.
The probe used was a Brüel & Kjær sound intensity probe type 3520, it consisted of two ½" microphones mounted opposite each other, separated by a 12mm spacer[11]. Intensity meters have directional response. As the probe is moved around the source being measured, an energy flow indicator on the meter indicates the orientation of the source in relation to the microphones. This energy flow indicator enables the operator to pinpoint the strongest source in the vicinity of measurement. The microphones can be covered with a foam windshield to protect from the effects of air movement. This use of the windshield was important in this work, due to the high airflow that resulted in the lab, while the open circuit tunnel was operated.

[10] Figure from Brüel & Kjær Product Data catalogue BP1650 – 11
[11] There are a variety of spacer sizes available from 6 to 50mm. The 12mm spacer was chosen because it had good high frequency response characteristics without sacrificing the lower part of the spectrum.

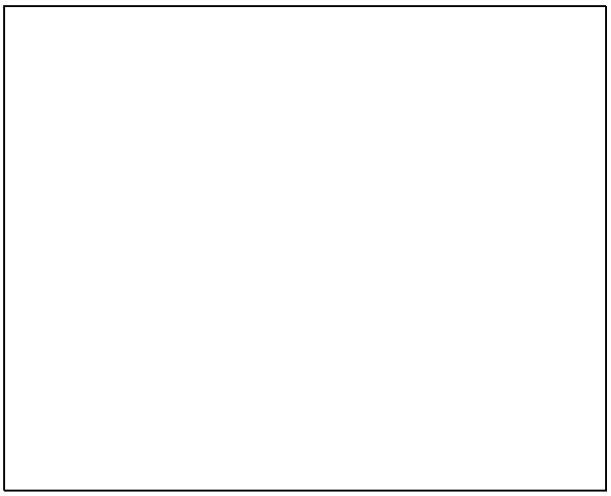

Figure 3-6 4433 analyser with probe and windshield.

3.5.2 Aerodynamics Equipment

Operation of Wind tunnel

The wind tunnel experiments were conducted with both fans operating. Although a single fan unit would run the tunnel sufficiently fast to achieve the desired velocity head in the working section, it was discovered that in this configuration a resonant mechanical vibration is set up. This is due most likely to the large blade angle on the fan. When this happens the noise level is augmented excessively.
The speed controller unit was operated on the mezzanine floor close to the working section.

Pitot Tube and Water Manometer

For accurate measurement and monitoring of the air velocity in the tunnel, a 6mm round nose Pitot tube was used in conjunction with a Betz water manometer model AVA. This gave highly accurate readings of velocity head to $\pm 0.1 mm_{H2O}$ accuracy as long as the zero datum had been set and the manometer positioned vertical using its fluid level. The Pitot tube was mounted parallel to the flow in the working section, held in place with a simple clamp.

3.5.3 Procedure

It was the intention at the outset, that testing of the sound radiated from the roof racks would be done inside the low noise working section, halfway down its length with a microphone mounted just behind the rack below the wake. The noise investigation was therefore initially concerned with the noise level at that location.

The initial test using the 2260 investigator was conducted at the mid-way point of the low noise working section in two positions, an upper and a lower. The geometry of the upper and lower positions was 200mm from the ceiling and the floor of the tunnel respectively, half way along the working section laterally centred. The microphone was mounted on a telescopic boom with an aerodynamic nose cone and was held in the flow by hand. The orientation of the boom parallel to the flow, would minimise the noise emitted by the wind moving across it. Tests were conducted while workshop noise was at a minimum. They were done at 3 speeds, 15.5m/s or 56km/h in both the upper and lower position, at 22.2m/s or 80km/h in the upper position and at 29m/s or 104km/h in the upper position. An ambient reading was also done in the wind tunnel with no airflow. The sound measurements were 15s L_{Leq} tests. The $1/3^{rd}$ octave band spectrums were downloaded to a PC where they were graphed and analysed.

The tests revealed mainly broadband noise a few various bands displaying local frequency peaks. One peak that appeared consistently at each speed was the 160Hz 1/3rd octave interval, this has a range from 141-178Hz. The peak was attributed to the blade passing frequency of the fans, calculated at 147.5Hz[12]. The overall A-weighted sound levels were 81.5, 88.7 and 100dBA[13] for the 15.5, 22.2 and 29km/h tests respectively with an ambient level of 49dBA. Figure 3.7 shows the spectrum for the 22.2km/h test[14].

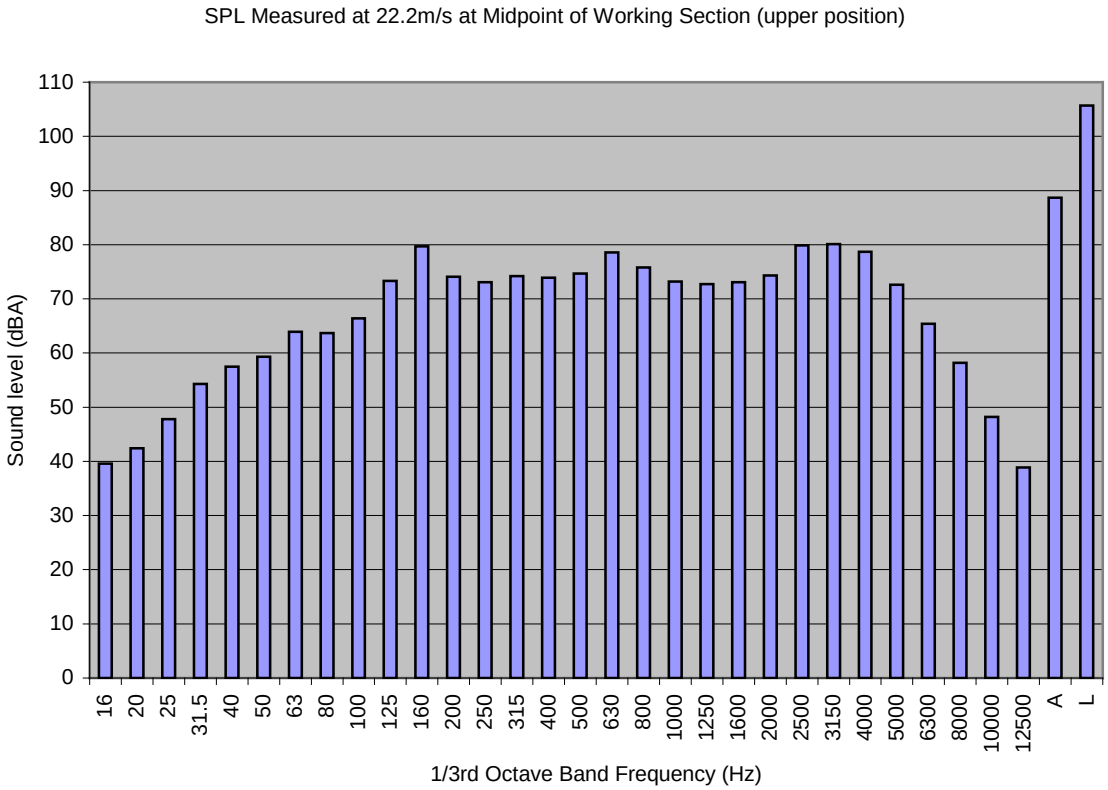

Figure 3-7 Sound spectrum measured in working section at 22.2m/s (80km/h).

Each of the bars represents the SPL of a 1/3rd octave band. The last two are the A weighted and linear overall SPLs respectively.
As stated previously, low noise level in the range from 200-1000Hz was important for this work. The presence of a dominant frequency, in the 630Hz 1/3rd octave band, as shown in fig. 3.7 was unacceptable.

A treatment program was needed to reduce the sound levels to an acceptable level.

[12] Calculation of blade passing frequency in Appendix B
[13] All dB and dBA measurements in this thesis are re. 0.00002 N/m^2
[14] Spectrums for other tests in Appendix D

3.6 Treatment of Noise Sources

In order to find out where to focus noise treatment work on the wind tunnel, a series of spectrums were measured inside the tunnel, down the length of the acoustically treated section, to determine the evolution of the noise profile. These were needed for the verification of the effectiveness of the existing noise treatment.

3.6.1 Verification of Effectiveness of Existing Silencers

Method

Holes were drilled in the roof of the wind tunnel in positions between each silencing section. They were labeled positions A through to D and were the upstream end of the first diffuser, splitter silencer, second diffuser and settling chamber respectively. See fig. 3.8. These were plugged after the tests.

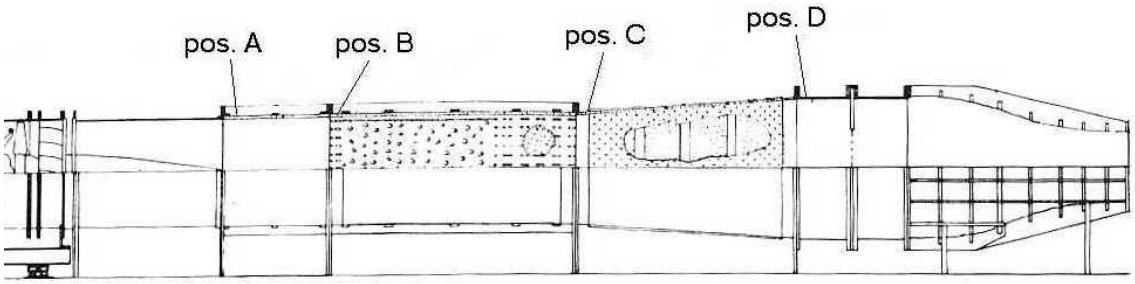

Figure 3-8 The Positions of test holes.

The 2260 was used to measure the sound spectrums at these positions. The microphone was mounted at the end of a gooseneck with an aerodynamic nosecone. While the tunnel was running at test speed, the microphone was lowered into the wind tunnel and orientated so that the wind-induced noise was at a minimum. This was determined by reading the overall SPL as the microphone direction was altered. Measurements taken were 10s L_{Leq} tests. They were conducted at two airspeeds, the minimum speed of the tunnel with both fans operating, 16.7m/s in the working section and the speed at which the main experimentation would be done, 22.2km/h in the working section.

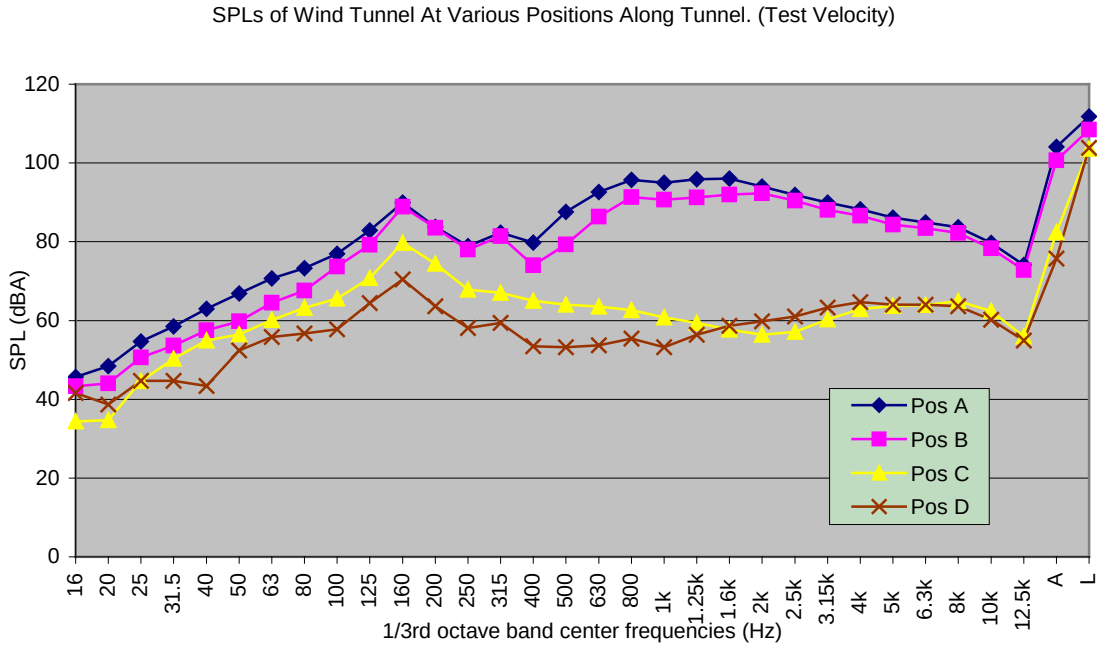

Figure 3-9 Sound spectrums at each position, measured at test velocity.

Results and Conclusions

The sound spectrum differed at each position, there was a consistent decrease in the overall SPL, more than could be explained by the inverse square law (assuming the fan unit is the noise source). Each of the silencers seemed to be effective at reducing different frequencies of the spectrum. Figure 3.9 shows the development of the sound spectrum at the test velocity of 22.2m/s (80km/h)[15].

The first Diffuser: Position A – Position B

There was not a lot of sound energy removed through this section. This is an expected result, as this diffuser has no sound treatment in it. There was however a general decrease in the mid range sound from 400Hz through to 1.6kHz. There was also some attenuation in the low frequency 20Hz to 80Hz range. The OASPL (overall sound pressure level) decreased from 104.1 to 100.7 dBA.

The Splitter Silencer: Position B – Position C

This section was very effective across the whole spectrum. There was a dramatic decrease in SPL in the range from 500Hz to 12.5kHz. The OASPL decreased from 100.7 to 82.4 dBA.

The second Diffuser: Position C – Position D

This was an effective noise abating section for the middle to lower frequencies from 100Hz to 1kHz. The OASPL decreased from 82.4 to 75.7 dBA. An interesting feature of this test was that the noise level increased slightly in the range from 1.6kHz to 5kHz. Assuming that there were no additions inside the wind tunnel that were large sound producers, this result reveals that the propagation of sound was not just in the downstream direction. There were sources of noise external to the tunnel circuit and sound was entering the tunnel at the exit or working section area.

This also explains why the initial 22.2m/s spectrum in the working section measured with the boom pole was much higher than the gooseneck test at position D.

There may also have been sound being reflected from the open end of the wind tunnel back upstream.

3.6.2 Acoustic Termination

To combat the entrance of sound at the exit of the wind tunnel and reflections from the open end, it was decided that an acoustic termination was needed. As described earlier, there was an acoustic termination

[15] Sound spectrums at the minimum velocity in Appendix D

built for the wind tunnel when it was first constructed. Nugyen[16] described it as a basic straight wind tunnel section with a 100mm fibreglass lining, retained by perforated steel sheets. This is not the only type of noise abatement device that could be constructed. Embleton[17] describes various muffler types that would be suitable for a duct-device such as a wind tunnel. A dissipative muffler similar to that originally built was finally decided upon. This type has a low flow resistance and sound absorption is relatively wideband.
For porous absorbent material, with a solid reflective backing, to effectively absorb a sound, it must be a least ¼ the wavelength thick. This guarantees that the antinode of the sound wave encounters the material. At the antinode of the compression wave, the air velocities are greatest and the most energy will be absorbed through viscous losses in the material. The lowest frequency absorbed by an absorber assuming normal incidence is:

$f = c/4t$

where t is the thickness of the absorber and c is the speed of sound in air (340m/s at 25˚C)
In real life, the incidence of the sound wave is not always normal, and lower frequencies will be absorbed to some extent. This is particularly true in the case of a lined duct where the immediate assumption is that planar sound waves travel more or less longitudinally in the duct. Of course, if the waves are ideally planar and parallel to the lining, there will be no absorption at all. Embleton points out however that, "a truly plane wave cannot exist in a duct. Because of losses at the boundary, the wave front near the side walls is bent toward them". There would also be reflections off the walls of the tunnel. For these reasons, the acoustic termination would be effective.

Frequencies of interest were, the blade passing frequency of 147.5Hz and the aforementioned range around 500Hz. Calculations of desired absorber thickness were based on 147.5Hz as this is the lowest frequency and hardest to remove.
$t = c/4f$
$= 340/(4*147.5)$
$= 0.58m$

This is a very high value and was both difficult and expensive to achieve. The actual thickness was based upon availability and cost.

Attenuating Material Selection

The choice of lining material was based on absorption curves measured by Parkinson, J.P.[18] in the University of Canterbury Reverberation Room. Parkinson's work investigated the effectiveness of various configurations of open and closed cell foams and films for use in noise control work. The material chosen as most suitable for use in the wind tunnel acoustic termination was an open cell polyester foam. The maximum thickness practically available was 100mm. The theoretical lowest frequency absorbed by this foam at normal incidence is:
$f = 340/4*0.1$
$= 850Hz$[19]

[16] Nguyen, H. B. *Aerodynamic Noise in Separated Flow*
[17] Embleton, T. F. W. *Mufflers*
[18] Parkinson, J. P. *Acoustic Absorber Design*
[19] Experimental absorption curve in Appendix A

Description of Termination

The acoustic termination (fig. 3.10) is a 1.5m long straight wind tunnel section with 1m square external cross-section. It is constructed of timber and MDF and internally lined with 100mm thick foam, this reduces the internal cross section to 0.76m square. It is supported on castors to enable easy removal when not in use.

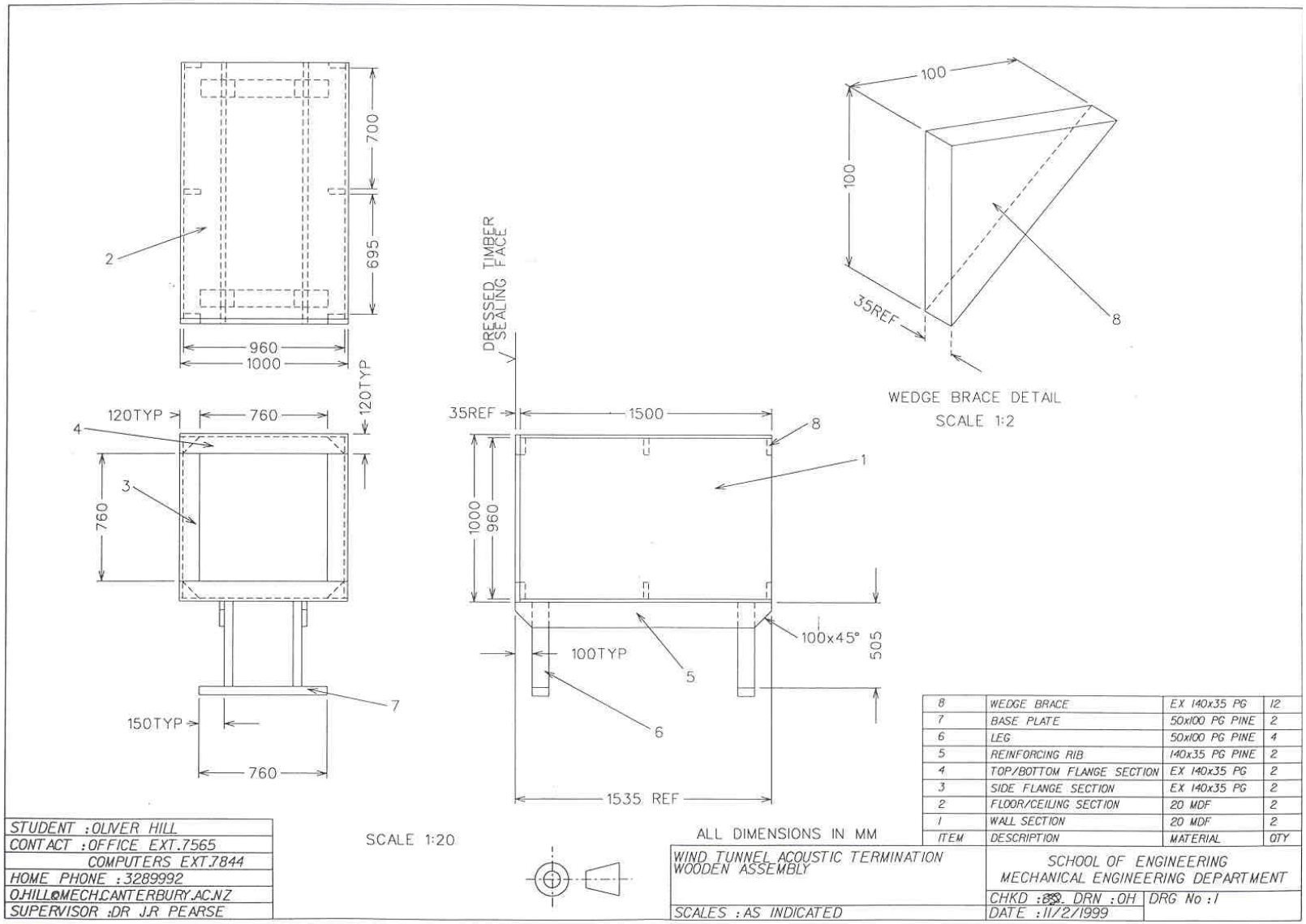

ITEM	DESCRIPTION	MATERIAL	QTY
8	WEDGE BRACE	EX 140x35 PG	12
7	BASE PLATE	50x100 PG PINE	2
6	LEG	50x100 PG PINE	4
5	REINFORCING RIB	140x35 PG PINE	2
4	TOP/BOTTOM FLANGE SECTION	EX 140x35 PG	2
3	SIDE FLANGE SECTION	EX 140x35 PG	2
2	FLOOR/CEILING SECTION	20 MDF	2
1	WALL SECTION	20 MDF	2

Figure 3-10 The acoustic termination.

3.7 Performance of Termination

To see whether the signal to noise level of the wind tunnel was low enough, the A-bar was placed in the working section, halfway down its length with a microphone positioned in the typical experimental configuration. The microphone was mounted in a transverse boom microphone holder with an aerodynamic nosecone just behind the rack below the wake. See fig 3.11. The transverse boom was constructed from a slender aerodynamic aluminum extrusion that was filled with fibre glass and polyester resin. A slot was milled into the boom for the placement of the microphone cable.

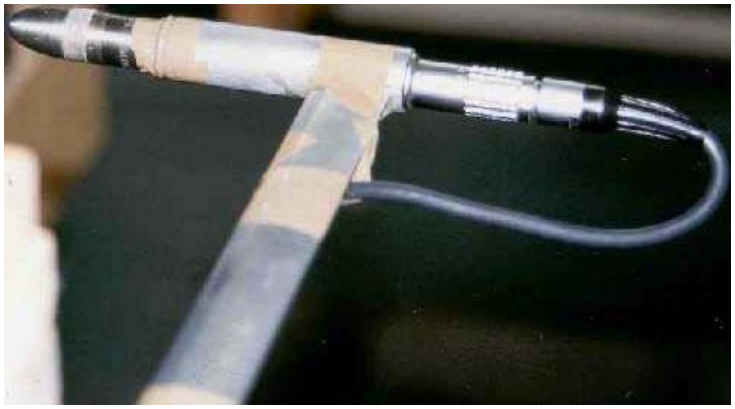

Figure 3-11 Microphone on transverse boom with aerodynamic nosecone.

The tunnel was run at the test speed of $30mm_{H2O}$ and sound spectrum measurements were taken. Although it was clear that the noise level increased with the presence of the roof rack, the tonal peak could not be identified in the spectrum. It was also very difficult to hear the tone with the ear, the presence of the walls of the working section prevented the transmission of the sound.

It was decided that for the SPL tests a different configuration would be run: The roof rack would be mounted on test mounts at the end of the acoustic termination in the free jet. The working section would be removed and the acoustic termination attached to the end of the contraction. It was assumed that the velocity profile of the jet was undeveloped and uniform owing to the short length of the acoustic termination and the close proximity of the roof rack to the exit (135mm to leading edge), reducing the effect of jet entrainment. (See fig 3.12) In this configuration the tone was very audible. The noise in the wind tunnel laboratory would however, need further reduction for the tone to be seen clearly on the sound level meter spectrum.

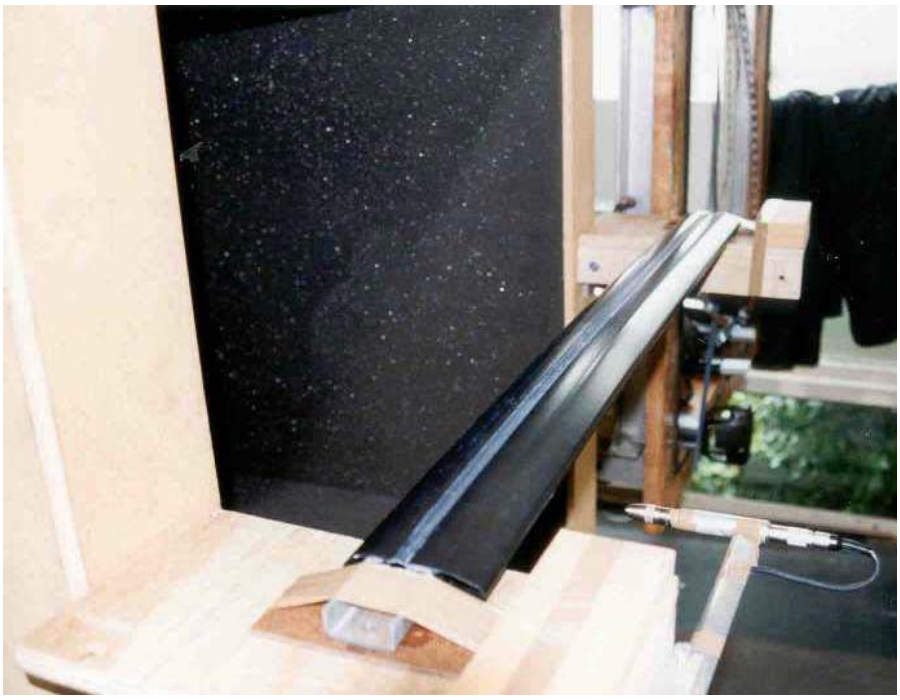

Figure 3-12 Final test configuration.

3.7.1 Grill Sealing and Intake Lining

The 4433 Intensity Analyser was used to find the loudest source in relation to the wind tunnel exit. The probe was held near the exit, external to the airflow with the tunnel operating at test velocity. It was rotated until the energy flow indicator was at maximum deflection and the display showed the highest intensity. The loudest source was clearly the intake area on ground floor.
The first treatment to combat this was to seal the grill with sound absorbent panels. Initially these were 25mm thick fibreglass absorbers framed in aluminum, but due to the nature of these to deteriorate and release dangerous fibres, were soon changed. The fibreglass panels were replaced with 10mm gib-board panels with 50mm polyester foam adhered to each side. See fig 3.13 An area next to the windows was also sealed up to prevent transmission of noise up to the mezzanine floor.

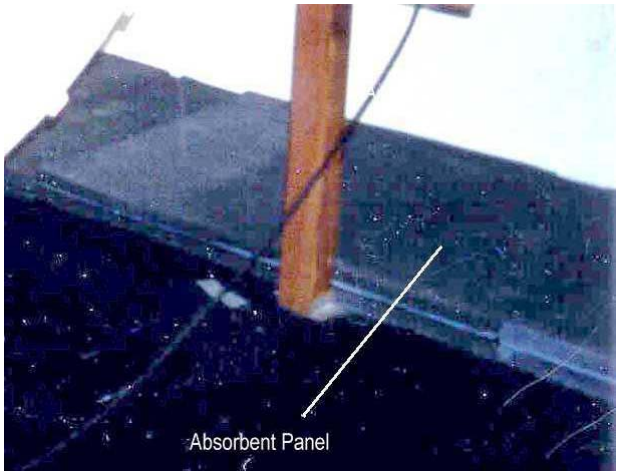

Figure 3-13 Grill sealing absorbent panels.

Secondly, the wind tunnel intake area was lined with the same 50mm absorbent foam. The walls were framed with 25mm square timber and the foam adhered to this. Having the air gap behind the foam gave better sound absorption.[20] The exterior of the intake itself was also lined with absorbent foam.

3.7.2 End Wall Lining and Placement of Jet Deflector

As previously, the 4433 Intensity Analyser was used to scan the area around the wind tunnel exit. This time it was noted that the moving air from the jet was buffeting the flexible end wall, this produced high levels of noise. Initially, the wall was lined with absorbent foam and although this removed some of the sound, it did not prevent the buffeting. A free jet is an unstable fluid motion and at high Reynolds numbers, because of the viscosity in the shear layers, turbulence leading to buffeting is induced in the downstream flow.

Closer to the exit the air motion is less oscillatory. It was decided the placement of an acoustic jet deflector in between the end wall and the jet exit, prior to the onset of major oscillation in the airstream, would prevent the emission of the buffeting noise. A deflector[21] was constructed with timber framing and ribbing skinned with 3mm MDF sheet. The dimensions of the deflector were 1.7m high by 2.1m wide with a 1.2m radius curve. The sheet was overlaid with 50mm polyester foam to prevent acoustic reflections. The deflector was given an inflection at the upstream end to prevent impingement of the airstream on its leading edge. See fig. 3.14. The deflector directed the airflow up towards the ceiling of the building, preventing turbulent gusting in the test area. This gave a more controlled environment.

Figure 3-14 Acoustic jet deflector.

3.7.3 Fan Unit Lining and Leak Sealing

Once again, the wind tunnel area was scanned with the 4433. It was determined that the region near the fan unit was emitting high levels of noise. The intensity probe was moved along the tunnel wall in the local area around the fan unit. It was determined that the strongest emissions were coming from the regions surrounding the impellers.
The fan unit had three linings applied to it, 2 layers of 25mm sound absorbent foam material and a mass loaded barrier product, designed to prevent the transmission of sound.
To monitor the effectiveness of the treatment, three positions along the fan unit were chosen and the intensity level of each one was measured with the 4433 in between lining applications. Figure 3.15 shows

[20] Ref Parkinson, J. P. *Acoustic Absorber Design.*
[21] Drawings in Appendix E

the approximate positions. The windshield of the probe was held against the housing and pointed radially into the tunnel.

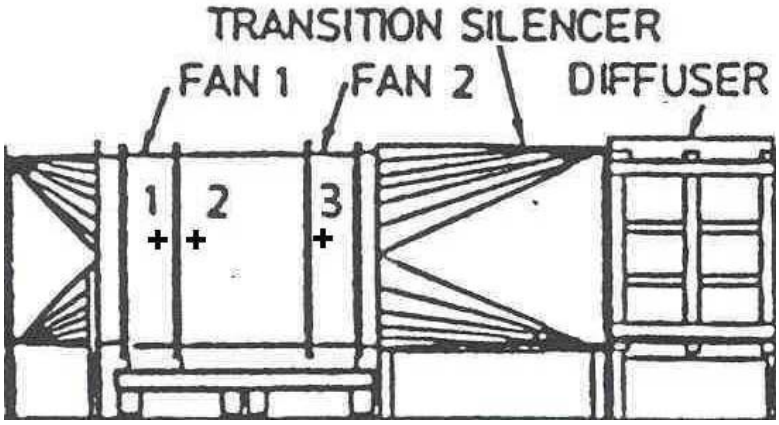

Figure 3-15 Positions of SPL measurements.

The intensity levels varied as follows…

	Position 1	Position 2	Position 3
Untreated	77.8 dBA	78 dBA	76 dBA
After 1st foam layer	69.9 dBA	68.3 dBA	71 dBA
After 2nd foam layer	63.5 dBA	61.4 dBA	66.6 dBA
After sound blanket	60 dBA	61.7 dBA	58.3 dBA

Absorber foam was also applied to the walls, base and ceiling of the 1st diffuser and the square to round transition upstream of the fan unit. Sealant was inserted into any gaps that were present between the flanges of sections and taped over. This prevented the production of noise from air leaks.

3.8 Noise Reductions from Treatment

The sound spectrum of the tunnel was measured between each treatment. These tests were performed in two positions with the 2260 outside the air stream. The microphone was mounted in the default position on the 2260 with a windshield in place. The positions are shown in figure 3.16. Position 1 was relevant only for the first test, prior to the placement of the acoustic termination. In subsequent tests, only position 2 was used.

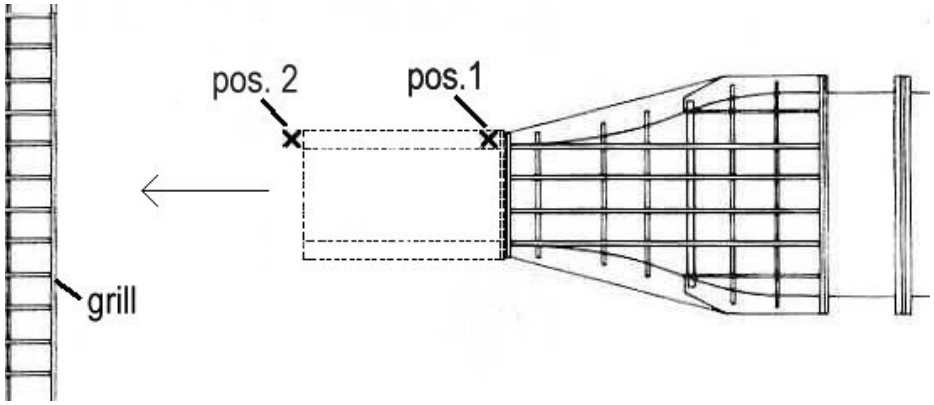

Figure 3-16 Test positions for monitoring of noise treatment.

Each treatment changed the sound spectrum in a different way, but each time there was a decrease in the OASPL. Each of the treatments seemed to reduce different frequencies of the spectrum. Figure 3.17 shows the development of the sound spectrum at the test velocity of 22.2m/s[22]. The measurements taken at

[22] Sound spectrums at the minimum velocity in Appendix F

position 2 between each stage of work will be compared with the initial measurement at position 1. During the initial measurement at position 2, the airflow from the jet was impinging on the microphone and there was much psuedo sound. This can account for the high sound pressure levels in the lower half of the spectrum.

The Acoustic Termination (Position 2).

The main effect that the acoustic termination had was the reduction in high frequency sound. There was a dramatic decrease in sound from 2.5kHz upward. The points where the curve was higher than that of the initial measurement at position 1 can be explained by the presence of the grill, as explained earlier, a strong noise source. The overall sound pressure level decreased from 79.3 to 77.3 dBA

The Sealing of the Grill with Fibreglass Absorbers (Position 2)

This modification was most effective in the mid-range of the sound spectrum from 400Hz to 3.15kHz. It was especially valuable in removing the dramatic peak at 800Hz, likely to be caused by the presence of a tone. As a result, the OASPL dropped from 77.3 to 72.9 dBA.

Replacement of the Fibreglass with Foam and Lining of the Intake Area (Position 2)
These spectrums mapped each other almost identically everywhere on the spectrum except in the low frequency range from 31.5 to 80Hz where there was a dramatic drop in SPL. The OASPL decreased from 72.9 to 72.6 dBA.

The Lining of the Fan Unit and Addition of Acoustic Jet Deflector (Position 2)
This was effective in abating the noise in the mid range from 315Hz to 3.15kHz. The peak that had persisted at 315Hz was almost eliminated. The OASPL decreased from 72.6 to 69.6 dBA
The total noise abatement work reduced the OASPL by almost 10 dB from 79.3 dBA to 69.6 dBA

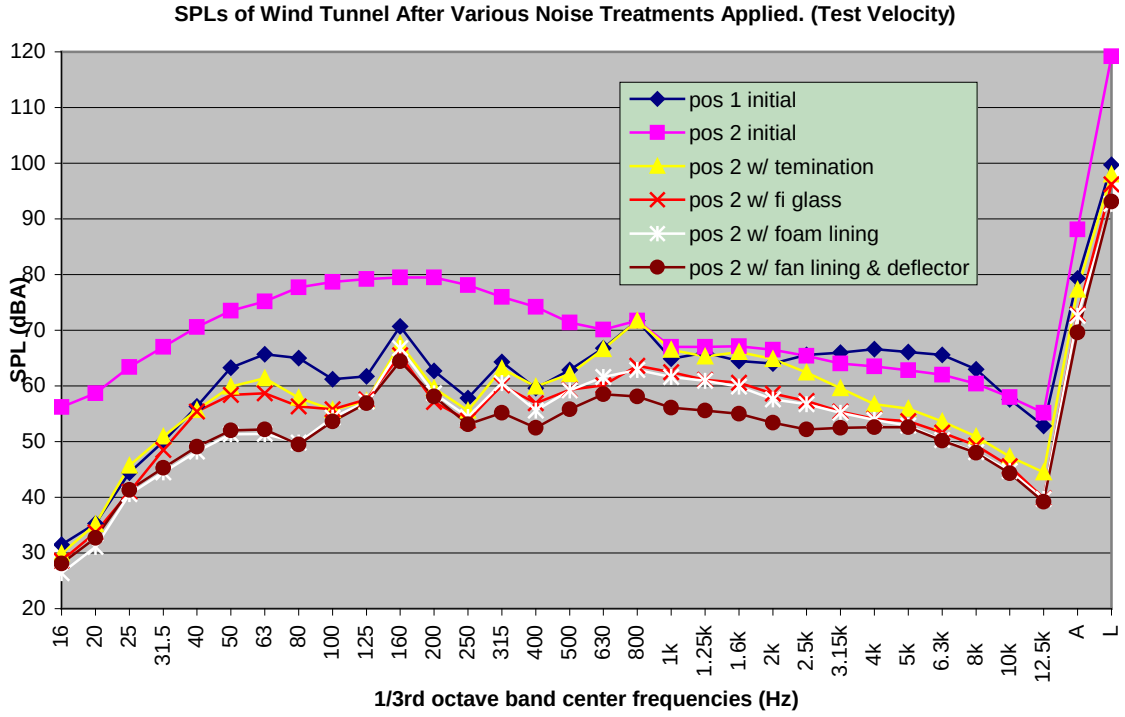

Figure 3-17 Evolution of Sound Spectrum with each treatment.

3.8.1 Signal to Noise Ratio

The improvement in the wind tunnel's OASPL was significant but more important was the increase in signal to noise ratio. This was due to the large abatement of noise in the region of the spectrum around the 500Hz 1/3 octave band. The SNR increased in this band from 0.91 to a final value of 1.04[23]. This was an ideal result, the SNR increase to above unity would enable the sound level meter to detect the signal.

3.9 New Description/Arrangement

The wind tunnel configuration is as before with only minor changes. (See fig. 3.18) These are as follows…

xvi) Contraction to 0.76m square cross-section. (As before)
xvii) Acoustic termination with test mounts.
xviii) Acoustic jet deflector

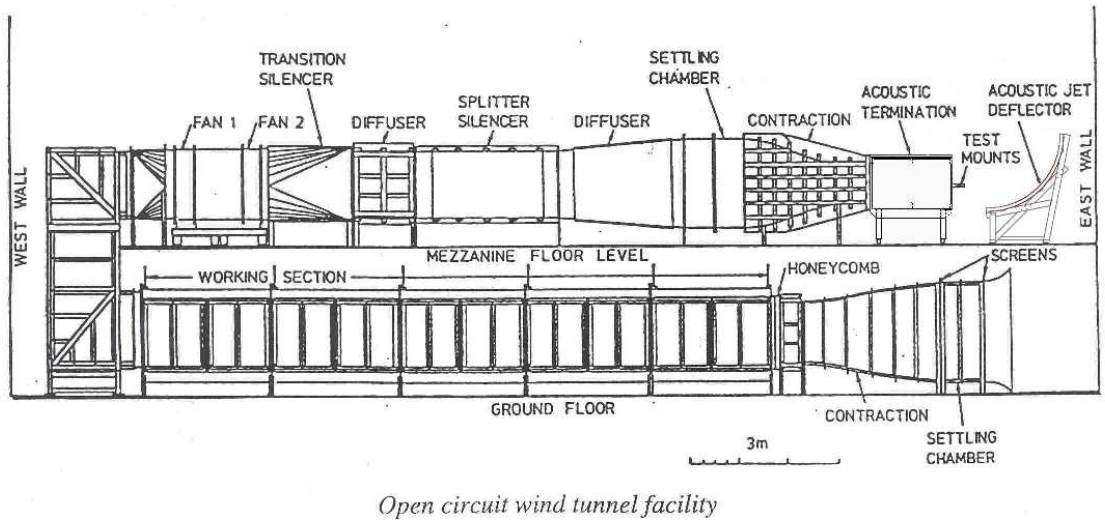

Figure 3-18 The final configuration of the tunnel

[23] Calculation of Signal to Noise Ratio in Appendix B

Chapter 4

INVESTIGATION OF THE NOISE EMISSION OF THE ROOF RACK AND THE IDENTIFICATION OF THE RESPONSIBLE MECHANISMS

4.1 Introduction to Chapter

In this, the first part of the experimental program, the noise emission of the A-bar was analysed in detail through a series of field and laboratory experiments. There are two clearly defined parts in this chapter: 1) the identification of the noise spectrum of the A-bar and comparison with competitor's roof racks and 2) the identification of the mechanisms in the flow responsible for the noise emissions. In this chapter, the issue of whether or not the presence of the car roof affects the flow over the rack and subsequent noise production is addressed. Full-scale roof rack specimens were used in all experiments. Most experiments were carried out at a test speed of 80km/h (22.2m/s). It was established in preliminary field tests that from this speed upward, the telltale roof rack noise was easily distinguished.

4.2 Description of Instruments

The following instruments were used in the experiments described in this chapter:

1. Sound Spectrum Measurement Equipment. This included

a) The Bruel & Kjaer 2260 Investigator sound level meter was used with the microphone mounted on the transverse boom with an aerodynamic nosecone. This is described in detail in chapter 3.

b) A Hung Chang Oscilloscope Model no. OS-620. (See fig 4.1a)

c) A 486 33MHz PC with a 16 channel 200kHz data capture card. (See fig 4.1a)

2. A Metrix GX245 Function Generator and Frequency Meter with small paper diaphragm speaker for the production of pure tones. (See fig 4.1b)

3. The 6mm round nose Pitot tube and Betz water manometer Model AVA were used, as described in chapter 3. (See fig 4.1c & d)

4. A Cole Parmer Temperature and Humidity Meter Model No. 37000-00 with Relative Humidity and Temperature Probe Model No. 37000-50. This was used to determine the temperature and relative humidity of the airstream. This gave accurate measurements of temperature to ±0.1°C and relative humidity to ±0.1%. (See fig 4.1e)

5. Digital and Mercury Thermometers. Measurements were accurate to ±0.1° and ±1° respectively. (Fig 4.1f shows digital thermometer)

6. Mercury Barometer. Measurements were accurate to $\pm 1 mm_{Hg}$.

7. A 70mm cotton fibre tuft wand. (See fig 4.1h)

8. Indicator paint –TiO_2 powder suspended in vitrea 32 mineral oil (or automatic transmission oil) with oleic acid used as an emulsifier.

9. A Sage Action Inc. Model 5 Twin-Vortex Bubble generator was used to produce neutral buoyancy helium bubbles. (See fig 4.1i)

10. Digital image capture equipment. This included:

a) Kodak Megaplus Camera

b) PII 450MHz PC with Megaplus Interface Card

c) ILC Technology Xenon Arc Lamp model LX 300-F & power supply model PS 300-1 (See fig 4.1g)

11. Hotwire Anemometry. This included:

a) A TSI Monitor and Power Supply Unit Model Nos. 1051-2, 1054B and 1056.

b) DISA probes type 55 P14 (See fig 4.1j)

c) A TSI Calibrator Model no. 1125.

d) A 2-D manual traverser

e) 486 33MHz PC with Data Capture Card

12. Frequency excitation equipment. This included:

a) A BWD electronics' minilab model 603A function generator with small paper diaphragm speaker.

b) An Advance Vibrator type VI, driven by Advance frequency generator type J mod.2.

c) A Topward digital function generator 8112 with frequency measurement.

13. Natural Frequency Measurement equipment. This included:

a) Bruel and Kjaer accelerometer models 4335 and 4344

b) Systel AC3 Dual charge amplifier and integrator

c) A Yokogawa DL1540 digital oscilloscope with fast Fourier transform function.

Figure 4-1 Equipment used in experiments.

4.3 Detailed Description of A-bar

In general, a roof rack consists of a cross bar with end pieces designed for the attachment to vehicle roofs. The A-bar conforms to this basic configuration.

The A-bar is an aerodynamic design, based on the Clark Y aerofoil, thus it has a camber and a high thickness to chord ratio. This last feature is important for a roof rack application as it gives increased load carrying strength. The strength of the crossbar comes from a formed galvanised steel member that is inserted into the extruded plastic aerodynamic shroud. There is a slot in the middle of the upper surface for the attachment of accessories, an extruded elastomer infill seals this when not in use. The dimensions of the A-bar are as follows: chord length 80mm and maximum thickness 27mm.

Figure 4.2 shows various details of the A-bar: a) cross bar in detail showing the steel member, b) A-bar test specimen with test mounts, c) mounting of cross bar to end piece, d) end view of end piece, e) front view of end piece, f) cross sectional detail of cross bar showing plastic extrusion, steel member and elastomer infill, g) detail of test specimen foot mount.

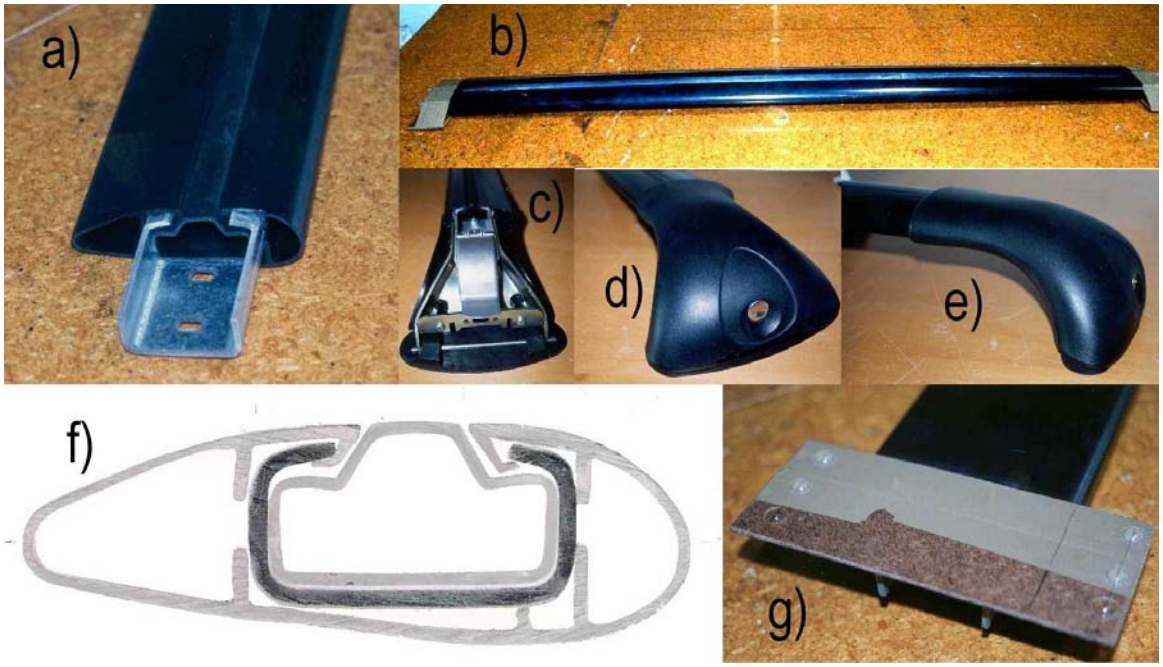

Figure 4-2 Various details of the A-bar.

4.4 Sound Spectrum Analysis

The following experiments were used to determine the sound spectrum emitted from the A-bar and competitors' racks.

4.4.1 Laboratory Sound Spectrum Tests

Method

In these tests the roof rack under investigation was mounted on the test mounts at the end of the acoustic termination of the wind tunnel. The leading edge of the roof rack was positioned 135mm back from the jet exit.

The 2260 investigator sound level meter was used for the measurement of the sound spectrum. The microphone was mounted behind the roof rack, 151mm below the underside of the roof rack in the transverse boom microphone holder with an aerodynamic nose cone fitted. The leading edge of the nosecone was positioned 95mm behind the leading edge of the rack. The transverse boom extended 150mm from the edge of the tunnel.

It was important for the microphone to be located as close to the noise source as possible because of the low signal to noise ratio, in this position the microphone would be completely submerged in the sound field of interest and yet have minimal effect on the flow field around the roof rack. An external microphone was conceived to be too far from the source of noise.

Plastic tape was used to secure the microphone in the microphone holder and cover any sharp edges or transitions that existed in the boom arrangement. The test of the sound spectrum of one roof rack consisted of two measurements with the roof rack in place and four measurements of the empty tunnel. The empty tunnel tests were done both before and after the roof rack tests to eliminate the possibility of anomalous readings. The tests were 10s unweighted L_{Leq} tests.

In order to obtain a narrow band sound spectrum, the AC output from the 2260 was fed into the PC via its data capture card. The signal was sampled at 20kHz for 3.6s. This data was processed in Matlab, a fast Fourier transform (FFT) function was used to obtain power spectra revealing the dominant frequencies present in the sound field. The AC signal was also fed concurrently into the Hung Chang oscilloscope, this gave a quick visual indication of the signal level.

The Metrix function generator and speaker were used for the identification of roof rack tones. The frequency from the signal generator could be changed very slightly by careful adjustment of the controls. Correlation between the generated tone and the tone produced by the roof rack could be accurately identified by the author through listening for the presence of beats. The beats would become slower as the frequency of the generated tone converged with that of the roof rack.

The airspeed was measured using the pitot tube and manometer. The Cole Parmer probe was mounted on a clamp stand and submerged in the free jet for the measurement of the relative humidity and temperature of the air stream. The atmospheric pressure was also recorded in between each test.

In order to mount each roof rack at the same height relative to the microphone, wooden spacer blocks were employed.

These tests were carried out at times when the laboratory ambient noise levels were low.

Results

There were three types of results achieved from the laboratory tests, these were:

a. 1/3rd Octave Band Sound Spectrum.

This result was produced by removing the base sound spectrum of the empty wind tunnel from the roof rack sound spectrum[1], this then had an A-weighting applied to it. Peak frequency bands were evident in this result.

b. Narrow Band Sound Spectrum.

This was useful for pinpointing the exact frequencies of the dominant tones (the previous result revealed only frequency bands). Background noise could not be removed from this result of this test and so distinction between those tones produced by the roof rack and those generated by other sources could not be made based on the narrow band sound spectrum test alone.

c. Peak Frequency.

This was a subjective result, gained with the function generator and speaker and the author's ear. If there were two dominant frequencies, it was often hard to determine them both. Usually however, this was a very accurate method.

[1] This process is described in Appendix C

4.4.2 Preliminary A-bar Test

To establish the sound spectrum of the A-bar, it was tested as described. The assumption was made that the noise was being emitted from the cross bar and not the end pieces. This assumption was based on subjective tests in which the A-bar end pieces were held in the free jet while listening for tones. It was also assumed at this stage that the car roof did not affect the flow around the roof rack and thus the roof rack would produce the same sound spectrum with no roof present. This was yet to be confirmed. (see sections 4.5.1.1 and 4.5.1.2)

The A-bar results were as follows:

- 1/3rd Octave Band Sound Spectrum (See fig 4.3)

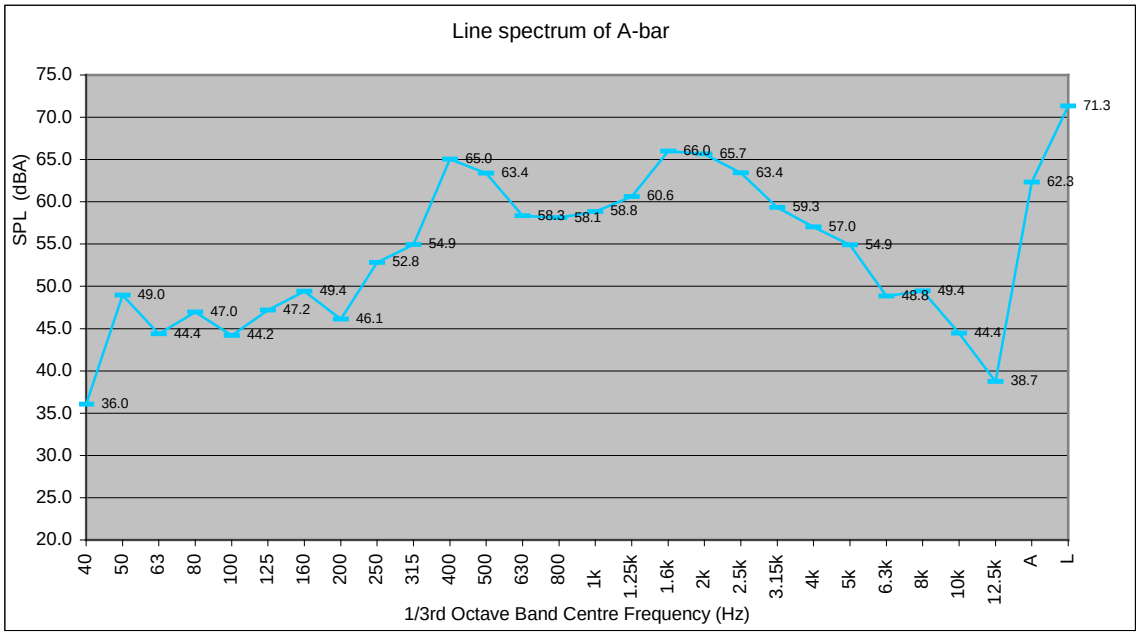

Figure 4-3 A-bar 1/3rd octave band sound spectrum.

The A-bar sound spectrum showed two dominant peaks, one in the 400Hz 1/3rd octave band and another in 1.6kHz 1/3rd octave band. The 400Hz peak corresponds to the peak noticed in preliminary field tests at Ruapuna described in chapters 1 and 3. The overall sound pressure level (OASPL) was 62.3dBA.

- Narrow Band Sound Spectrum. (See fig 4.4)

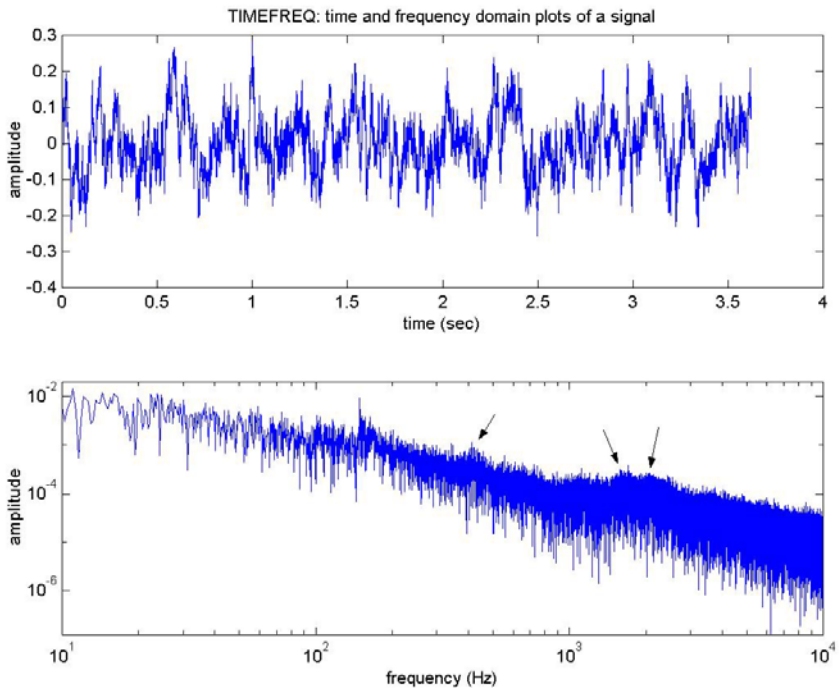

Figure 4-4 The time and frequency domain plots of emitted A-bar sound.

Unlike the 1/3rd octave band sound spectrum, the narrow band sound spectrum (the second figure) was not A-weighted. This is why the overall shape differs between the two. The peak experienced at around 160Hz is the blade passing frequency of the wind tunnel fans and so was ignored. The three arrows point to the peaks of interest. The first peak around 410Hz was pronounced but showed some scatter, the second, around 1.6kHz was less prominent and the third, around 2.1kHz was flatter than the previous two but was not to be ignored. These frequencies lay in the 400Hz, 1.6kHz and 2kHz 1/3rd octave bands respectively. This was very consistent with the1/3rd octave band sound spectrum.

- Peak Frequency.

In these subjective tests, the author detected two dominant frequencies, as in the 1/3rd octave band spectrum, these were: 443Hz and 2.3kHz. These lie in the 400Hz and 2.5kHz 1/3rd octave bands respectively.

4.4.3 Benchmark Testing

In these tests, competitor racks were tested in the same configuration to the A-bar to establish the relative loudnesses and give clues as to what features are likely to cause the generation of tones. The roof racks were placed the same distance away from the jet exit. As with the A-bar, the microphone was mounted behind the roof rack, 151mm below the underside of the roof rack on the transverse boom. The leading edge of the nosecone was positioned 95mm behind the leading edge of the rack.

Description of Competitor Racks

Figure 4.5 shows the competitor roof racks.

a) Hubco Standard 30mm by 20mm Bar.

A Standard configuration, produced by many manufacturers, this bar has a rectangular cross section with rounded edges.

b) Nomadic Glider Bar.

This has an asymmetric aerofoil profile with a sharp trailing edge, it has a rubber seal on its top surface that is removed for the installation of accessories. The cross bar is a aluminium extrusion.

c) Sportrack Jeep Bar.

This is a roll formed sheet steel rack, it has a slim symmetrical aerofoil-like profile.

d) Mondial Rack.

This has an approximately rectangular cross section. It is constructed from aluminium extrusions with an elastomer insert in the top surface.

e) RAK Bar.

This is an aluminium extrusion of asymmetric aerofoil profile, similar to the Glider bar, this has a rubber seal which is removed for the placement of accessories.

f) Rola Bar.

This is an aluminium extrusion of ellipsoidal shape, it has an elastomer insert in the top surface.

g) S-bar.

This is a Hubco roof rack, based on the standard 30mm by 20mm crossbar. It has an aerodynamic sleeve that is removed for the fitting of accessories. When the sleeve is in place the profile resembles a symmetric aerofoil.

h) Sportrack St-St Bar.

This is a roll formed sheet stainless steel rack. It has a similar profile to the Sportrack Jeep Bar but with a rubber insert in the upper surface.

i) Wellington Bar.

This is based on the standard 30mm by 20mm crossbar, it has diagonal slices cut out of the leading edge designed to induce spanwise motion in the airflow over its surface.

Figure 4-5 The competitor roof racks.

The results for the benchmark testing were as follows:

- 1/3rd Octave Band Sound Spectrums (See fig 4.6)

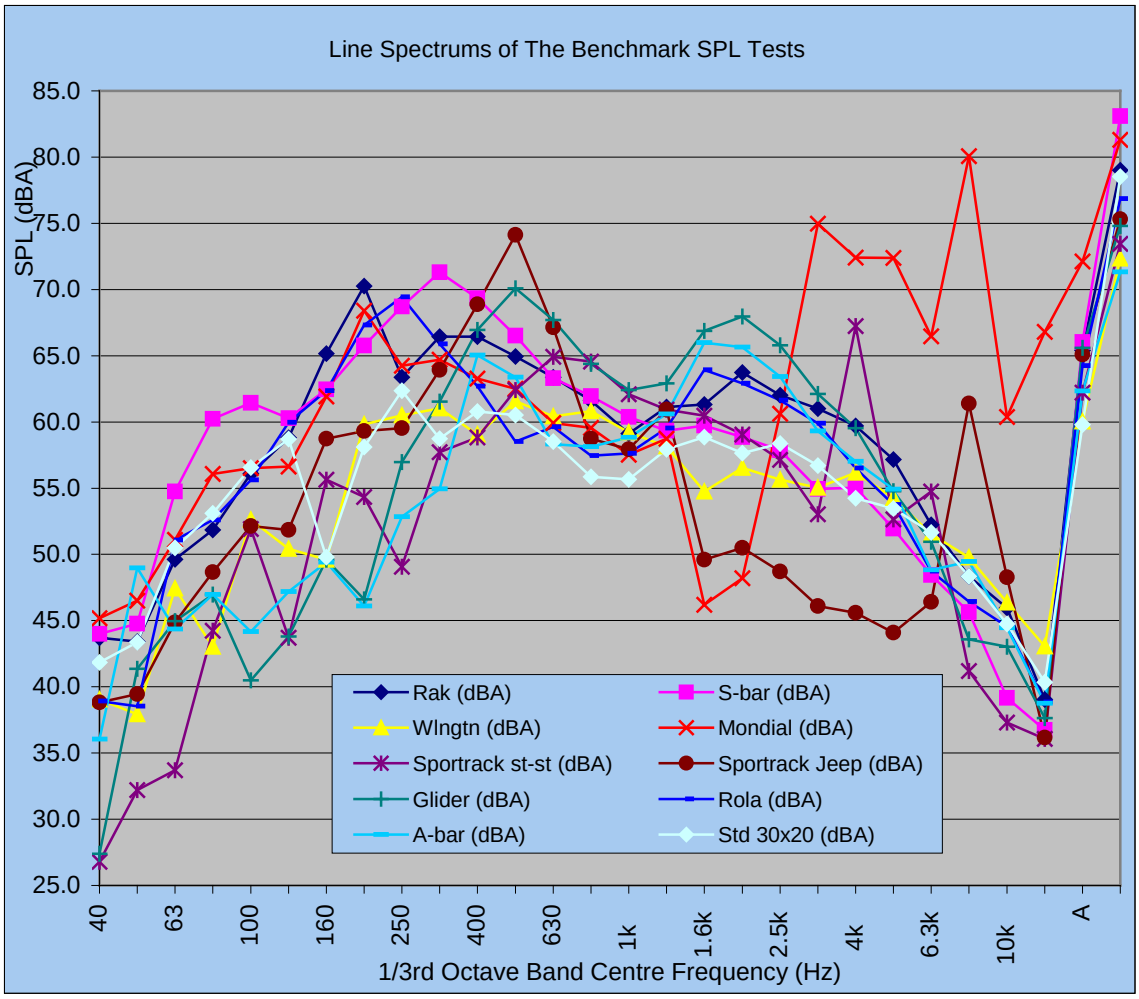

Figure 4-6 Line spectrums of the 1/3rd octave SPL benchmark tests.

As figure 4.6 shows, each of the racks displayed peaks in different bands of the spectrum. There are two separate ranges in which the peaks occur, 1) from 200Hz to 630Hz and 2) from 1.6kHz to 8kHz. If the peaks in the first range are examined, the trend of increasing frequency follows:

i. Rak at 200Hz
ii. Mondial at 200Hz
iii. Rola at 250Hz
iv. Std 30 x 20 at 250Hz
v. S-bar at 315Hz
vi. A-bar at 400Hz
vii. Glider at 500Hz
viii. Sportrack Jeep at 500Hz
ix. Sportrack St-St at 630Hz

The general trend of the above list is from those racks that have thick profiles towards those with slimmer lines. It is interesting to note that the Rak bar displayed the lowest frequency even though it has an aerofoil shape. These peaks may be caused by vortex shedding as this phenomenon exhibits this type of behaviour. (See chapter 2 section 2.2.2). If this is the case then the diagonal slices in the front edge of the Wellington bar must effect this mechanism as it did not display any prominent frequency. (See chapter 2 section 2.3.2).

The second range of peaks follow less of a trend with some racks displaying multiple peaks. Of particular interest is the Mondial spectrum that shows peaks from 3.15kHz through to 8kHz. Other racks displaying dramatic peaks in this range are the Sportrack Jeep bar and the Sportrack St-St bar. Racks that did not display any peaks in this range were the Standard 30mm by 20mm bar, the S-bar and the Wellington bar. These are all racks that have simple lines and lack fine features. They do not have sharp edges or fine cracks as all of the others do. These peaks are likely to be caused by cavity resonances (as described in chapter 2 section 2.2.3).

The OASPLs of the racks varied as follows:

Mondial	72.1 dBA
S-bar	66.0 dBA
Glider	65.6 dBA
Rak	65.4 dBA
Sportrack Jeep	65.1 dBA
Rola	64.3 dBA
A-bar	62.3 dBA
Sportrack St-St	62.2 dBA
Wlngtn	60.0 dBA
Std 30x20	59.8 dBA

It is important to note however, that because the Wellington bar exhibited no tonal sound, it had the lowest perceived noise level.

- Narrow Band Sound Spectrum.

The narrow band sound spectrum figures showed the same trends as the 1/3rd octave spectrums but displayed peaks at the actual frequencies of the emitted tones. These figures are found in appendix G paired with their respective unprocessed 1/3rd octave band sound spectrums.

- Peak Frequency.

Once again, in the these tests the operator detected many of dominant frequencies displayed in the1/3rd octave band spectrums and the narrow band sound spectrums, they were as follows:

a. Hubco Standard 30mm by 20mm Bar.

A frequency was heard at around 238Hz, this lies in the 250Hz 1/3rd octave band.

b. Nomadic Glider Bar.

A frequency was heard at around 452Hz, this lies in the 500Hz 1/3rd octave band.

c. Sportrack Jeep Bar.

A frequency was heard at around 454Hz, this lies in the 500Hz 1/3rd octave band.

d. Mondial Rack.

A frequency was heard at around 7.2kHz, this lies in the 8kHz 1/3rd octave band.

e. RAK Bar.

A transient frequency was heard at around 3.22kHz, this lies in the 3.15kHz 1/3rd octave band.

f. Rola Bar.

Frequencies were heard at 226Hz and 3.36kHz, these lie in the 250Hz and 3.15kHz 1/3rd octave bands respectively.

g. S-bar.

Frequencies were heard at 279Hz and 375Hz, these lie in the 250Hz and 400Hz 1/3rd octave bands respectively.

h. Sportrack Stainless Bar.

A frequency was heard at around 3.89-4.29kHz, this range lies in the 4kHz 1/3rd octave band.

i. Wellington Bar.

j. No frequencies worth noting were heard. There was however, a great deal of broadband noise produced by this roof rack.

4.4.4 A-bar Noise Emission with Angle of Attack

In these tests, the sound spectrum of the A-bar was measured at various attack angles. This was to establish the effect the incident flow angle has on the noise produced. The A-bar was placed the same distance away from the jet exit but closer to the microphone than in previous tests. The microphone was mounted behind the roof rack, 41mm below the underside of the roof rack on the transverse boom. The leading edge of the nosecone was positioned 95mm behind the leading edge of the rack. The roof rack was moved through 14 discrete angles of attack from 9.9° nose up to 12.6° nose down. The default incidence of the A -bar, the no lift angle, was considered the 0° angle of attack position. In reality, because the A-bar is a cambered aerofoil (that is asymmetric) the no lift angle is slightly nose down, approximately 1°.

- 1/3rd Octave Band Sound Spectrums

These were presented as a 3-D surface to show the development of the spectrum as the angle is varied[2]. (See fig 4.7)

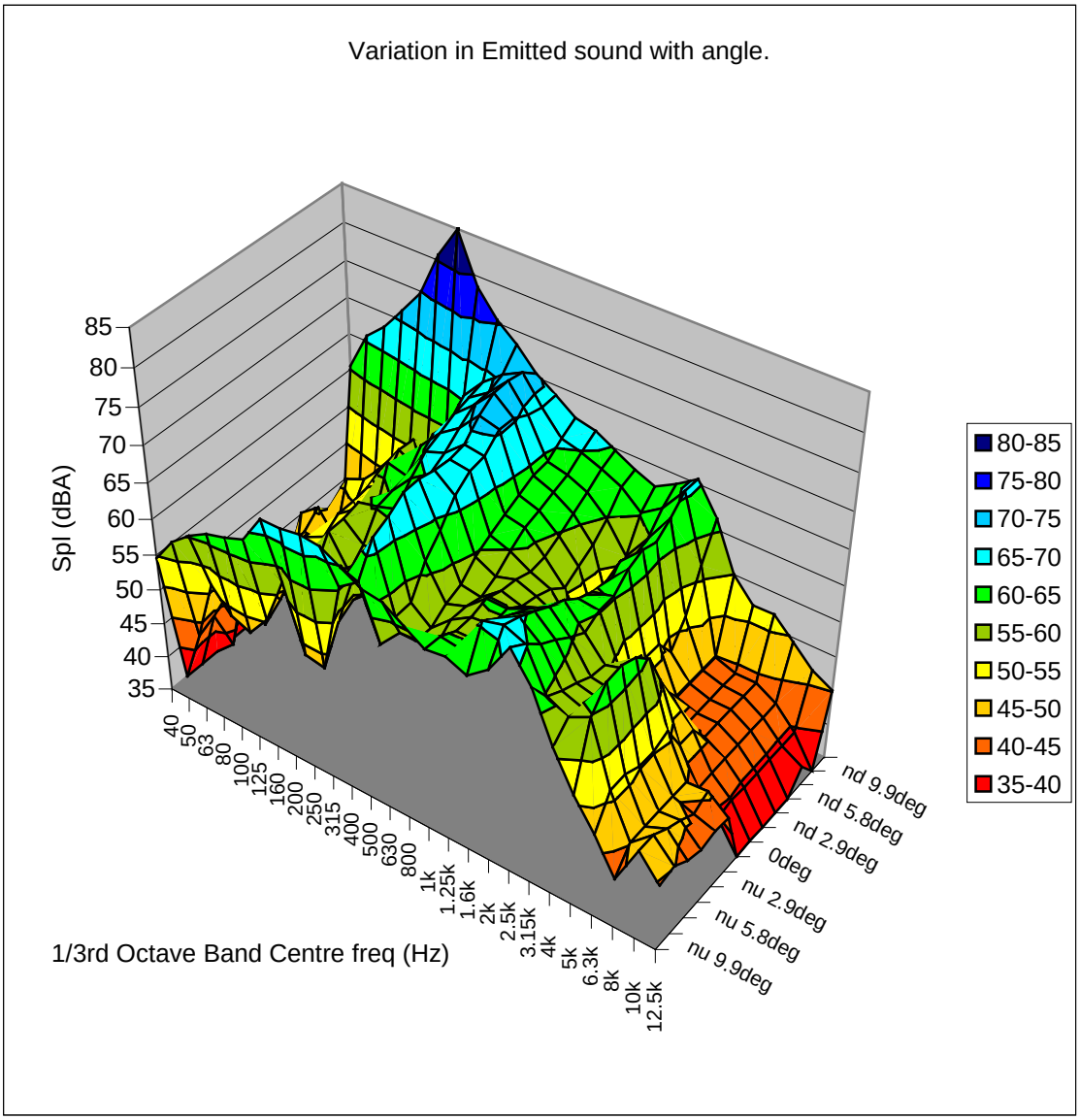

Figure 4-7 Emission of sound at various angles of attack.

There are two ridges that stand out in the figure, these are at 400Hz and 2.5kHz. A small ridge can also be seen in the 5kHz 1/3rd octave band in the range from nose up 2.9˚ to 7.3˚.
Figure 4.8 below shows the development of the two main ridges and the OASPL.

[2] Line spectrums are presented in Appendix G

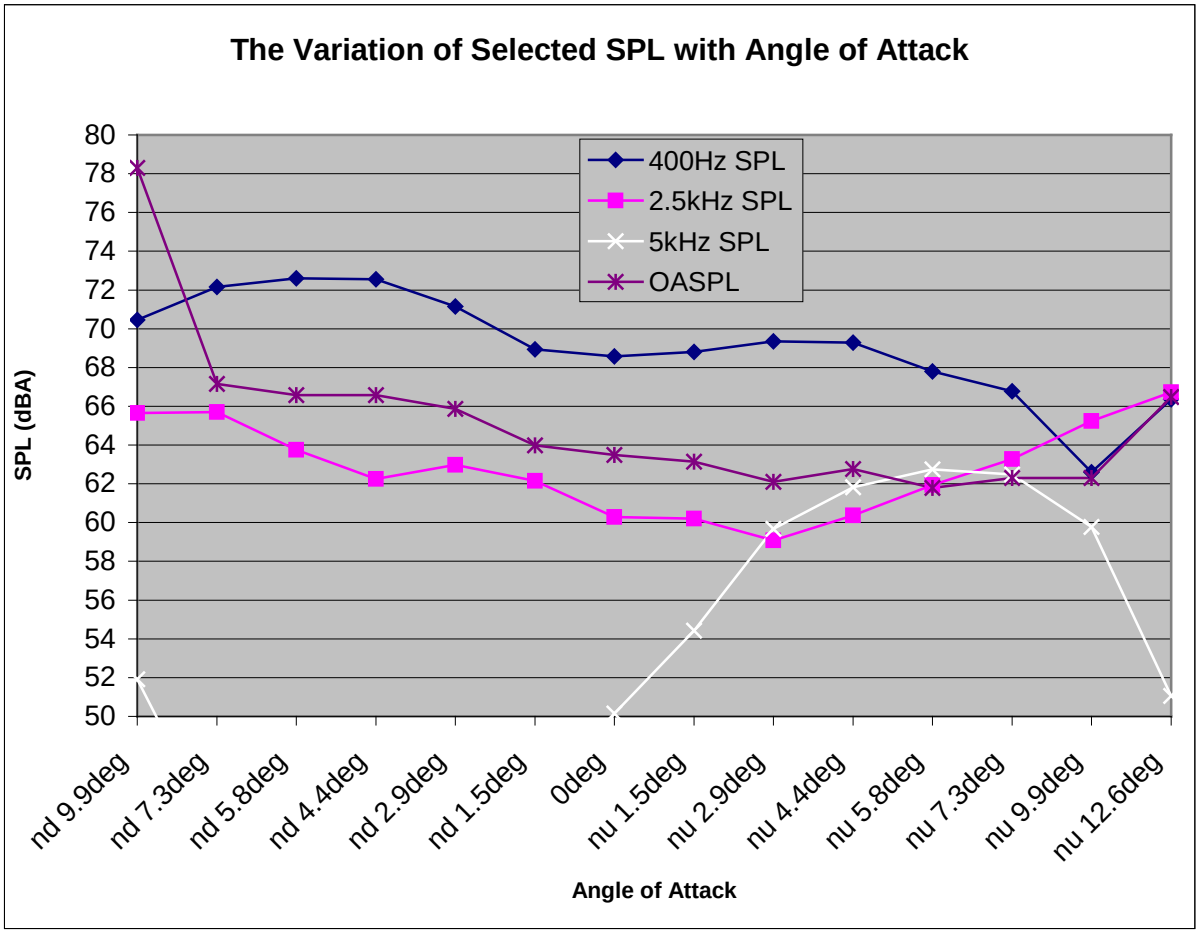

Figure 4-8 The development of the SPL of the A-bar with changing angle of attack.

The 400Hz ridge is dominant, displaying a maximum value at nose down 5.8° and 7.3° of 72.6dBA. At these nose down angles of attack, the peak is broader than at the nose up values where it is sharply defined. At the 0° angle of attack the ridge reaches a local minimum of 68.6dBA.

The 2.5kHz ridge increases with increases in angles of attack be they positive or negative, with maximum values occurring at the graph limits. At nose down 9.9° the maximum value of the 2.5kHz band was 65.7dBA and at nose up 12.6° the maximum value of the 2.5kHz band was 66.7dBA.

At these high angles of attack, the level of broad band noise started to increase considerably, it is likely that the A-bar had reached a stall condition, generating a large wake. This explains the sharp increase in the OASPL at the boundaries of the graph. The maximum OASPL measured was 78.3dBA at nose down 9.9°.

The small ridge at 5kHz is very well defined feature, it did not exist at nose down angles of attack.

- Narrow Band Sound Spectrum.

The narrow band sound spectrum figures can be found in appendix G. They display the same peak frequencies as the 1/3rd octave results and reveal the definition of each. The 400Hz peak is clear in the low nose up and nose down angle becoming more difficult to see in the higher angles of attacks. It is a slightly sharper peak (when visible) in the nose up range.

The 2.5kHz peak is a very broad peak and is visible in all the narrow band sound spectrum figures. It was noted however, that this peak was also present in the ambient (empty tunnel) spectrum measurement and thus this peak may not be caused by the roof rack alone.

The small 5kHz peak shows up very clearly in the range from 2.9° to 9.9° nose up. It is a very sharp peak with no scatter corresponding to a pure tone. This tone was produced by the roof rack because the peak is not present in the ambient spectrum.

- Peak Frequency.

In these tests, the author distinguished frequencies responsible for the 400Hz and 5kHz peaks.
In many cases there were two discrete tones affecting the 400Hz 1/3rd octave band, a dominant one in the range from 409Hz to 427Hz and a slightly lower one in the range from 449Hz to 460Hz. This explains why, in the A-bar sound spectrum, the 500Hz 1/3rd octave band is also prominent. At the higher nose up angles of attack the higher frequency tone was not heard. This type of behaviour in which the emitted frequencies follow a discrete variation is similar to that observed with trailing edge tonal noise as described in chapter 2 (section 2.2.1).
There was a 5kHz tone detected from 2.9to 9.9° nose up. This is consistent with both the 1/3 rd octave band and narrow band sound spectrums.

4.4.5 Field Sound Spectrum Tests

In these experiments, the roof rack was mounted in the usual position on the roof of a test car. The car was accelerated up to a higher test speed of 100km/h (27.8m/s) and held constant while the sound spectrum inside the car was measured with the 2260 Investigator sound level meter. 100km/h was chosen as the test speed as this is a common operational speed. The car used in these was a 1999 Ford Falcon Sedan. The microphone was located at the approximate position of the ear of the front seat passenger. Background noise removal was carried out on this spectrum. Results were as follows:

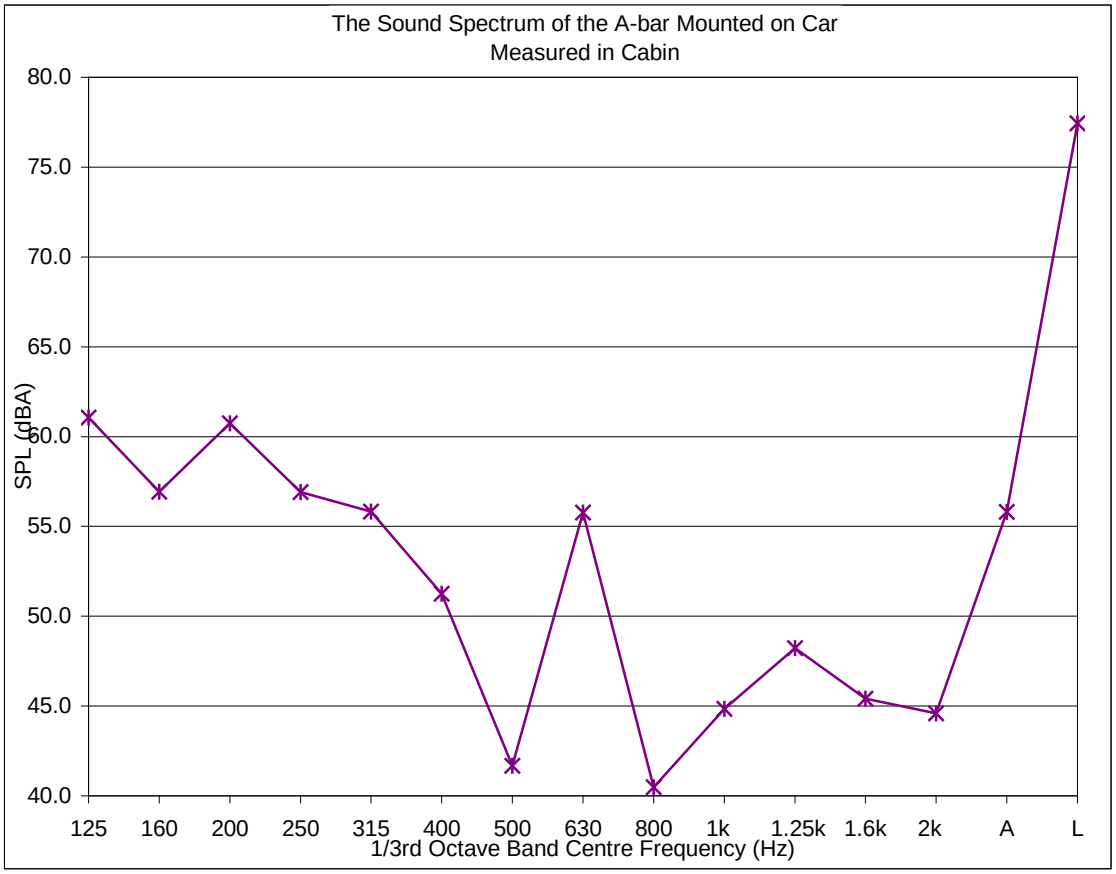

Figure 4-9 The sound spectrum of the A-bar (field test).

The spectrum in figure 4.9 differs considerably from that measured in the lab (fig. 4.3), there is much more noise in the low frequency region it decreases rapidly at the high frequencies, in fact the sound pressure levels of the 1/3rd octave bands above 2kHz were so low that they lay outside the dynamic range of the sound level meter. (Dynamic range for this measurement was 39 – 119dB). The most prominent peak in the spectrum was in the 630Hz band. There was also a peak at the 200Hz band, but due to the broadness of this peak, it is doubtful that it was caused by a tonal sound.
The 630Hz peak is caused by the same mechanism that produced the 400Hz – 500Hz peaks in the laboratory experiments. The increase in the frequency was proportional to the increase in test velocity.
The sound that produced the higher frequency peaks at around 2.5kHz and 5kHz in the laboratory experiments does not appear in the field sound spectrums. This is most likely due to attenuation of the higher frequency sound, by the car roof. For an equivalent sound level, a high frequency sound has less energy than one of low frequency, and according to the mass law, the more easily it is absorbed by transmission through a panel.
To compare the OASPL of the field experiment with that of the laboratory experiment would be inappropriate due to the large differences between the experimental methods. The main difference was the positioning of the microphone, it was not only in a different location with respect to the roof rack but it was also outside of the air stream, removing the effect of pseudo sound.

4.5 Flow Field Analysis

The analysis of the flow field around the A-bar was done using both flow visualisation and hotwire anemometry techniques.

4.5.1 Flow Visualisation

To gain understanding of flow patterns and mechanisms present in the case of a transparent homogeneous fluid, flow visualisation is often used. As the name suggests, it is the art of making invisible flow visible. There were three flow visualisation techniques used in this work: tufting, indicator paint and particle illumination.
Figure 4.10 shows the profile of the A-bar and points that will be referred to in this section.

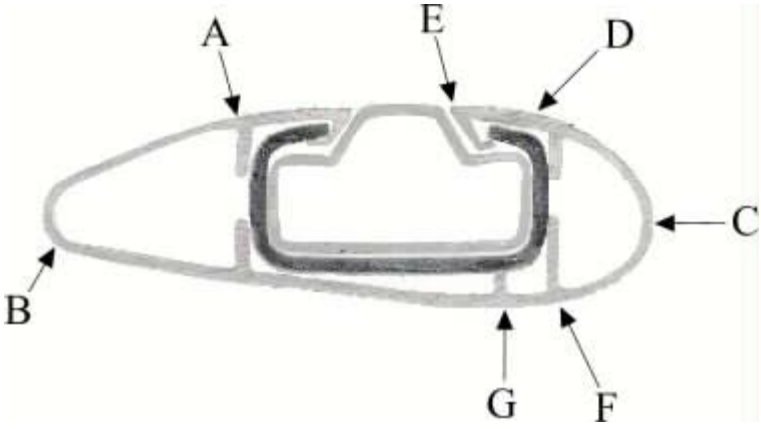

Figure 4-10 A-bar profile and points of relevance.

Tufting Tests

These were carried out both in the laboratory and in the field. The results of these experiments will be presented together.
In these tests, the roof rack was placed in an airflow and a tuft wand moved through the flow around it. By the motion of the tuft, one could determine many properties of the flow, including the local flow directions and the separation regions.
In the laboratory experiment, the roof rack was mounted on the floor of the working section of the wind tunnel. The wind tunnel was operated at a wind speed of 22.2m/s. Areas of interest for this test were:

1) The upper and lower separation points
2) The stagnation point
3) Any unusual air motion

In the field experiment, the roof rack was mounted on the roof of a test car. Once again, the test speed was 22.2m/s (80km/h). The car used was a 1994 Toyota Camry Sedan. Areas of interest were:
1) The angle of the incident flow onto the roof rack.
2) Separation regions over the car roof, particularly in the area around the windscreen to roof transition.
3) Any unusual air motion or motion inconsistent with the lab test.

Results were as follows:
The lab experiments revealed that a flow separation occurred on the top surface where there was a dramatic slope change upstream of the trailing edge, this is point A in figure 4.10. Separation on the lower surface occurred just upstream of the trailing edge, point B. The stagnation point occurred at the leading edge, point C. The flow over the roof rack was 2 dimensional, that is the tuft remained perpendicular to the span.
In the field experiments, it was discovered that flow separation did not occur in any dramatic way at the transition from the car windscreen to the roof. The tuft remained straight, close to the roof surface, implying attached flow. (See fig. 4.11). The shapes of older model cars showing less aerodynamic development may exhibit a separation region.

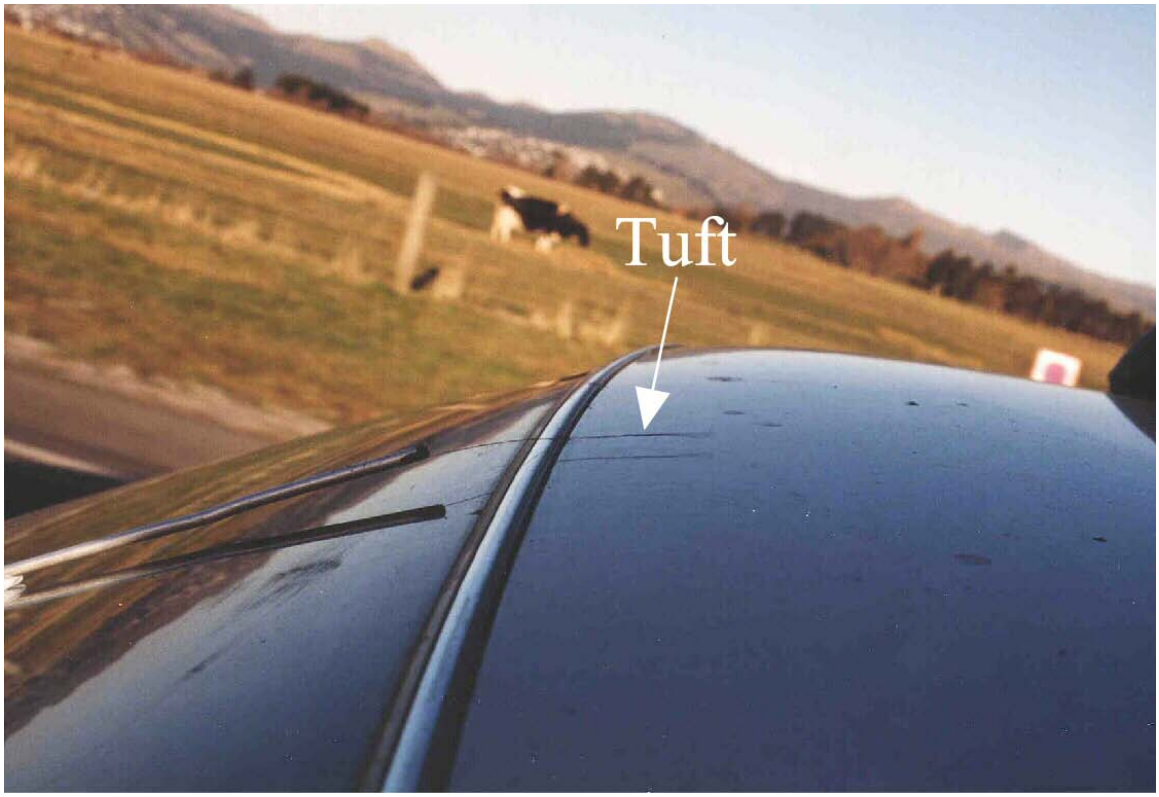

Figure 4-11 Tuft experiment showing the attached flow at the windscreen to roof transition.

In a similar experiment in which the tuft was placed in the flow upstream of the roof rack, it was seen that the incident flow onto the roof rack was parallel to the car roof. (See fig. 4.12) This confirmed the assumption made in section 4.4.2, that the car roof did not affect the flow around the roof rack.

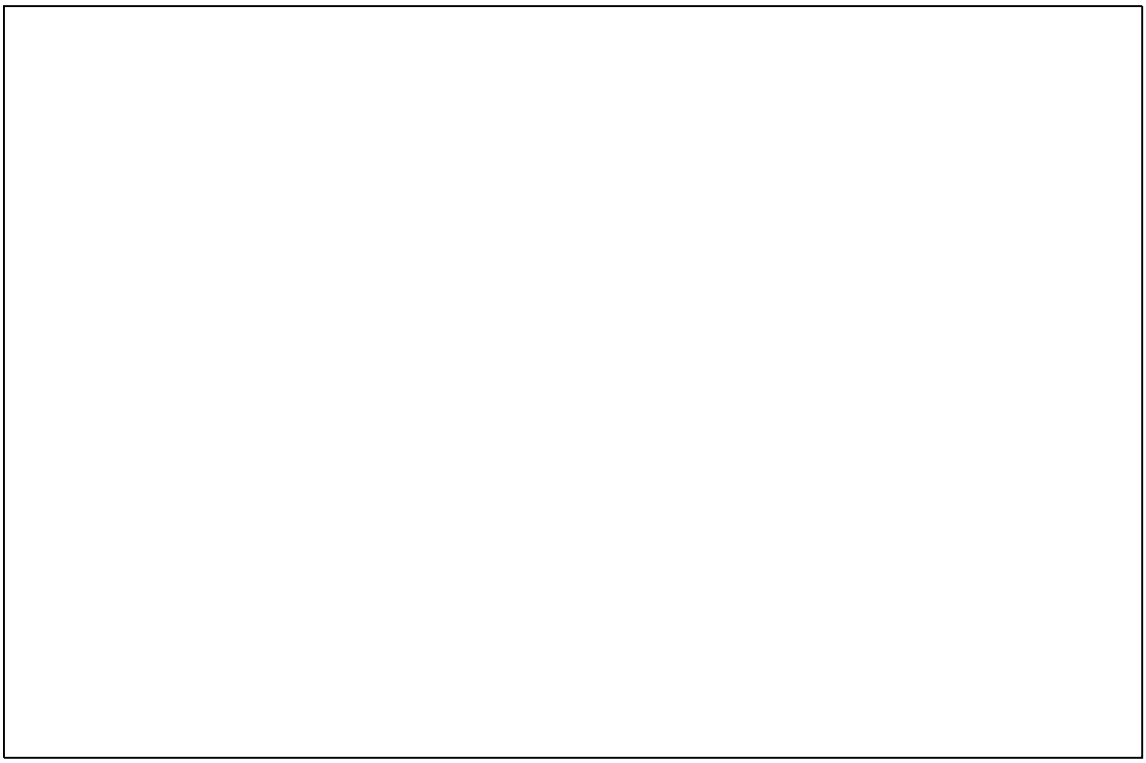

Figure 4-12 Tuft experiment showing the incident flow onto the roof rack.

Indicator Paint Tests

In indicator paint type experiments, the body under investigation is painted with a fluid containing suspended solid particles and exposed to an airflow. This paint is very fluid and affected by air movement, revealing the flow patterns on (or very close to) the surface of the body. The paint pools in separation regions and streaks where the flow is attached. At stagnation points where there is not a lot of air motion, the paint settles.

These tests were performed both in the field and in the laboratory. In the laboratory tests, the A-bar was painted then mounted on the test mounts in the free jet. In the field tests it was mounted on the car roof, painted and then the car accelerated up to test speed.

Figure 4.13 shows three views of the A-bar following the indicator paint test.

Figure 4-13 Top, bottom and front views of the A-bar with indicator paint.

Results were as follows:
The paint appeared to be unmoved at the leading edge (point C in figure 4.10), streaking away from this line. On the top surface, the paint accumulated in a small region around the maximum thickness point, that is, from point D to point E. This also occurred on the under surface between points F and G. Downstream of these regions the paint shows parallel chord-wise streak lines until points A and B on the top and bottom surfaces respectively.
The settling of the indicator paint at the leading edge is due to stagnation, the flow away from this line is attached and likely to be laminar. At points D and F the flow separates. This is a result of the retarding of the flow because of the lower pressure gradient experienced near the maximum thickness point. Reattachment occurs at points E and G due most likely to a laminar to turbulent transition in the shear layer and re-energising of the flow. Separation into the wake finally occurs at points A and B, a result of dramatic changes in the profile angle. The separation region or bubble on the upper surface was approximately 12mm long whereas the separation region on the lower surface was shorter at around 10mm long. The vertical distance between the upper surface separation point (point A) and the lower surface separation point (point B) was 17.8mm.

During the field tests, the indicator paint was painted on the car roof in the region around the transition from the windscreen to the roof in order to detect the presence of a separation bubble. (See fig. 4.14). The only place that the indicator paint pooled was directly behind the windscreen trim for a length of approximately 4mm. Outside of this region streaking of the paint revealed attached flow.

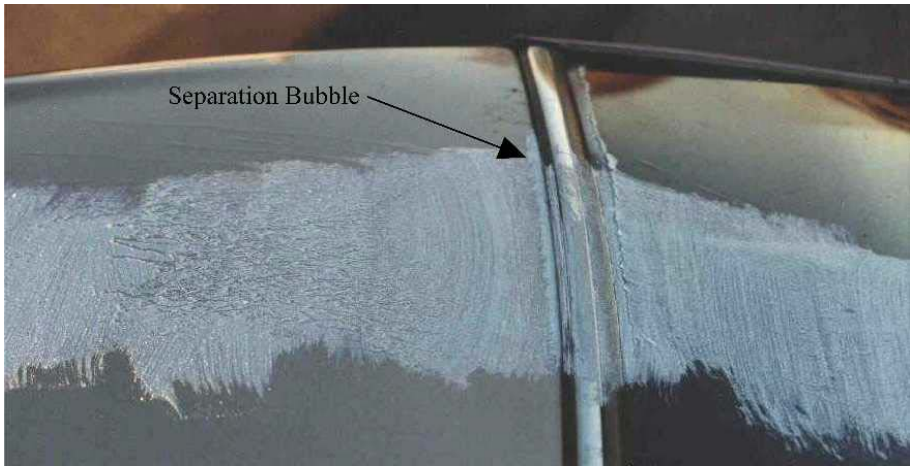

Figure 4-14 The test car roof with indicator paint (brush marks in transverse direction).

Particle illumination

In these tests, neutral buoyancy helium bubbles were released into the airstream upstream of the roof rack. These were generated inside canisters in the bubble generator unit and delivered via a transparent plastic tube to where they were released. They were illuminated with a thin light sheet generated by the Xenon arc lamp and photographed using a high-speed digital camera. The photographs were taken late in the day when the light in the laboratory was diminishing, against a backdrop of black cardboard. Figure 4.15 shows the experimental arrangement. The A-bar was placed inside the wind tunnel working section. The light sheet projected through the working section roof onto the rack's upper surface. The camera was mounted on a tripod outside of the airstream with its aperture pointed toward the illuminated area.

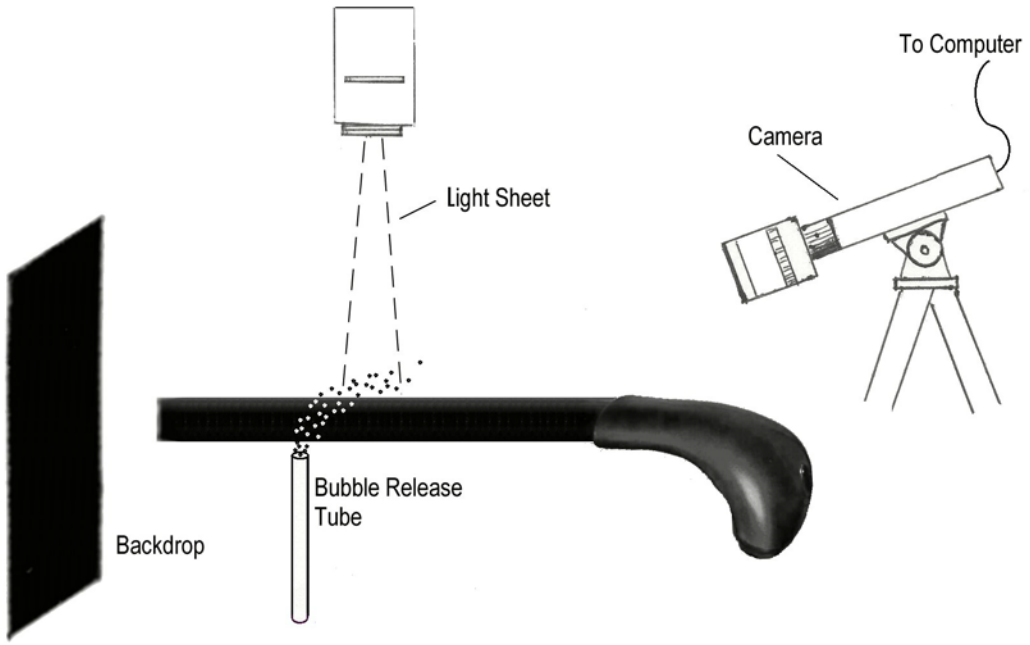

Figure 4-15 Experimental arrangement for particle illumination experiment.

Using the computer program XCAP™, images were captured at various exposure times. Figure 4.16 and 4.17 show typical images captured at 10m/s or 36km/h airspeed. Due to the nature of the particles chosen, this lower velocity was needed.

Figure 4.16 was captured with an exposure time of 33ms, it reveals streamlines over the top surface, it is quite clear that the flow is separating off this surface upstream of the trailing edge at the point established in the indicator paint experiments (point A fig 4.10). The fluctuation of the wake can also be seen. Note the circular motion of the particles.

Figure 4-16 Illuminated helium bubbles in airflow around A-bar.

Figure 4.17 was captured with an exposure time of 3ms. In this test, the bubbles accumulated in a foam on the upper surface to clearly show the separation point.

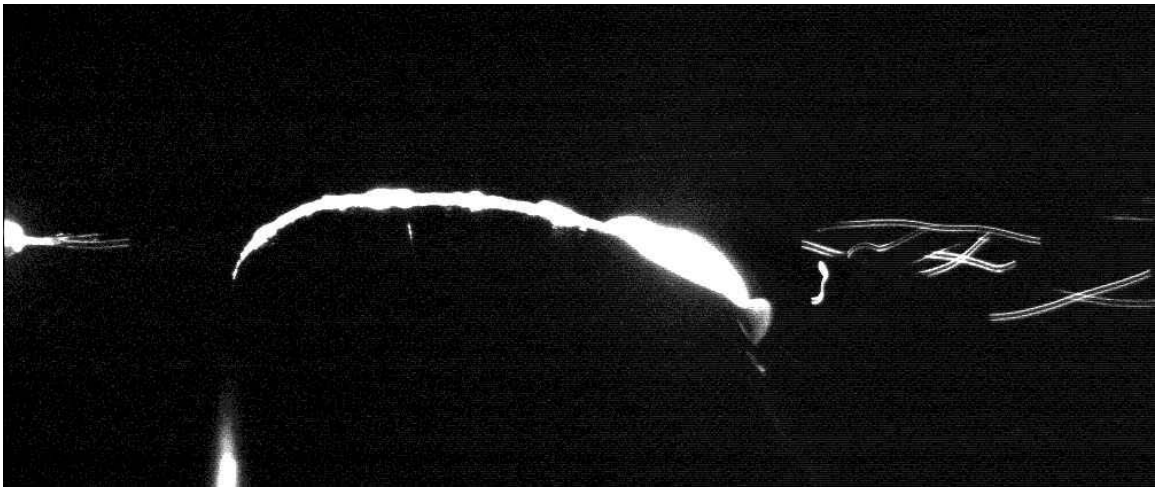

Figure 4-17 Illuminated helium bubbles and foam conglomeration on A-bar.

4.5.2 Hotwire Anemometry

Hotwire anemometry is a technique used for the accurate measurement of small-scale local velocities in airflows. This practice involves the placement of a very slender probe in the region of interest. The probe holds a fine wire (5μm thick) of known resistivity, which is part of an electrical circuit. The wire's resistance changes according to its temperature variation. The higher the local velocity, the faster the rate of cooling it experiences. By monitoring these resistance fluctuations, the flow velocities are measured.

The TSI monitor and power supply unit were used to control the electronics of the probe outputting an electrical voltage related to the velocity. This voltage was converted to a velocity measurement in m/s. The turbulence intensity was calculated from velocity fluctuations. The probe was mounted on a 2-dimensional traverser that could be manually traversed to within ±0.1mm.
Prior to each experiment, the hotwire probe was cleaned in alcohol and the equipment calibrated using the TSI calibrator and Betz manometer.

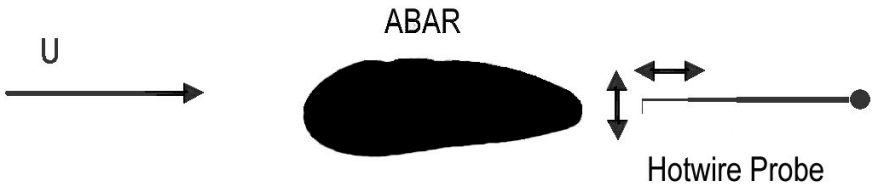

Figure 4-18 Diagram showing location of hotwire probe.

The local velocities and turbulence intensities were measured over an area 13mm downstream of the trailing edge in the centre of the wake. It was a rectangular area, 32mm by 27mm. The measurements were 1mm apart in the transverse direction and 4mm apart in the longitudinal direction. Each measurement was sampled at 2kHz for 2 seconds. Linear interpolation was used to predict values between these. The results were as follows:

The velocity profile is shown in figure 4.19, it resembles what one would expect in the wake of any bluff body, with lower velocity at the heart of the wake rising toward the free stream velocity at the outer edges. The vertical and longitudinal direction distances are with respect to the centre of the trailing edge.
Note, in actual fact, the velocity at the outer edges exceeds that of the free stream, this is due to the contraction of the streamlines around the roof rack. The width of the wake within this area averaged 13mm.

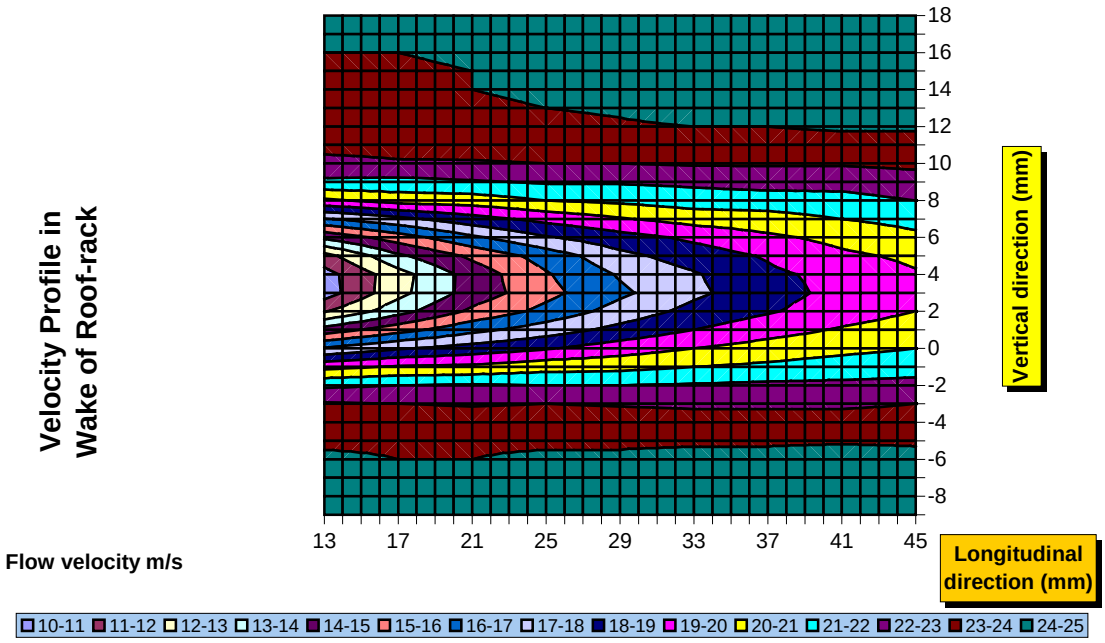

Figure 4-19 Velocity profile in A-bar wake as measured using hotwire anemometry.

Figure 4.20 shows the RMS turbulence relative to the free stream velocity. This result reveals the existence of two separate regions or lobes of high turbulence separated by a low turbulence region. Note that the accuracy of the measurement equipment drops in areas of high turbulence. The values toward the centre of the lobes are approximate only. The lobes represent eddy regions or regions of high of vorticity.

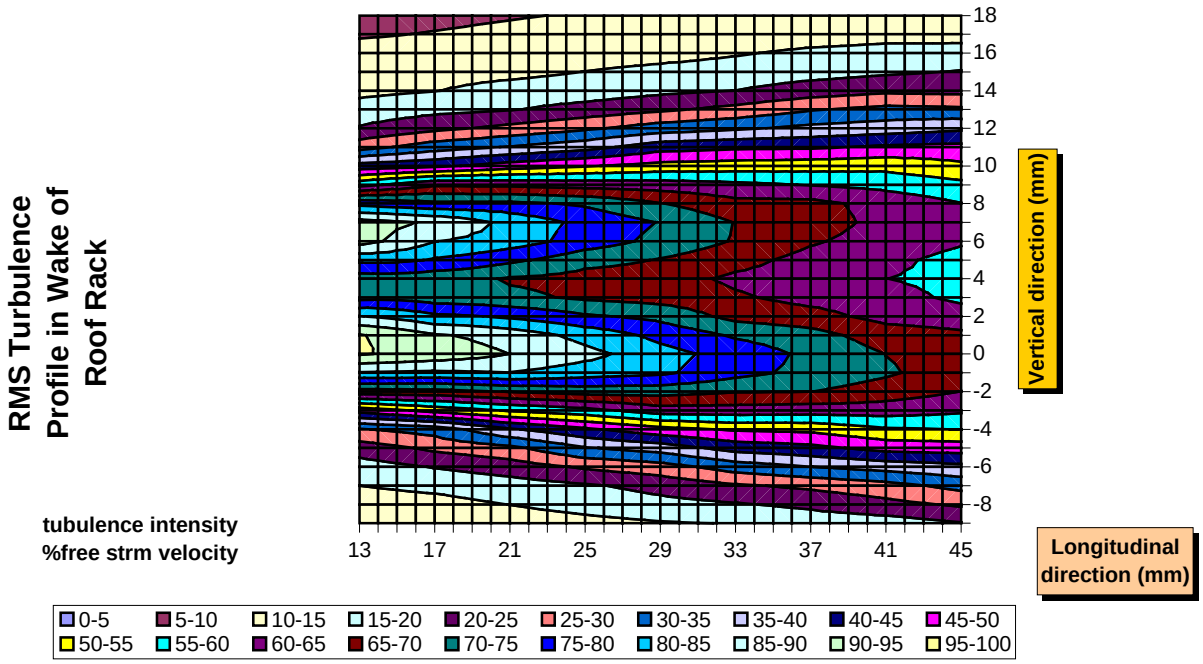

Figure 4-20 Turbulence profile in A-bar wake as measured using hotwire anemometry.

To find out whether the eddies are breaking off to form a stable vortex street the hotwire equipment was used to measure the frequencies in the wake. The hotwire probe was vertically traversed13mm downstream of the roof rack trailing edge and sampled at positions in the free stream (18mm above trailing edge), the edge of the wake (10mm above T.E.), the centre of the upper turbulence lobe (7mm above T.E.), the centre of the wake (4mm above T.E.), the centre of the lower turbulence lobe (0mm above T.E.), the bottom edge of the wake (3mm below T.E.) and the free stream (9mm below T.E.). 17100 samples were taken at each point at a sampling rate of 20kHz. A fast Fourier transform was performed on the data to produce a power spectrum. Figure 4.21 shows the time and frequency domain spectrums at the centre of the upper turbulence lobe.

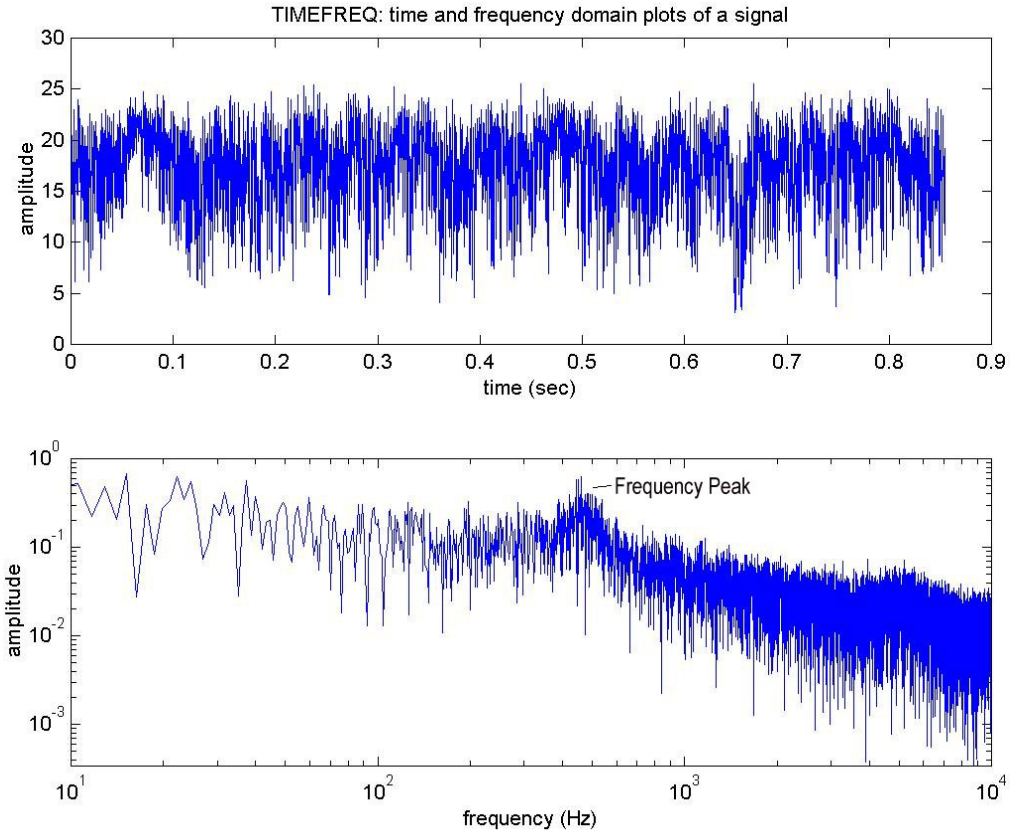

Figure 4-21 The velocity variation at the centre of the turbulence lobe.

It is very clear from the result that there is a dominant frequency in the wake. This lies around 460Hz, very close to that of the sound emissions. This peak frequency is recognisable at the edges of the wake and strongest at the centre of the turbulence lobes but fades at the centre of the wake (14mm point) and in the free stream[3].

A 2-dimensional wake exhibiting two discrete turbulence regions with periodicity clearly indicates the phenomenon of blunt trailing edge vortex shedding. This is certainly the case in the flow over the A-bar.

[3] The power spectrums for each position can be found in Appendix H

4.6 Analysis of the Natural Frequencies of the A-bar

The roof rack assembly has various natural frequencies, if these are being excited by the vortex shedding or other mechanisms this will amplify the sound emissions. The three most easily excited natural frequencies were evaluated to see whether they lay in the range of the 400Hz and 500Hz 1/3rd octave bands. These were: the mechanical natural frequency of the assembly, the natural frequency of the air column inside the A-bar and the natural frequency of the air gap between the roof rack and the car.

4.6.1 Mechanical Natural Frequency Evaluation

Procedure

The initial method proposed to detect the mechanical natural frequency of the A-bar was to supply an input signal with varying frequency exciting the roof rack and measure the amplitude of vibration. The frequency at which the amplitude peaked would be the natural frequency.

The vibrations were detected with Brüel and Kjaer accelerometer models 4335 and 4344, their output signals were amplified using the Systel Amplifier. The Yokogawa digital oscilloscope was used to view the signal, it contained a fast Fourier transform function and was also used to view the power spectrum of the signal. The Topward digital function generator was used to measure the frequency produced. Initially the A-bar was fastened to a laboratory table for the experiment, but it was soon discovered that the natural frequencies of the table itself interfered with the results. As a result the roof rack was set up on a solid steel bed and held in place with clamps.

Various methods were used to try to excite the A-bar's mechanical natural frequency. The first used an acoustic signal produced by the BWD function generator and loudspeaker, unfortunately the power of the output sound was not constant due to the frequency response of the speaker. The amplitude of vibration of the rack more accurately represented the signal strength than the resonance characteristics of the A-bar. Excitation via a mechanical signal was tried using the Advance vibrator and frequency generator but similar problems were also encountered with this system.

In the end the roof rack was excited by tapping it with a soft mallet. In the steady state, the roof rack oscillated at its natural frequencies. This method proved successful and the fundamental natural frequency of mechanical vibration was established as 82Hz[4], far removed from the vortex shedding frequency.

4.6.2 Acoustic Natural Frequency Evaluation

The natural frequencies of the air column inside the A-bar and the air gap between the roof rack and the car were calculated[5]. They were 190.6Hz and 4900Hz respectively, both were far enough removed from the vortex shedding frequency to assume that the effect they had on the noise emissions was negligible.

4.7 Summary of Results and Discussion for A-bar Analysis

The behaviour of the airflow around the roof rack has been discussed in this chapter. It has been established that the untreated A-bar has a region of laminar boundary layer growth on both the upper and lower surface from the stagnation point at the leading edge. On the upper surface, the boundary layer remains laminar until approximately 1/5 chord, where the pressure gradient becomes less favourable and the flow close to the surface of the rack becomes retarded to the extent of separation. This also occurs on the lower surface at around 1/5 chord. Transition to turbulent flow takes place in the separated region, causing the flow to reattach 12mm downstream on the top surface and 10mm downstream on the lower surface. This is due to increased mixing within the turbulent boundary layer that causes transferral of momentum from the free stream to the surface, restoring the motion of the stagnant fluid. Further downstream, the flow separates into the wake. This occurs at approximately 3/4 chord on the top surface

[4] The power spectrum for the mechanical vibration of the A-bar can be found in Appendix I
[5] Natural frequency calculations in Appendix B

and very close to the trailing edge on the lower surface. The wake is a periodic one, with the production of a typical blunt trailing edge Karman vortex street.

From the findings in this chapter, it has been established that this vortex shedding is the mechanism responsible for the production of noise. At 22.2m/s (80km/h), at normal incidence the frequency of this sound jumps between two discrete frequencies around 420Hz and 450Hz. The strongest of these two frequencies however, is the 420Hz. The SPL of the vortex shedding tone is highest when the angle of attack of the A-bar is slightly nose down (from 5.8˚ to 7.9˚).

The frequency at which the vortices are being shed is usually dependent either on the mechanical natural frequency or on the relevant Strouhal dimension. In the case of the A-bar, it has been established that the mechanical natural frequency is significantly different from the vortex shedding frequency (see section 4.6.1), therefore the shedding frequency must be dependent on the Strouhal dimension. In the case of a circular or square cylinder, the Strouhal dimension is the diameter of the cylinder and the Strouhal number is 0.2. In the case of an aerofoil, this dimension is not as well defined. If we base our calculation of the Strouhal number on the vertical distance between the upper and lower separation points, a distance of 17.8mm then for a vortex shedding frequency of 420Hz, the Strouhal number is 0.34. If the calculation is based upon the width of the wake, a value of 13mm, then for a vortex shedding frequency of 420Hz, the Strouhal number is 0.25. [6]

Massey[7] states that in the case of circular cylinder, vortex shedding occurs in the Reynolds number range from $250 < Re < 2 \times 10^5$. If in the case of the A-bar we base our calculation of Reynolds number on the length value of 17.8mm then $Re = 2.6 \times 10^4$ but if the calculation is based on the length value of 13mm then $Re = 1.9*10^4$. In both cases, Re lies within the vortex shedding range.

The A-bar also generates noise at higher frequencies, at around 1.6kHz to 2.5kHz and 5kHz at some incidence angles. These are produced by the interaction of the flow with the region around the elastomer infill via a mechanism described as a cavity resonance (see chapter 2 section 2.2.3). As seen in figure 4.9 these frequencies are not heard from within the car, this is due to there being attenuated by the roof and lining (as described in section 4.4.6).

Not only was the effect the car has on the production of noise from the roof rack addressed in this chapter but also the transmission of the sound through the roof of the car. It was established that there was no flow separation off the windscreen and a gentle roof angle as found on most modern cars would not dramatically affect the incident flow onto the roof rack. In the case of cars with unusually steep angles of attack, it could be possible that the incident flow be affected to the extent of increasing the noise production. The likelihood of resonance occurring in the air gap between the roof and the roof rack or in the air column inside the roof rack itself is very low, the resonant frequencies of these systems being far removed from the vortex shedding frequency.

Discussion of Experimental Method

The method used to remove the base 'empty tunnel' noise measurement from the 'roof rack in place' sound measurement[8] to produce a spectrum representing the signal produced by an isolated roof rack, proved very successful. The peak representing the fan blade passing noise was eliminated and tonal frequencies were revealed very clearly. A figure representing the empty tunnel sound profiles for measurements taken throughout a 4 month period during the experimentation program can be found in appendix F. The 84 profiles show very good consistency. The only major variation was in the 1.25kHz to 2.5kHz 1/3rd octave bands, thought to be due to cavity resonance from the microphone mount.

During the course of an experiment, the variation in the airflow was slight, however there was a slow rise in air temperature and a drop in the relative humidity. The longest experiment recorded in this work was for a period of 2hrs in which a temperature rise of 1.5˚C from 23.8˚ to 25.3˚ was recorded. The biggest drop in relative humidity recorded was 2.1% from 30% to 27.9%. over a 1hr 20min period.

---

[6] Strouhal number calculations in Appendix B

[7] Massey, B. S. *Mechanics of Fluids.*

[8] This process described in Appendix C

The variation of Strouhal number caused by these effects is negligible.
Similarly, the speed fluctuations were small, the maximum fluctuation experienced was 0.2m/s from 22.5m/s to 22.3m/s over a 2hr period. The Strouhal number fluctuation caused by this is insignificant.

EXPERIMENTAL INVESTIGATION OF METHODS FOR ELIMINATION OF ROOF RACK NOISE

5.1 Introduction to Chapter

This chapter describes the second part of the experimental program, the treatment of the A-bar noise emission. In this part, proposed methods for the treatment of blunt trailing edge vortex shedding were trialed. These were of type 1, 2 and 3 treatment types (as laid out in chapter 2 section 2.3.2). The effect the treatments had on the flow field was investigated using flow visualisation and the corresponding noise emissions were measured. Successful A-bar noise treatments were trialed on other "noisy" roof racks to see whether they were as effective.

5.2 Experimental Procedure

In chapter 4, it was established that through the measurement of the roof rack sound spectrum in the free jet of the wind tunnel, predictions of the roof rack noise perceivable from inside the car could be made. It was also established that subjective tests were accurate in determining the presence and frequency of vortex shedding tones. These techniques, as well as quantitative field tests were used in the noise-testing program described in this chapter. For consistency, the same A-bar was used in most of the experiments. In those cases where the treatment being tested was destructive to the roof rack, as in those involving the drilling of holes, additional A-bar roof racks were used. As in previous tests in chapter 4, full-scale roof rack specimens were used. All laboratory experiments were carried out at the test speed of 80km/h (22.2m/s), those performed in the field, at 100km/h (27.8m/s). All quantitative tests were performed as described in chapter 4, sections 4.4.1 and 4.4.5.

Indicator paint flow visualisation was employed to determine the flow around modified A-bar specimens. This was carried out as described in chapter 4 section 4.5.1.2.

5.2.1 Guidelines for A-bar Modifications

Because the A-bar roof rack was in production at the writing of this thesis, a focus of this work was to produce a treatment to the A-bar noise without changing the overall roof rack itself. The treatment ideally should not involve significant changes to the current A-bar because of the already significant tooling costs incurred. The ideal case scenario would be a treatment that involved either the addition of a minor process or slight modifications to an existing one. It is important that modifications to the A-bar do not jeopardise its performance or life, they should not reduce the strength or increase corrosion. Roof racks are generally designed to be robust, they must be able to take the occasional knock and be able to be used by people of varying abilities. Likewise any additions made to the A-bar must be tough and safe.

Perhaps one of the most important traits of a marketed product is its appearance, the treatment carried out on the A-bar must not sacrifice aesthetics.

5.2.2 Methods Trialed

Based upon the ideas gained from previous studies, as summarised in chapter 2, treatments to disrupt the vortex shedding sound emission from the A-bar were proposed. The treatment methods were either type 1, 2 or 3, or a combination of these. Some of the examined treatments had inherent limitations, in either manufacturability or maintaining the performance of the roof rack. These will be identified and explained.

The initial testing of all sound treatment methods was through subjective qualitative tests. The more practical methods were tested quantitatively, there were 3 series of quantitative tests performed in the lab and set of tests in the field. Of the laboratory experiments, series 1 and 2 were performed on the A-bar with a 0˚ angle of attack whereas the series 3 tests were performed at both 0˚ and 5.8˚ nose down. The laboratory tests followed the methods described in chapter 4 section 4.4.1, note comparison between the different series can only be made based on the trends of the spectrums and not the quantitative values. The field tests followed the method described in chapter 4 section 4.4.5, note these tests were of the more successful methods.

5.3 Splitter Plate

The practicality of a splitter plate was considered. A splitter plate is a thin plate that protrudes out of the trailing edge or base of a blunt body. It isolates the vorticity sheets cast off the separation points from each other, preventing the interaction that leads to vortex shedding. These have been used in the past for reducing the vortex shedding induced vibration of circular cylinders. Splitter plates, because they are very slender are, by their nature, sharp (and in some cases flimsy). The rough handling of a roof rack with splitter plate installed could be injurious or cause damage to the splitter plate itself. For this reason, a splitter plate arrangement was not tested.

5.4 Air Jets

5.4.1 Base Bleed from Trailing Edge Holes

Description

An alternative idea used to produce the same effect is base bleed, this is the injecting of a sheet of air from the trailing edge or base of a blunt body. Wood[1] showed that this could, in the case of blunt trailing edge aerofoils, reduce noise. An A-bar was prepared by drilling a series of 1.5mm holes with 5mm spacing along the trailing edge from which air was released. The air was supplied into the rear cavity from the laboratory compressed air supply line. This was tested qualitatively in the wind tunnel.

Results and Discussion

There was no perceived drop in SPL at the vortex shedding frequency but an increase in the broadband noise. This noise was produced by the small air jets from the trailing edge holes.

[1] Wood, C. J. *The effect of base bleed on a periodic wake*

Kovasznay's[2] experiments showed that vortices often form some distance downstream of the trailing edge. The presence of a short splitter plate or a weak base bleed is unlikely to affect the wake very far downstream of the body.

If this treatment had been successful, the major issue to address in implementing it would have been the source of the air supply to the trailing edge holes. The most likely source of high pressure air is the leading edge of the roof rack. Due to the construction of the A-bar, complex ducting would be needed to channel the flow into the rear cavity. The economic manufacture of the holes would be a simple problem to solve. A continuous punching operation could be introduced directly after the extrusion of the plastic shroud.

5.4.2 Air Jets at Turbulent Separation point

Description

The effect of a row of air releasing holes at the upper surface separation point was investigated. It was thought that this would break up the correlation of the vortex shedding or induce a 3-dimensional flow in the wake.

A series of 3mm holes with 11mm spacings were drilled in an A-bar specimen on the upper surface 22mm upstream of the trailing edge. Air was supplied to the rear cavity via the mains compressed air line. This specimen was tested qualitatively in the wind tunnel.

Results and Discussion

There was no noticeable difference between the sound level of this specimen and that of the untreated A-bar. Once again, if this treatment had been successful the issues would be the same as those presented by the trailing edge hole roof rack, the only major difference is that due to the position of the holes, it is more likely that rain would get inside the roof rack, increasing the risk of degradation of the rack.

The manufacturing method would be identical to the trailing edge hole specimen.

---

[2] Kovasznay, L. S. G. *Hotwire Investigation of the Wake Behind Cylinders at Low Reynolds Numbers*

5.4.3 Air Jets at the Laminar Separation Point

Description

The placement of a row of air releasing holes, at the laminar separation point, was investigated. The effect that these had on the vortex shedding noise was measured. The holes were 3mm diameter with a spacing of 22.5mm. A similar row of holes was drilled along the leading edge of the A-bar at the stagnation point. Air entered the front cavity through these holes due to the high pressure at the leading edge and flowed out of the top row where the pressure was lower. This A-bar specimen was tested in the wind tunnel in a subjective qualitative sound test.

Results and Discussion

There was an audible reduction in the sound pressure level of the vortex shedding tone when tested in the wind tunnel. This was the first method to produce a perceivable difference. (Subjective field tests with this specimen also revealed a dramatic reduction of this tone)

Flow Visualisation

An indicator paint flow visualisation test was carried out on the A-bar specimen. The method used was consistent with that described in chapter 4 section 4.5.1.2. Figure 5.1 shows the paint pattern that resulted from the addition of the two rows of holes.

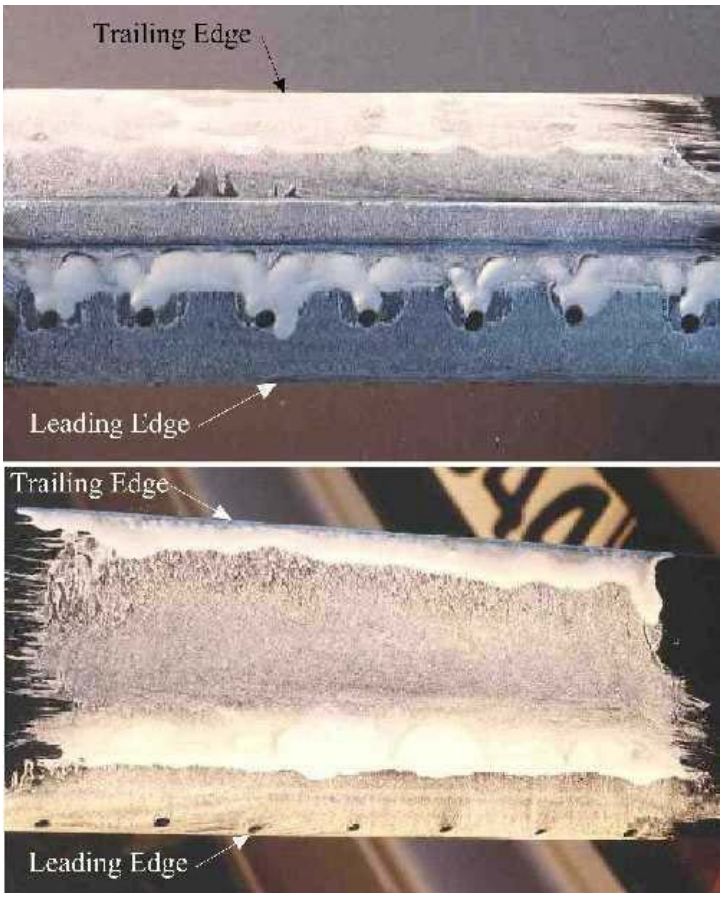

Figure 5-1 The top and bottom views of the double row holes modification.

The two most important features of the pattern were a) the areas surrounding the upper surface holes and b) the dimples in the upper surface turbulent separation-point line. There was an area of separated flow directly behind each of the holes in the top row, this is synonymous with what would be observed if there was a solid obstruction at each of the points. The air jets from the holes are physically similar to vertical cylinders of jet diameter extending from the roof rack surface (see fig 5.2). The flow of a fluid with a developed boundary layer around such an obstruction causes the production of a “horse shoe” vortex. These vortices trail downstream from each side of the obstruction causing the mixing of high energy free-stream flow with the lower energy boundary layer flow

(See inset[3]). It was this re-energising of the boundary layer that caused the early reattachment of the flow downstream of the hole.

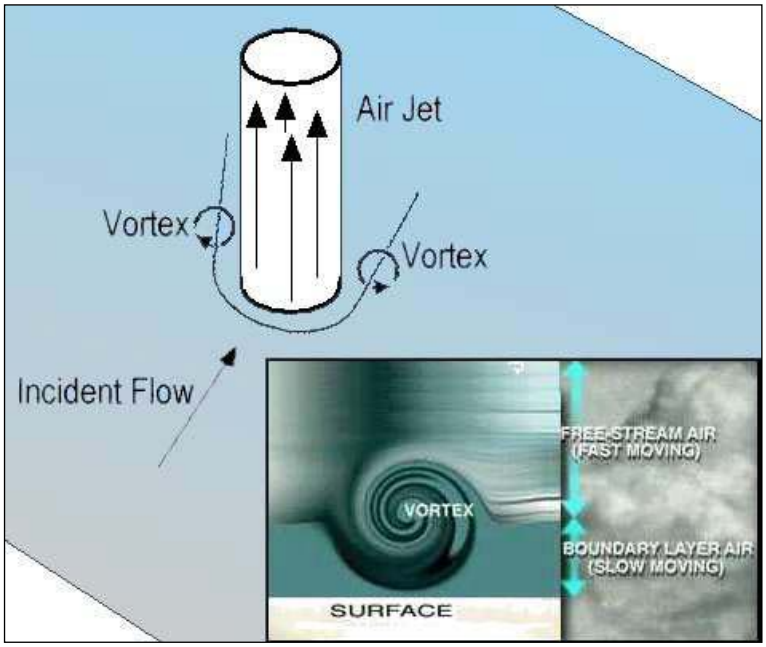

Figure 5-2 The cause and effect of horse shoe vortices.

The increased energy of the flow downstream of the holes also caused a delayed turbulent separation, evidenced by the dimple pattern in the turbulent separation-point line.

The dark areas flanking the top row holes were evidence of high velocity flow on the roof rack surface. This was caused by the convergence of streamlines as the airflow encountered the jet. The dark area just downstream of the accessory strip in the interval between two of the holes was an anomalous occurrence and no conclusions about the general flow pattern were drawn from it.

The reduction in noise is a result of the trailing vortices interacting with and weakening the vortex street.

The discontinuous disturbance to the vortex street may also break up the spanwise correlation of the vortex shedding. The flow pattern on the under-surface was unchanged from that of an unmodified A-bar.

[3] Inset from Internet site: http://www.microaero.com/

As with the previous two treatments investigated this modification is very easy to produce by the addition of a simple continuous punching operation into the production process. The only drawback of this design is the potential for water to accumulate inside the roof rack on rainy days, increasing the rate of degradation and corrosion. Treatments that are additions to the A-bar were considered a more practical idea.

During the course of this testing of the previous treatment, it was noticed that there was some reduction of sound from the roof rack when the leading edge holes were sealed with adhesive tape. The interaction of the airflow with the top row holes themselves without the release of air was enough to disturb the vortex street to a limited extent, reducing the vortex shedding sound slightly. On this basis, the placement of various additions at the laminar separation point was investigated.

5.5 Adhesive Plastic Hemispheres

Description

A series of tests were performed on the A-bar with a row of 7mm diameter adhesive plastic hemispheres forward of the laminar separation point on the upper surface. The hemispheres were 26mm apart and 18mm forward of the leading edge of the accessory slot. This arrangement was tested quantitatively in the free jet of the wind tunnel as described in chapter 4 section 4.4.1. This was part of the series 1 testing.

Results and Discussion

There was a perceivable decrease in the SPL of the vortex shedding tone when this modification was applied. Figure 5.7 shows the measured sound spectrum (spectrum Abar vor.) Although the 400 – 500Hz peak was still visible, there was an overall level reduction. At the 400Hz 1/3rd octave band the SPL dropped 2.6dB from 63.5dBa to 60.9dBA and at the 500Hz 1/3rd octave band the SPL dropped 1.5dB from 62.5dBA to 61dBA. The narrow band sound spectrum also shows a reduction of the vortex shedding tonal peak[4].

[4] Narrow band sound spectrums found in Appendix H

This sound treatment works in a similar way to the air jets at the laminar separation point. Chordwise vortices are generated by the presence of the hemispheres, upsetting the wake and reducing the strength of the vortex street. The spanwise correlation of the vortex street may also be reduced.

In terms of manufacture, this treatment is very practical. This treatment is easily applied to the A-bar, the hemispheres would be fastened onto the roof rack with a strong adhesive. This could be done either by hand or by machine. If attached securely they would stand up to rough treatment and not degrade the A-bar or reduce its life.

5.6 Leading Edge Serrations

Figure 5-3 Strips used for the reduction of vortex shedding noise.

They are (from left to right) the Owl strip #1, Owl strip #2, Pinking shear strip, Owl strip #1 dble thickness, Asymmetric serration and Jetting strip.

5.6.1 Pinking Shear Cut Strip

Description

The effect of leading edge serrations (as discussed in chapter 2 section 2.3.2) was trialed on the A-bar. A serrated adhesive strip of 10mm average width x 1.8mm thick was prepared using dressmaker's pinking shears. The serrations had 2mm amplitude and pitch 5mm (see figure 5.3). A series of tests were performed with this strip attached to the A-bar, it was positioned with the serrated edge upstream, its rear edge 12mm forward of the accessory slot on the top surface. This arrangement was tested quantitatively in the free jet of the wind tunnel as described in chapter 4 section 4.4.1. This was a series 1 test.

Results and Discussion

There was no perceivable decrease in the SPL of the vortex shedding tone with the application of this treatment, but a noticeable increase in the broadband sound. The 1/3rd octave band sound spectrum can be seen in figure 5.7 (spectrum: Abar pk). The 315Hz 1/3rd octave band shows a dramatic rise in SPL and the 400Hz 1/3rd octave band has increased slightly. This noise increase is likely to be due to the increased turbulence created by the serrations. In the narrow band sound spectrum[5] the vortex shedding peak appears to be further to the left than usual, revealing that the frequency of the sound had decreased. This decrease in frequency may be a result of the widening of the wake due to the turbulence induced by the strip. If this treatment had been successful, it would have been easily produced by the die cutting of an adhesive elastomer strip. This would be applied after the production of the extruded plastic shroud.

5.6.2 Saw Blade

Description

A serrated edge saw blade was trialed in a similar arrangement to the above test. The saw blade was 1mm thick with an average width of 10mm, the serrations were asymmetric (saw toothed) with 1.5mm amplitude and 2.5mm pitch. The blade was positioned on the

[5] Narrow band sound spectrums found in Appendix H

A-bar with its downstream edge 10mm forward of the accessory slot. It was attached to the A-bar with adhesive tape. Tests were performed on the modified roof rack in the same manner as described in chapter 4 section 4.4.1. This was a series 1 test.

Results and Discussion

Similar to the pinking shear cut strip treatment, there was no perceivable decrease in the SPL of the vortex shedding tone. The 1/3rd octave band sound spectrum can be seen in figure 5.7 (spectrum: Abar saw). There were some high frequency cavity resonance tones generated by this addition, these show up clearly in the figure. The narrow band sound spectrum also reveals the presence of one particularly loud high frequency tone at 2.5kHz (this may be influenced by the tones produced by the microphone holder). Similar to the effect of the previous treatment, the vortex shedding frequency decreased. If put into production, this treatment would be best manufactured from an adhesive elastomer strip similar to the previous specimen.

5.7 Roughness Strips

In both test series 1 and 3, tests were performed on specimens with modifications based on the attachment of strips of emery tape of varying size and position. These were attached towards the front of the A-bar on the upper surface. The purpose of using roughness strips is to trip the boundary layer to turbulent early on and increase the mixing of the higher energy flow of the free stream with the more stagnant boundary flow. This should cause the flow to stay attached further back towards the trailing edge rather than at the usual separation point. Theoretically, the bigger and rougher the strip, the more effective it should be. In terms of manufacture, the addition of roughness strips is very convenient, these could be adhered to the roof rack in the appropriate place very easily. If fastened securely they would be robust and durable and not degrade the life of the roof rack.

5.7.1 16mm P60 Strip Adjacent to the Accessory Slot

Description

A 16mm wide P60 emery strip was attached to the A-bar adjacent to the accessory slot on the upstream side. It was fastened to the A-bar with double-sided adhesive tape. This arrangement was tested quantitatively as described in chapter 4 section 4.4.1. This was part of the series 1 testing.

Results and Discussion

Figure 5.7 shows the sound spectrum that was produced by this specimen (spectrum: Abar snd). There was a broadening of the peak in the low frequency range with a slight drop in the SPLs of the 400Hz and 500Hz 1/3rd octave bands. The subjective test revealed that the vortex shedding frequency was not diminished even though the broadband noise had increased considerably. In the narrow band spectrum, the vortex shedding frequency peak is not clear, due most likely to the increased broadband noise. The increased broadband noise is produced from the turbulence caused by the interaction of the flow with the emery strip.

5.7.2 10mm P150 Strip at Leading Edge

Description

A 10mm wide P150 emery strip was attached to the A-bar at the leading edge. It was fastened to the A-bar with double-sided adhesive tape. This arrangement was tested quantitatively as described in chapter 4 section 4.4.1. This test was part of the series 3 experiments and was performed at two angles of attack, 0˚ and 5.8˚ nose down. (Note, the trends only and not the values can be compared between different series.)

Results and Discussion

The measured sound spectrum for the 0˚ and 5.8˚ nose down tests is shown in figures 5.9 and 5.10 respectively (spectrums: Abar 10mm strip). At both angles of attack, there was a dramatic decrease in the overall sound pressure level and SPL decreases in the 400Hz and 500Hz 1/3rd octave bands. At 0˚, the 500Hz 1/3rd octave band dropped 6.2dB from

68.1dBA to 61.9dBA and at 5.8˚, it dropped 5.2dB from 69.8dBA to 64.6dBA. At 0˚, the SPL of the 400Hz 1/3rd octave band dropped 0.5dB from 68dBA to 67.5dBA and at 5.8˚, it dropped 4.8dB from 72.3dBA to 67.5dBA. The narrow band spectrums for both angles show a significant decrease in the level of the vortex-shedding peak. In the subjective tests however, the vortex shedding tone was still audible.

5.7.3 15mm P60 Strip at Leading Edge

Description

A 15mm wide P60 emery strip was attached to the A-bar at the leading edge. As with the previous specimen, it was fastened to the A-bar with double-sided adhesive tape. This arrangement was tested quantitatively in both the lab and the field in the methods described in chapter 4 sections 4.4.1 and 4.4.5 respectively. The laboratory test was part of the series 3 experiments and was performed at two angles of attack, 0˚ and 5.8˚ nose down. An indicator paint flow visualisation test was performed on the roof rack specimen in the method described in chapter 4 section 4.5.1.2.

Results and Discussion

The 1/3rd octave sound spectrums for these tests are shown in figures 5.9 and 5.10 (spectrums: Abar 15mm strip). This treatment was more effective at the 5.8˚ nose down incidence angle than at 0˚, however the 500Hz 1/3rd octave band did show a 5.5dB drop at 0˚. At 5.8˚ nose down, the treatment produced a significant reduction in the SPLs in both the 400Hz and 500Hz bands. The 400Hz band dropped 6.5dB from 72.3dBA to 65.8dBA and the 500Hz band dropped 5.6dB from 69.8dBA to 64.2dBA. In the narrow band spectrums, the vortex shedding tonal peak decreased much more at the 5.8˚ nose down incidence angle. At this angle, the peak was undetectable in the spectrum. Similar to the previous test, the vortex shedding tone was perceivable with the ear at both angles. In the field test result (figure 5.11, spectrum: Abar 15mm strip) the SPL of the vortex shedding tone appears to be higher than that of the unmodified case. The curve however is much flatter, due to the increase broadband noise. It is likely that the increase in the tonal frequency is due to the overall spectrum increase from the broadband noise and not a result of a strengthening of the vortex street.

Flow Visualisation

The indicator paint result is shown in figure 5.4. It can be seen from this result that the emery strip causes the boundary layer to be turbulent over the whole chord. There is still a separation bubble at the maximum thickness point but this is much diminished. The turbulent separation into the wake occurs earlier on than usual on both the upper and lower surfaces creating a wider wake. The separation on the lower surface is very much advanced (around 1/3chord from the trailing edge). This early retardation of the flow over the A-bar is due to the early transition of the boundary layer to turbulent resulting in faster boundary layer growth and greater energy dissipation. The widening of the wake lowers the frequency of the vortex shedding, shown by the apparent movement of the 1/3rd octave band peak to the left.

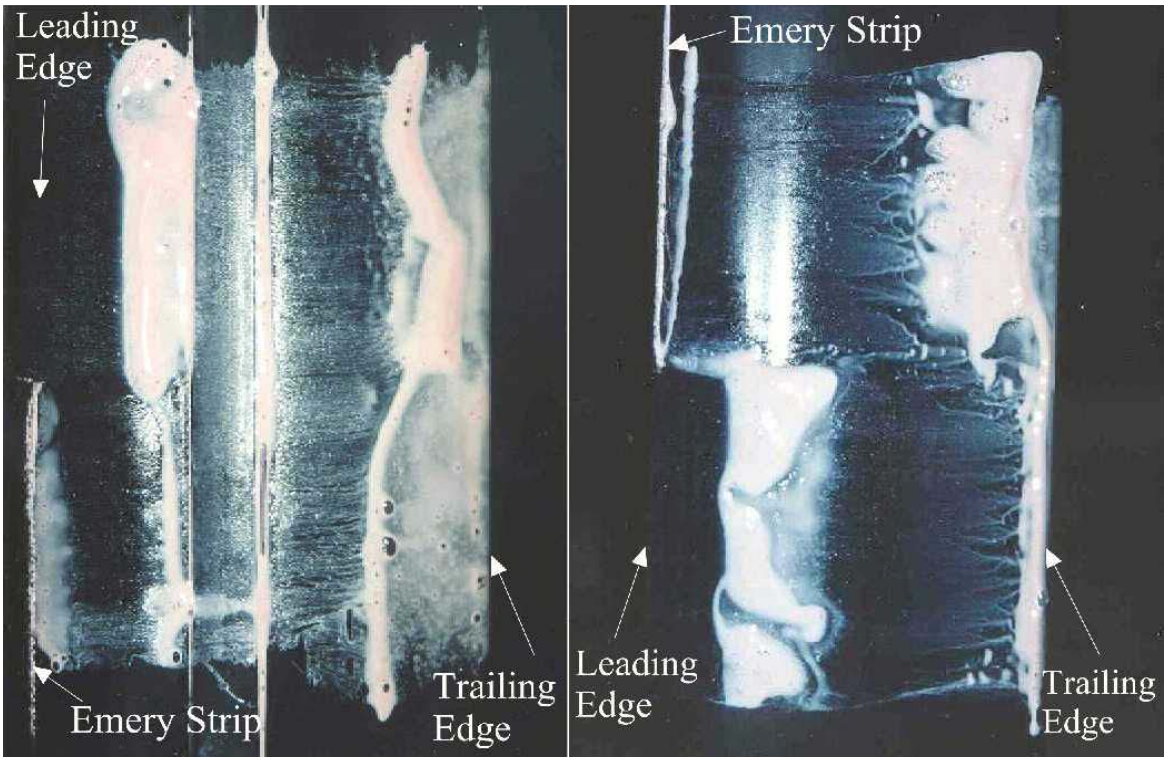

Figure 5-4 Top and bottom views of the A-bar with and without 15mm emery strip.

5.7.4 28mm P150 Strip at Leading Edge

Description

A 28mm wide P150 emery strip was attached to the A-bar at the leading edge. As with the previous two specimens, it was fastened to the A-bar with double-sided adhesive tape. This arrangement was tested quantitatively as described in chapter 4 section 4.4.1. This test was part of the series 3 experiments and was performed at two angles of attack, 0˚ and 5.8˚ nose down.

Results and Discussion

The measured 1/3rd octave sound spectrums for the 0˚ and 5.8˚ tests are shown in figures 5.9 and 5.10 respectively (spectrums: Abar 28mm strip). There was a dramatic increase in the OASPL when this modification was applied. This was mainly an increase in broadband noise in the low frequency range peaking at around the 160Hz 1/3rd octave band. The emery strips lacked flexibility and the 28mm strip, due to its width, would not conform to the curve in the leading edge of the roof rack, lifting up off the roof rack

surface during the test. This caused the increase in noise production. The OASPL increased by 8.4dB from 62.4dBA to 70.8dBA at 0˚ incidence and increased by 14.2dB from 65.8dBA to 86dBA at 5.8˚ nose down. There is a possibility that this strip may have deflected turbulent airflow into the path of the microphone, if this was the case, the sound spectrum will be affected by pseudo sound.

5.8 Irregular Leading Edge Serrations

These treatments were similar to the pinking shear cut strip but had intervals between each of the serrations. They were produced from adhesive elastomer strip using craft knives and scissors. In production, they could be produced by die cutting and attached with strong adhesive. They are robust and durable, they do not sacrifice the life or strength of the roof rack and can be made to add to the aesthetic appeal of the roof rack.

5.8.1 Owl Wing Strip No. 1

Description

Tests were performed on the A-bar with the addition of an adhesive serrated strip on the upper surface near the leading edge. The serrations on this strip were spaced 10mm apart. Strips of this type are referred to as owl wing strips because the first use of them arose from the study of the leading edge of owls wings. Some owls exhibit exceptionally quiet flight (this is discussed in chapter 2 section 2.3.2). The owl wing strip no. 1 had a 20mm pitch and 5mm amplitude with an original base width of 10mm, (see figure 5.3) it was positioned with the serrations pointed upstream. This first test was performed with the rear edge of the strip flush up against the accessory slot ie. the apexes of the serrations were 15mm forward of the accessory slot. This arrangement was tested quantitatively in the free jet of the wind tunnel as described in chapter 4 section 4.4.1. This was tested in the series 2 experiments and was tested at 0˚ incidence only.

Results and Discussion

Figure 5.8 shows the measured 1/3rd octave sound spectrum (spectrum: Abar owl 1). As the result shows, the 400Hz – 500Hz peak was affected by this modification. The SPL of the 500Hz 1/3rd octave band dropped 4.7dB from 67.9dBA to 63.2dBA. The peak

however, was still visible and a vortex shedding frequency was detected in the subjective tests. The serrations would have worked in a similar fashion to the hemispherical vortex generators, producing chordwise trailing vortices. These were not very strong as their influence on the vortex shedding tone is minor.

5.8.2 Owl Wing Strip No. 1 Forward Position

Description

The previous treatment was tested on the A-bar specimen a second time, this time, the owl wing strip was positioned 7mm forward of the accessory slot ie. the apexes of the serrations were 22mm forward of the accessory slot. This arrangement was tested quantitatively in the free jet of the wind tunnel as described in chapter 4 section 4.4.1 and as above was part of the series 2 experiments.

Results and Discussion

The 1/3rd octave sound spectrum measured with the 2260 Investigator is shown in figure 5.8 (spectrum: Abar owl 1 fwd). This position proved to be much more effective for the removal of the vortex shedding peak. The SPL of the 400Hz 1/3rd octave band dropped 0.5dB from 67.4dBA to 66.9dBA. The SPL of the 500Hz 1/3rd octave band dropped 3.7dB from 67.9dBA to 64.2dBA. The peak is hardly visible in the 1/3rd octave sound spectrum for this treatment and the usual vortex shedding frequency was so faint that it was not able to be well-defined in the subjective test. It is likely that this position is more effective in reducing noise because the serrations are forward of the separation bubble and in the laminar boundary layer region. In this unstable region, the serrations would have more influence on the flow, whereas in a separated region, the flow (or lack of it) is more stable.

5.8.3 Owl Wing Strip No. 1 Forward Position Double Thickness

Description

Once again, an A-bar specimen based upon the use of the owl wing strip no. 1 was used. In this case, adhesive triangles were placed onto the serrations of strip (see figure 5.3). As in the previous test, it was positioned 7mm forward of the accessory slot ie. The apexes of the serrations were 22mm forward of the accessory slot. This arrangement was tested quantitatively in the free jet of the wind tunnel as described in chapter 4 section 4.4.1 and was part of the series 2 experiments. An indicator paint flow visualisation test

was performed on this roof rack specimen in the method described in chapter 4 section 4.5.1.2.

Results and Discussion

The measured 1/3rd octave sound spectrum of this specimen is shown in figure 5.8 (spectrum: Abar owl 1 dble fwd). This treatment proved to be even more effective than the last for the removal of the vortex shedding tone. The SPL of the 400Hz 1/3rd octave band dropped a further 0.2dB to 66.7dBA with a slight rise in the SPL of the 500Hz band to a value of 65.1dBA. The sound spectrum shows a general rise in SPLs from 250Hz to 1kHz due to an increased broadband emission, this seems to have overshadowed any tonal noise that may have remained. The vortex shedding tone was even less apparent in the subjective test than in the case of the previous specimen.

Flow Visualisation

The indicator paint result is shown in figure 5.5. It can be seen from this result that this treatment affects the flow over the roof rack dramatically. This paint pattern on the upper surface of this specimen noticeably resembles that of the specimen with air jets at the laminar separation point, the turbulent separation point showing a regular pattern such as what would be observed with the presence of a series of chordwise vortices. In this case, these vortices are produced by the forward facing serrations. Stagnation of the flow causes a high-pressure region at the front of each of the serrations, this coupled with a lower pressure region on the top surface of each serration generates local vorticity that grows to form a developed chordwise vortex. The small triangular separation bubbles trailing from the apexes of the serrations are a result of the growth of the vortices down the serration. The chordwise vortices generated from this treatment are much stronger than those generated by the air jets at the laminar separation point, as a result, the paint in the separated region on the upper surface shows a very clear circulation. Consequently, the vortex street is highly disrupted, decreasing its periodicity and tonal noise production. The increased turbulence in the wake causes the increase in broadband noise.

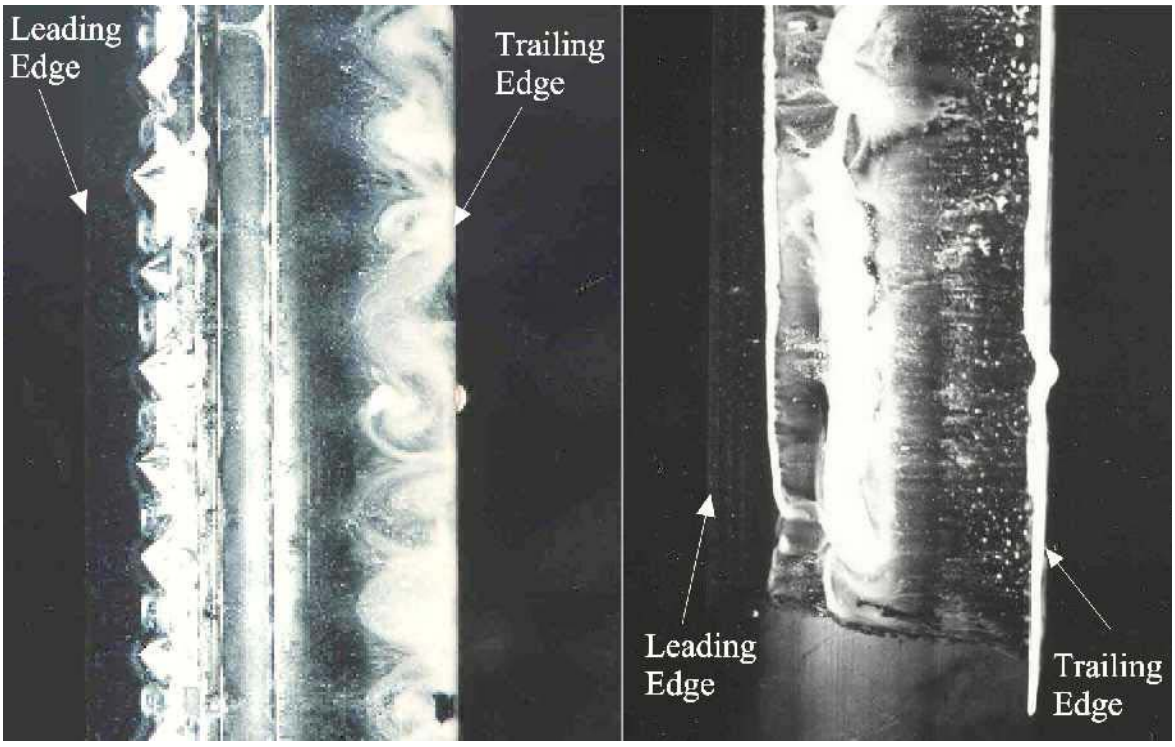

Figure 5-5 Top and bottom views of the A-bar with double thickness owl strip no. 1 in forward position.

5.8.4 Owl Wing Strip No. 2

Description

A smaller owl wing strip was produced with 10mm pitch and 2mm amplitude. It was made from a pinking shear cut strip with every second serration removed (see figure 5.3). The base width of the owl wing strip no. 2 was 10mm, it was positioned with the rear edge of the strip 3mm forward of the accessory slot. In this position the apexes of the serrations were 12mm forward of the accessory slot. Quantitative tests were performed on the specimen in the free jet of the wind tunnel and in the field as described in chapter 4 sections 4.4.1 and 4.4.5 respectively. The laboratory test was part of the series 3 experiments, and was tested at 2 attack angles, 0˚ and 5.8˚ nose down.

Results and Discussion

There was a decrease in the vortex shedding tone with this modification at both angles. Figures 5.9 and 5.10 show the measured 1/3rd octave sound spectrums (spectrums: Abar owl 2). Although the 400 – 500Hz peak is still visible, there was a reduction, particularly in the 500Hz band. At 0˚ incidence, the SPL of the 400Hz 1/3rd octave band dropped 1dB from 68dBa to 67dBA and the SPL of the 500Hz 1/3rd octave band dropped 3.3dB from 68.1dBA to 64.8dBA. At 5.8˚ nose down, the SPL of the 400Hz 1/3rd octave band dropped 3.8dB from 72.3dBa to 68.5dBA and the SPL of the 500Hz 1/3rd octave band dropped 3.5dB from 69.8dBA to 66.3dBA, this treatment works in the same way as the owl wing strip no. 1, by creating chordwise vortices that disturb the regular vortex street. Because the serrations are small and frequent, there is quite a lot of broadband noise produced, more than the other treatments in the series (neglecting the 28mm emery strip). The narrow band sound spectrums show dramatic reductions of the tonal peaks[6]. The field test result shows a flattening of the peak with the lowest broadband noise production of the treatments tested in the field. Similar to the 15mm emery strip test, the peak band shows a slight increase in SPL.

5.8.5 Asymmetric Strip

Description

Some tests were performed on the A-bar with the addition of an asymmetrically serrated strip, once again, with the serrations pointing upstream on the upper surface near the leading edge. This strip can be seen in figure 5.3. The serrations on this strip were right-angled triangles as opposed to isosceles as in the usual owl wing strip configuration. The orientation of each triangle varied alternately in a similar fashion to vortex generators on aircraft wings. The distance between the apexes of the serrations was, 15mm between those sloping away from each other in the downstream direction and 25mm between those sloping towards each other in the downstream direction. The serrations protruded 5mm from the base strip, which had a width of 5mm. The strip was placed with the rear

[6] Narrow band sound spectrums found in Appendix H

edge of the base strip flush with the accessory slot. This treatment was tested in a subjective sound test and an indicator paint flow visualisation test. In a second set of tests, the 15mm emery strip was placed at the leading edge of the A-bar along with the asymmetric strip.

Results and Discussion

There was no audible advantage in the use of the asymmetric strip in preference to the owl wing strips. The result from the flow visualisation test can be seen in figure 5.6. Downstream of the 15mm spaces between the serrations the flow is unaffected, showing no evidence of vorticity, however downstream of the 25mm spaces, the flow shows the effects of chordwise vortices, with swirling in the separated region. In the tests with the 15mm emery strip in place, the noise level was perceivably lower than without. The SPL of the vortex shedding tone had decreased significantly. The flow pattern on the surface of the roof rack was also changed by the presence of the emery strip, the upper surface was not significantly different but the lower surface showed the same turbulent boundary layer and advanced separation as in the case of the specimen with just the 15mm emery strip. Because this treatment involves the placement of two separate strips, the manufacture of this treatment would be more involved than others discussed. The treatment would however be robust, durable and not sacrifice the strength or life of the A-bar.

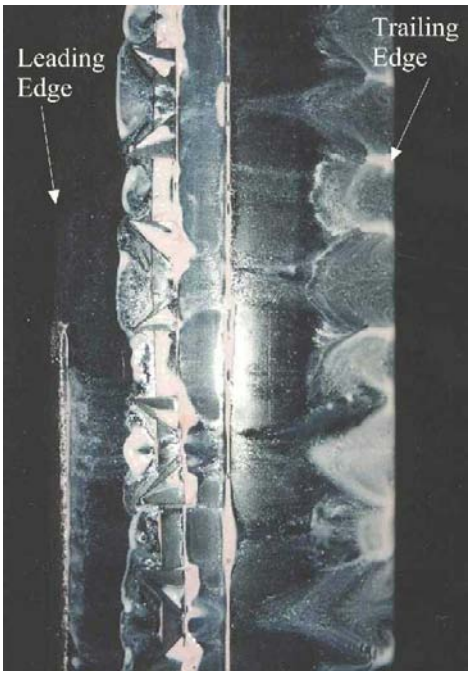

Figure 5-6 Upper surface of the asymmetric serrated strip.

5.9 Combinations

5.9.1 Roughness Strip and Owl Wing Strip No. 2

Description

A treatment was tested, based upon the use of the smaller owl wing strip no. 2 in combination with the 15mm emery strip placed at the leading edge. As in the previous owl wing strip no. 2 test, the strip was positioned with the rear edge of the strip 3mm forward of the accessory slot. Quantitative tests were performed on the specimen in the free jet of the wind tunnel and in the field as described in chapter 4 sections 4.4.1 and 4.4.5 respectively. The laboratory testing was part of the series 3 experiments, carried out at 2 attack angles, 0˚ and 5.8˚ nose down.

Results and Discussion

This strip exhibited a very good reduction in the vortex shedding tone. Figures 5.9 and 5.10 show the sound spectrums as measured with the 2260 Investigator (spectrum: Abar owl 2 & 15mm strip). A peak is still visible in the 0˚ incidence spectrum but it has moved to a lower frequency, present in the 315Hz 1/3rd octave band, this deviation of the peak frequency can also be seen in the narrow band spectrum[7]. At 0˚ incidence, the reduction of the SPL of the 400Hz 1/3rd octave band was 3dB from 68dBa to 65dBA while the SPL of the 500Hz 1/3rd octave band dropped 4.3dB from 68.1dBA to 63.8dBA. At 5.8˚ nose down, the peak is much diminished, the SPL of the 400Hz 1/3rd octave band dropped 5.8dB from 72.3dBa to 66.5dBA and the SPL of the 500Hz 1/3rd octave band dropped 4.7dB from 69.8dBA to 65.1dBA. The main difference in the flow around this specimen and that of the owl wing strip on its own is that the boundary layer on the lower surface is turbulent and separates at a point upstream of the trailing edge. This causes a wider wake and a lower vortex shedding frequency. The field test sound spectrum is shown in figure 5.11. Once again, there is a general increase in SPL right across the spectrum due to the increased broadband noise. In reconciling this spectrum with the result gained from the laboratory tests, it is likely that the slight increase in SPL exhibited

[7] Narrow band sound spectrums found in Appendix H

at the vortex shedding frequency is a result of the broadband noise and not an increase in the tonal frequency.

Similarly to the previous treatment, the manufacture of this treatment would be more involved than other types, because this treatment involves the placement of two separate strips. Nevertheless, it would be robust, durable and not sacrifice the strength or life of the A-bar.

5.9.2 Jetting Strip

Description

A strip was designed with the purpose of combining the effects of a leading edge emery strip with the effect of an owl wing strip, to generate both a turbulent boundary layer on the lower surface as well as chordwise trailing vortices. It was made from 24mm wide emery strip and had 10mm deep trapezium shaped notches cut from it. (See figure 5.3) The resulting tabs were thickened with two layers of the 1.8mm thick adhesive strip. The distance between the tabs was 13mm at their base and 3mm at their tips. The strip was referred to as the jetting strip because it was thought that higher velocity air would be expelled downstream from the gaps between the tabs. The jetting strip was attached with double-sided adhesive tape to the leading edge of the A-bar. This arrangement was tested quantitatively in laboratory and field tests as described in chapter 4 sections 4.4.1 and 4.4.5 respectively.

Results and Discussion

Figures 5.9 and 5.10 show the laboratory sound spectrums at 0˚ and 5.8˚ nose down incidence respectively and figure 5.11 shows the sound spectrum from the field test. There was generally a decrease in the vortex shedding tone with the application of this modification. The most dramatic reduction can be seen in the 5.8˚ nose down test in the laboratory, the SPL of the 400Hz 1/3rd octave band dropped 6.9dB from 72.3dBA to 65.4dBA and the SPL of the 500Hz 1/3rd octave band dropped 5.1dB from 69.8dBA to 64.7dBA. Similar to the previous cases, the field spectrums show a SPL increase at the vortex shedding frequency. This is however due to the increase in broadband noise produced by the addition, the prominence of the peak is much less dramatic and the tone

is not as audible. Of the four treatments used in the field test, this case shows the lowest vortex shedding frequency SPL.

This strip works by generating chordwise trailing vortices from the diagonal sides of the tabs, the interaction of these with the wake produces a much weakened vortex street. This strip may also reduce the spanwise correlation of the vortex street, reducing the intensity of the tone produced. The manufacture of this strip would be just as simple as that of the owl wing strips. Instead of being die cut from smooth strip, strip with texture or roughness would be used. The treatment would be robust, durable and not sacrifice the strength or life of the A-bar.

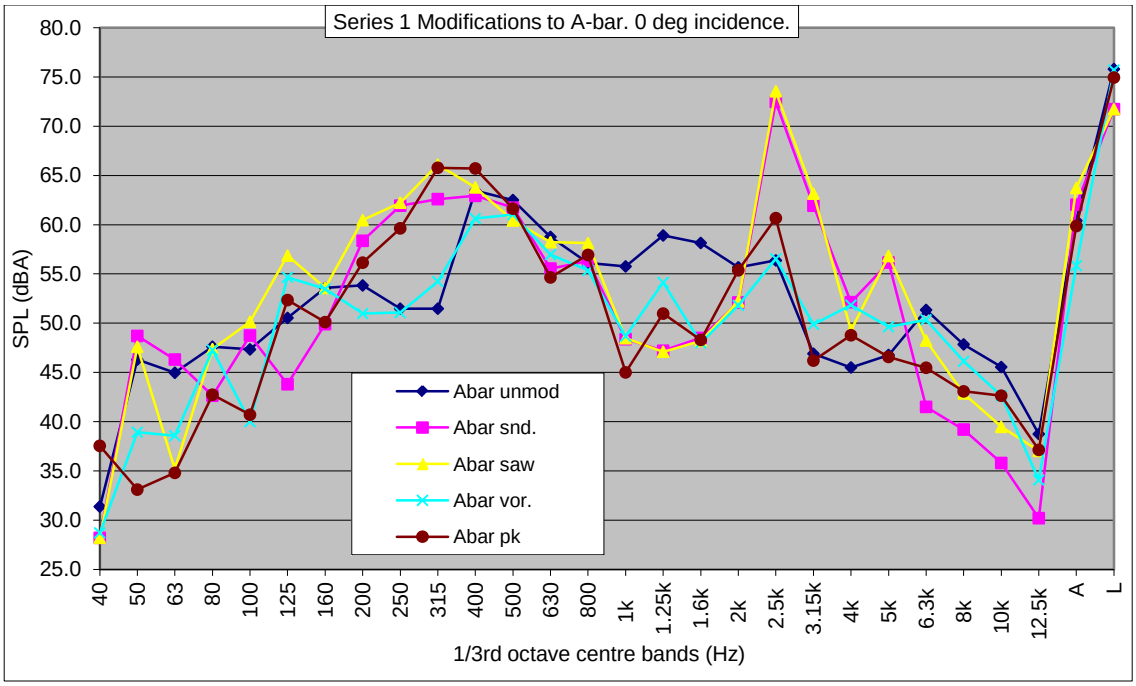

Figure 5-7 1/3rd octave sound spectrums of the series 1 treatment tests.

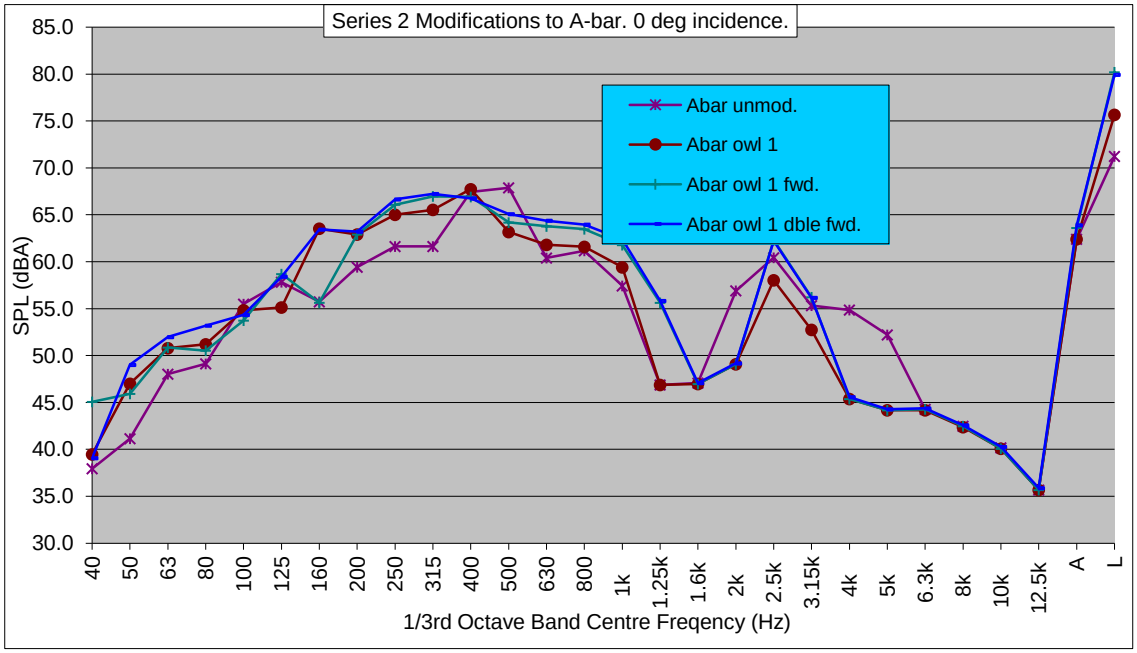

Figure 5-8 1/3rd octave sound spectrums of the series 2 treatment tests.

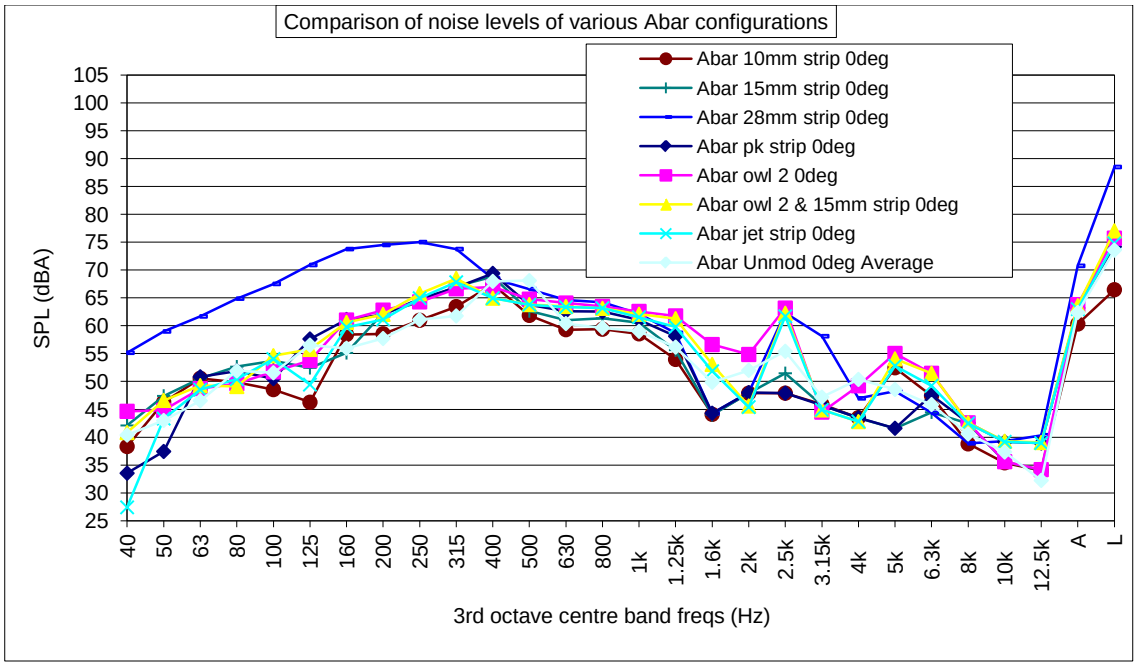

Figure 5-9 1/3rd octave sound spectrums of the series 3 treatment tests 0˚ attack angle.

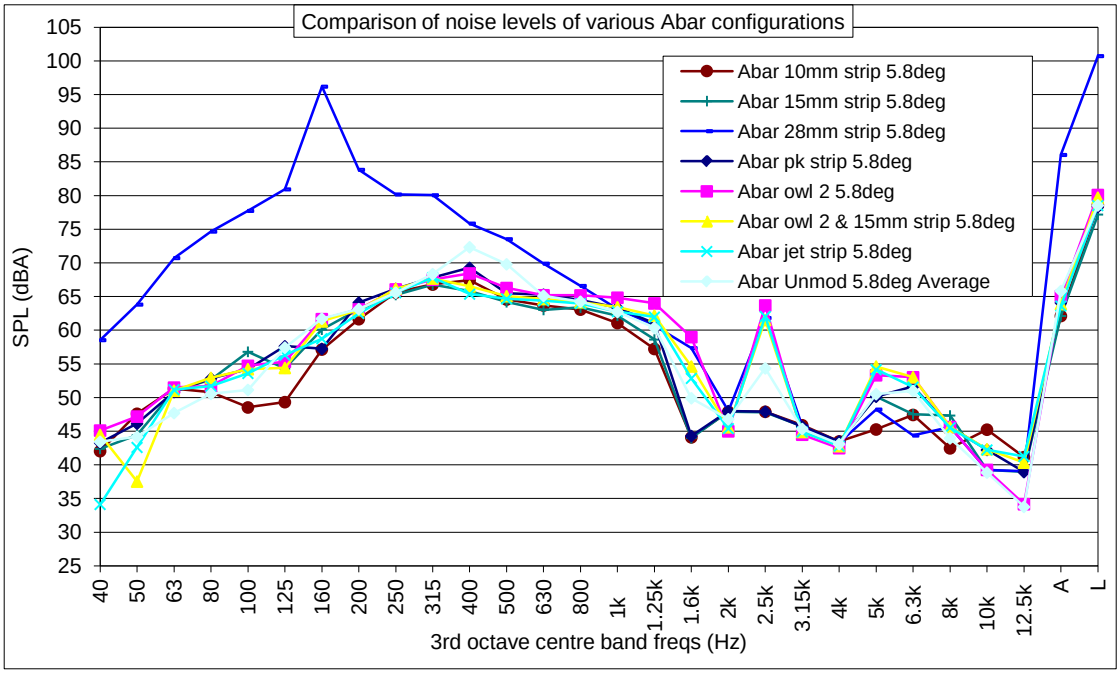

Figure 5-10 1/3rd octave sound spectrums of the series 3 treatment tests 5.8˚ nose down attack angle.

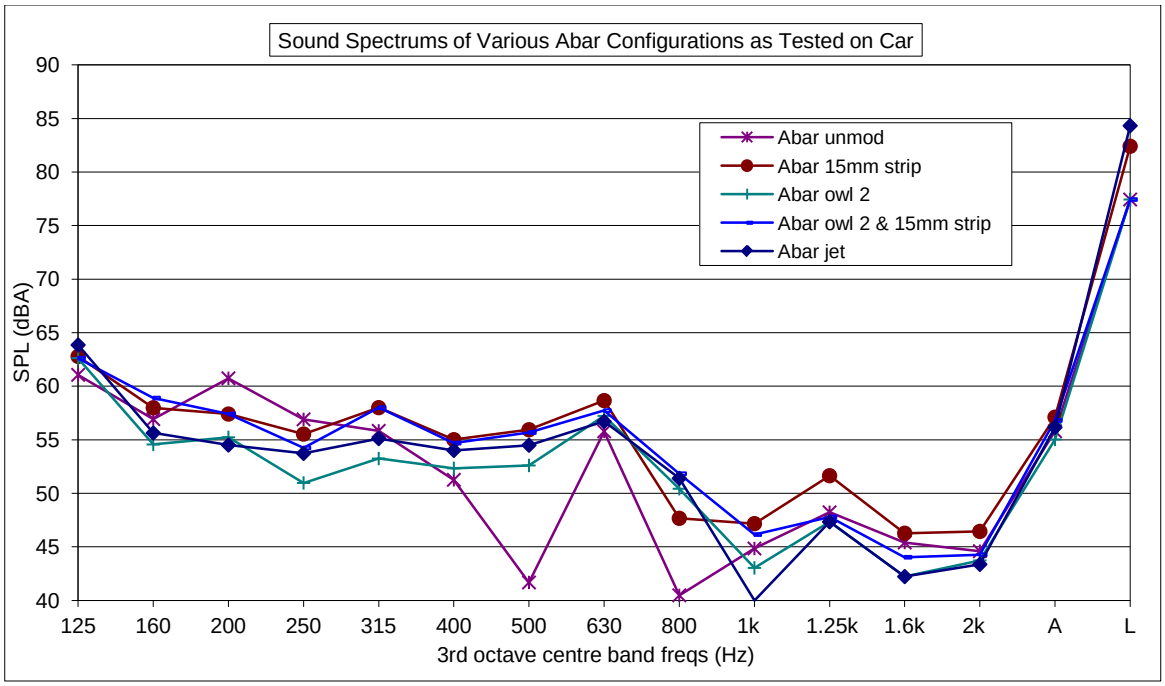

Figure 5-11 1/3rd octave sound spectrums of field tests.

5.10 Trials on Other Roof Racks

The owl wing strip no. 1 was trialed on a number of other "noisy" roof racks with excellent results. Two roof racks showing dramatic improvements were the Nomadic Glider bar and the Sportrack Jeep bar. These were tested in a standard quantitative laboratory sound spectrum test in the wind tunnel. The vortex shedding tonal peak was virtually eliminated, yielding a reduction in SPL of the dominant frequency band of 17.3dB and 12.4dB for the Glider and Jeep bar respectively. These are considerably large reductions. Figure 5.12 shows the spectrum of the Glider test before and after treatment[8].

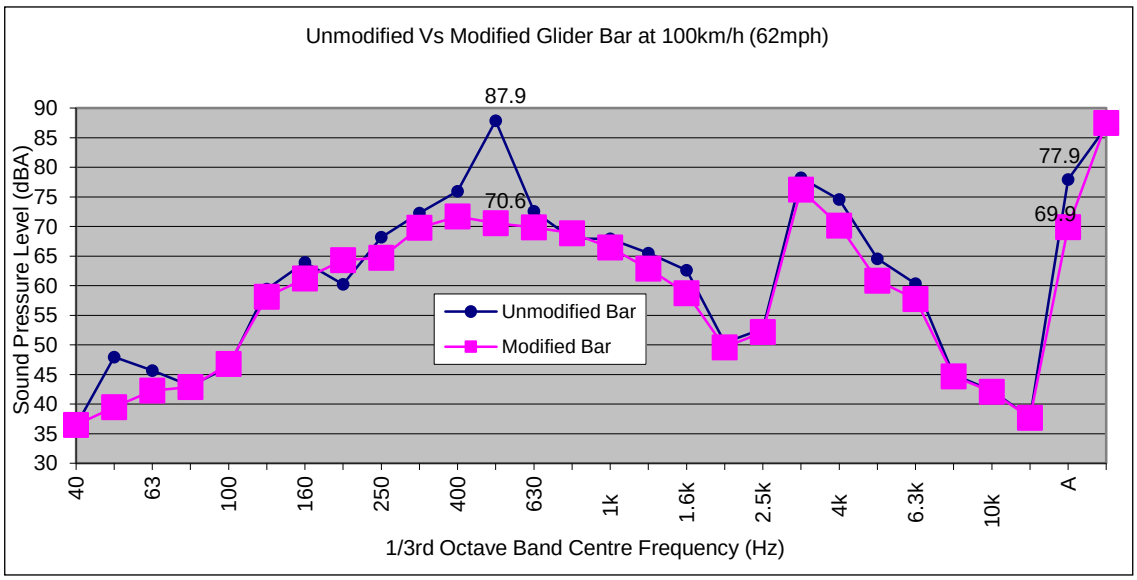

Figure 5-12 The sound spectrum of the Glider bar before and after treatment.

The Glider bar is similar to the A-bar in that it is primarily a plastic extrusion. In the case of roof racks that are roll formed from sheet metal eg. the Sportrack Jeep bar, the serrations may be more practically produced by a forming operation.

[8] The 1/3rd octave sound spectrum showing the effect of the Sportrack Jeep bar modifications in Appendix J

5.11 Summary

Various treatments appeared to be effective in reducing vortex shedding tonal emission. These were based mainly on the production of chordwise vortices that interacted with the wake, disrupting the formation of a regular vortex street. The quietest competitor roof rack tested, the Wellington bar also worked on this principle. The large diagonal slots cut from its leading edge induced strong chordwise vorticity in the flow over the roof rack[9]. It was found that in the case of the A-bar, the most effective systems for doing this appear to be those based on forward facing serrations similar to those trialed by Hersh et al[10] to reduce the noise of sharp trailing edged aerofoils. The successful serrations described in their paper were of a much smaller scale than those found to be effective in the current work. Perhaps this is because the NACA0012 aerofoils they tested were assumed to have a laminar boundary layer over the whole chord. As shown, the A-bar has a turbulent boundary layer over much of its surface and much larger flow disturbances are needed to create the required vorticity in the wake for noise abatement. The larger the disturbance to the flow, the greater the abatement of the vortex shedding tone. The cost of this reduction in the tonal frequency is a greater level of broadband noise.

A roughness strip at the leading edge of the A-bar was found to be effective in causing the boundary layer to be turbulent over the whole chord. This causes an advanced separation and a wider wake, lowering the frequency of the vortex shedding tone. The energy of the tone will be lower due to the larger losses in the augmented wake.

The jetting strip, combining the two phenomena was also found to be a particularly effective treatment.

It was also found that the placement of the vortex generating strips removed the tonal noise sometimes produced by the accessory slot. This noise generally occurred after the removal of accessories when the elastomer infill did not immediately return to its default position.

---

[9] Indicator paint flow visualisation test results for the Wellington bar in Appendix J

[10] Hersh, A. S. Soderman, P. T. Hayden, R. E. *Investigation of Acoustic Effects of Leading Edge Serrations on Airfoils*.

Chapter 6

CONCLUSIONS, RECOMMENDATIONS AND FUTURE WORK

6.1 Conclusions

From this experimental study of the aerodynamic noise generated by roof racks and possible methods for its reduction, the following conclusions have been drawn:

1) The noise primarily responsible for causing annoyance to car occupants is a tone. This tone is caused by the phenomenon known as vortex shedding.
2) Vortex shedding from the A-bar is a result of both its boundary layer separating upstream of the trailing edge and the bluntness of the trailing edge itself. The boundary layer is turbulent when it separates, this does not prevent the vortex shedding.
3) The vortex street can be weakened by the generation of chordwise trailing vortices on the surface of the roof rack. These interact with the wake, disrupting the regular vortex formation.
4) Strong chordwise vortices also decrease the spanwise correlation of the vortex street, reducing the sound emission.
5) These chordwise vortices can be generated by additions on the surface of the roof rack near the leading edge. These additions must induce cross flow in the incident airstream. Examples of additions that do this are: cylinders, hemispheres, serrations and diagonal steps.
6) Additions based upon serrated strips can be manufactured and applied easily to the A-bar with minor changes to the production process.

6.2 Recommendations

In terms of reducing the noise of the current A-bar roof rack model, the addition of strips such as the owl wing strip no. 1 would be highly advantageous. These could readily be manufactured with unpretentious aesthetic appeal. They are robust, durable and safe and can be fitted by hand with sufficient accuracy. The strips should be adhered to the A-bar surface sufficiently well to ensure continual service.

Concerning the fundamental design of a roof rack cross bar, the basic idea to use an aerofoil profile is good in many respects. Primarily, an aerofoil section is aerodynamically favourable with low drag. In terms of aesthetics, an aerofoil is an attractive shape and in the case of a well designed aerofoil, will have a low noise level. As has been addressed, the larger the wake, the more likely vortex shedding will be present. The most fundamental way to reduce the size of the wake is to sharpen the trailing edge. Lowson[1] describes that the way vortex-shedding noise has been reduced in the case of wind turbines is through the sharpening of the trailing edge. He describes noise reductions in the order of 15dB. Similarly, in Brooks and Hodgson's work[2] with aerofoils with fully developed turbulent boundary layers, they identified that the far-field sound pressure level differs between those aerofoils with a sharp trailing edge and those with a blunt edge, with the blunt case being typically louder. Based upon these studies and basic intuition, future crossbar profiles should be produced with as sharp a trailing edge as practicable. They should be based upon well known aerofoil sections that display good flow attachment at the Reynolds numbers concerned.

---

[1] Lowson, Martin V. *Applications of Aero-Acoustic Analysis to Wind Turbine Noise Control*

[2] Brooks T. F. and Hodgson T. H. *Trailing Edge Noise Prediction from Measured Surface Pressures*

6.3 Future Work

6.3.1 Transmission Loss through Car Roof

A more elaborate investigation could be done on the transmission of sound through the roofs of cars. This would give a much clearer understanding of those frequencies that are permissible and those that it is critical to remove. This may also present new ways for reducing the roof rack noise heard inside the car i.e. rather than removing the vortex shedding tone altogether, it may be possible to move it into a frequency range attenuated by the car roof.

6.3.2 The Noise Control of Roof Rack Accessories

Roof rack crossbar accessories are known to produce noise. A study to present guidelines for the production of quiet accessories would be very useful. This study could also look at the abatement of noise generated by the A-bar end pieces.

6.3.3 The Drag Coefficient of the A-bar

Drag is an important issue in the automotive industry. A helpful study would be one on the effect the noise abating additions have on the drag coefficient of the A-bar. This study may reveal a relationship between noise production and drag and give guidelines for more efficient noise treatment systems.

6.3.4 The Effect of Humidity and Temperature

In differing driving conditions, the level of noise heard from the roof racks varies. In wet or cold weather, the vortex shedding tone is more distinct. A useful study would be on the effect of temperature and humidity changes on the vortex street and its noise production. This study would include the influence these factors have on the sound transmission through air.

BIBLIOGRAPHY

In Alphabetical order…

Abernathy, F. H. and Kronauer, R. E. *The formation of Vortex Streets.* J. of Fluid Mech. Vol 13 1962

Arbey, H. and Bataille, J. *Noise generated by Aerofoil profiles Placed in a Uniform Laminar Flow*, J. Fluid Mechanics. Vol 134 1983 pp33-47

Baird, R. C. *Wind-Induced Vibration of a Pipe-Line Suspension Bridge and its Cure*. ASME Trans. Vol 77 No. 6 Aug 1955

Betchov, Robert and Criminale, Jr, William O. *Stability of Parallel Flows,* **Applied Mathematics and Mechanics Vol 10. Academic Press 1967**

Blake W. K. *Mechanics of Flow-Induced Sound and Vibration.* **Applied Mathematics and Mechanics. Academic Press INC Vol 17 – 1 1986**

Brooks T. F. and Hodgson T. H. *Trailing Edge Noise Prediction from Measured Surface Pressures,* **J. Sound and Vibration. 78(1) 1981 pp69 – 117**

Collins *English Dictionary and Thesaurus*, 1st Edition, HarperCollins Publishers 1993

Crighton, D. G. *Airframe Noise*. In Hubbard, H. H. **Aeroacoustics of flight vehicles: theory and practice**. NASA reference publication v1258 Aug 1991

Donohue, B. *Prediction of Aerodynamic Noise from Automotive Roof Carrier Systems – Final Report*. IRL Report 93301.00 TBG Project HUB301 Dec 1995

Embleton, T. F. W. *Mufflers*. In Beranek, L. L. **Noise and Vibration Control**. McGraw Hill Inc. 1971

Fink M. R. *Prediction of Airfoil tone frequencies.* **J. Aircraft** Vol **12 1975 pp 118 – 120**

Glorig, A. *Noise and Your Ear*. Grune and Stratton NY 1958

Hersh, A. S. Soderman, P. T. Hayden, R. E. *Investigation of Acoustic Effects of Leading Edge Serrations on Airfoils*. J. Aircraft. Vol 11 No. 4 April 1974

Hirsh, I. J. *The measurement of Hearing*. McGraw Hill NY 1952

Howe, M. S. *Noise produced by a Sawtooth Trailing Edge*. J. Acoust. Soc. Am. 90(1) July 1991

Kovasznay, L. S. G. *Hotwire Investigation of the Wake Behind Cylinders at Low Reynolds Numbers.* Proc. Roy. Soc. (London) A198 p174-190 1949

Kretch, B. and Crutchfield, R. S. *Elements of psychology*. Univ. of California Press Berkeley and LA.

Lighthill, M. J. *On Sound Generated Aerodynamically. 1: General Theory*, Proc. Roy. Soc. A 211 1952, pp 564 – 587

Lowson, Martin V. *Applications of Aero-Acoustic Analysis to Wind Turbine Noise Control,* **Wind Engineering Vol 16 No. 3 1992**

Massey, B. S. *Mechanics of Fluids***. Chapman & Hall 6th edition 1989**

Nguyen, H. B. *Aerodynamic Noise in Separated Flow*. Mech. Eng. Masters Thesis Canterbury University April 1971

Olson, H. F. *Music, Physics and Engineering*. Dover Pub. 2nd ed. 1967

Parkinson, J. P. *Acoustic Absorber Design.* Mech. Eng. Masters Thesis Canterbury University 1999

Paterson, Robert W. Vogt, Paul G. Fink, Martin R. and Munch, C. Lee *Vortex Noise of Isolated Airfoils*. J. Aircraft Vol 10 No. 5 1973 pp296 – 302

Price, P. *Suppression of the fluid-induced vibration of circular cylinders*. J. Eng. Mech. No. EM3 Proc. Of the Amer. soc. of Civil Eng. Vol 82 1956

Raine, J. K. *Modeling the Natural Wind Protection by Fences.* Mech. Eng. Ph.D Thesis Canterbury University 1974

Rodda, M. *Noise and Society*. Oliver and Boyd Ltd. London 1967

Schlichting, H. *Boundary Layer Theory*. McGraw Hill. 6th ed. 1968.

Steinman, D. B. *Pipeline Bridge Stabilized with Diagonal Rope Stays*. Civil Eng. Vol 22 No 3 March 1952

Stevenson, D.C. and **Raine, J. K.** *Dual Working Section Wind Tunnel at the University of Canterbury.* **New Zealand Engineering 15th April 1976**

Strouhal, V. *Uber eine besondere ort der Tonne regung***. Ann. Phys. Chem. 5(10) 1878 pp 216 – 251**

Tam C. K. W. *Discrete tones of isolated airfoils***. J. Acoust. Soc. Am. Vol 55 1974 pp 1173 – 1177**

Tang, T. T. *Aerodynamic Noise in Tube-Bank Systems*, Mech. Eng. Masters Thesis Canterbury University April 1971

Von Karman, T. and Rubach, H. *Uber den Mechqnismus des Flussigkeits und Luft-widerstandes*. Phys. Z.,13(2) 1912 pp 49 – 59

Wood, C. J. *The effect of base bleed on a periodic wake*. J. Roy. Aero. Soc. Vol 68 p 477-482 1964

APPENDIX A

Acoustics Related Tables and Figures.

APPENDIX B

B.1 Calculation of Blade Passing Frequency of Fans.

Each fan has 6 blades, with a run speed of 1475rpm
1475rev/min * 1min/60s = 24.583 rev/s
6 blade passes per revolution…
24.583 rev/s * 6 blade passes/rev = 147.5 blade passes/s (Hz)

B.2 Signal to Noise Ratio Before and After Noise Abatement Work.

In the 500Hz 1/3 octave frequency band…
The wind tunnel SPL prior to work, measured in the low noise working section at 80km/h
SPL_{0wt} = 74.7 dBA (500Hz)
The average wind tunnel SPL after noise abatement work, measured in the free jet at 80km/h
SPL_{1wt} = 65.2 dBA (500Hz)
The average value of the roof rack signal emitted at 80km/h, measured 20mm below, 60mm downstream of the trailing edge.
SPL_{rr} = 67.9 dBA (500Hz)

Signal to Noise Ratio (SNR) = Signal (dBA) / Background Noise Level (dBA)
Initially…
$SNR_0 = SPL_{rr} / SPL_{0wt}$
$= 67.9 / 74.7$
$= 0.91$
After noise work…
$SNR_1 = SPL_{rr} / SPL_{1wt}$
$= 67.9 / 65.2$
$= 1.04$

B.3 Calculation of the Resonant Frequency of the Air Gap between the Roof Rack and the Roof of the Car.

Resonance occurs when the relevant dimension is equal to half the wavelength of the exciting frequency. In other words the resonant frequency has a wavelength twice that of the dimension.

In the case of the Toyota Camry, the front roof rack had a gap of around 35mm between its lower surface and the surface of the roof.

$d = 0.035$
$\lambda = 2*d$
$= 0.07$
$f = c/\lambda$
where c (the speed of sound) = $343ms^{-1}$
$f = 343/0.07$
$= 4900Hz$

B.4 Calculation of the resonant frequency of the air column inside the roof rack.

As in the above calculation, resonance occurs when the relevant dimension is equal to half the wavelength of the exciting frequency.

The Abar crossbar length was approximately 900mm.

$d = 0.9$
$\lambda = 2*d$
$= 1.8$
$f = c/\lambda$
where c (the speed of sound) = $343ms^{-1}$
$f = 343/1.8$
$= 190.6Hz$

B.5 Calculation of the Reynolds number of the Abar.

The formula for the non dimensional Reynolds number is:
Re based on chord length
$Re = \rho Uc/\mu$
c = 80mm
$Re = 1.2*22.2*0.08/1.8*10^{-5}$
$= 1.18*10^{5}$
Re based on vertical thickness at flow separation
$Re = \rho Ut/\mu$
t = 17.8
$Re = 1.2*22.2*0.0178/1.8*10^{-5}$
$= 2.6*10^{4}$
Re based on wake thickness
$Re = \rho Ut/\mu$
t = 13mm
$Re = 1.2*22.2*0.013/1.8*10^{5}$
$= 1.9*10^{4}$

B.6 Calculation of the Strouhal number for vortex shedding from the Abar.

The formula for the non dimensional Strouhal number is:
S = ft/U
S based on vertical thickness at flow separation
t = 17.8mm
And f = 420Hz
S = 420*0.0178/22.2
= 0.34
S based on wake thickness
t = 13mm
And f = 420Hz
S = 420*0.013/22.2
= 0.25

APPENDIX C

Base/Background Noise Removal

The purpose of base noise removal is to produce a sound spectrum that represents the noise emitted solely from the roof rack itself. In order to do this an ambient noise reading is needed. In the case of this thesis, the two most used ambient noise readings were the empty tunnel 1/3rd octave spectrum and the bare car 1/3rd octave spectrum.

There were two methods of base noise removal considered, these are:

1) Numerical dB subtraction

In this method, the SPLs (in dB or dBA) of each 1/3rd octave band in the ambient sound spectrum are subtracted numerically from those of the specimen test sound spectrum. Decibels are a logarithmic unit and so these values do not represent a physical quantity

2) Linear sound pressure level subtraction

In this method, the SPLs (in dB) of each 1/3rd octave band are converted to their equivalent linear sound pressure (squared) ratio prior to subtraction, the difference is then converted back to dB (or dBA).

The linear sound pressure level is an rms value measured in N/m^2. It is non-dimensionalised by dividing by a reference rms sound pressure, of 2 x 10^{-5}N/m^2.

$SPL\ (dB) = 10\log p^2/p^2_{ref}$

$p^2/p^2_{ref} = 10^{(SPL/10)}$

Sample Calculation

If in a roof rack sound spectrum test, the 400Hz 1/3rd octave band has an SPL of 74.2dB and in an empty tunnel sound spectrum test, the same band has an SPL of 70dB.

Using the first method, the level of the 400Hz 1/3rd octave band representing the emission of the roof rack would be a simple difference of 4.2dB.

Using the second method, the levels in dB must first be converted to linear sound pressure levels.

For SPL = 74.2dB,

$p^2/p^2_{ref} = 10^{(74.2/10)}$

$= 26302679.9$

For SPL = 70dB

$p^2/p^2_{ref} = 10^{(70/10)}$

$= 10000000$

The difference is then taken:

$P^2/p^2_{ref} = 26302679.9 - 10000000$

$= 16302679.9$

This is converted back to a logarithmic value:

$SPL\ (dB) = 10\log(16302679.9)$

$= 72.1dB$

This can then be A-weighed:

$SPL_{400}\ (dBA) = SPL_{400}\ (dB) - 4.8dB$

$= 72.1 - 4.8$

$= 67.3dBA$

The second method was chosen as it yields values that represent the sound emission from the isolated roof rack, without reference to a particular experimental arrangement.

APPENDIX D

Sound Spectrums of the Unmodified Wind Tunnel

APPENDIX E

Acoustic Deflector Drawings

APPENDIX F

Sound Spectrums of Modified Wind Tunnel

APPENDIX G

1/3rd Octave and Narrow Band Sound Spectrums for Benchmark and Angle Variation Tests

APPENDIX H

Velocity Spectrums in A-bar Wake

APPENDIX I

Spectrum Showing Mechanical Natural Frequency of A-bar

APPENDIX J

Narrow Band Sound Spectrums for Treatment Tests Series 1 and 3

Competitor Rack Tests

Wellington Bar Indicator Paint Test

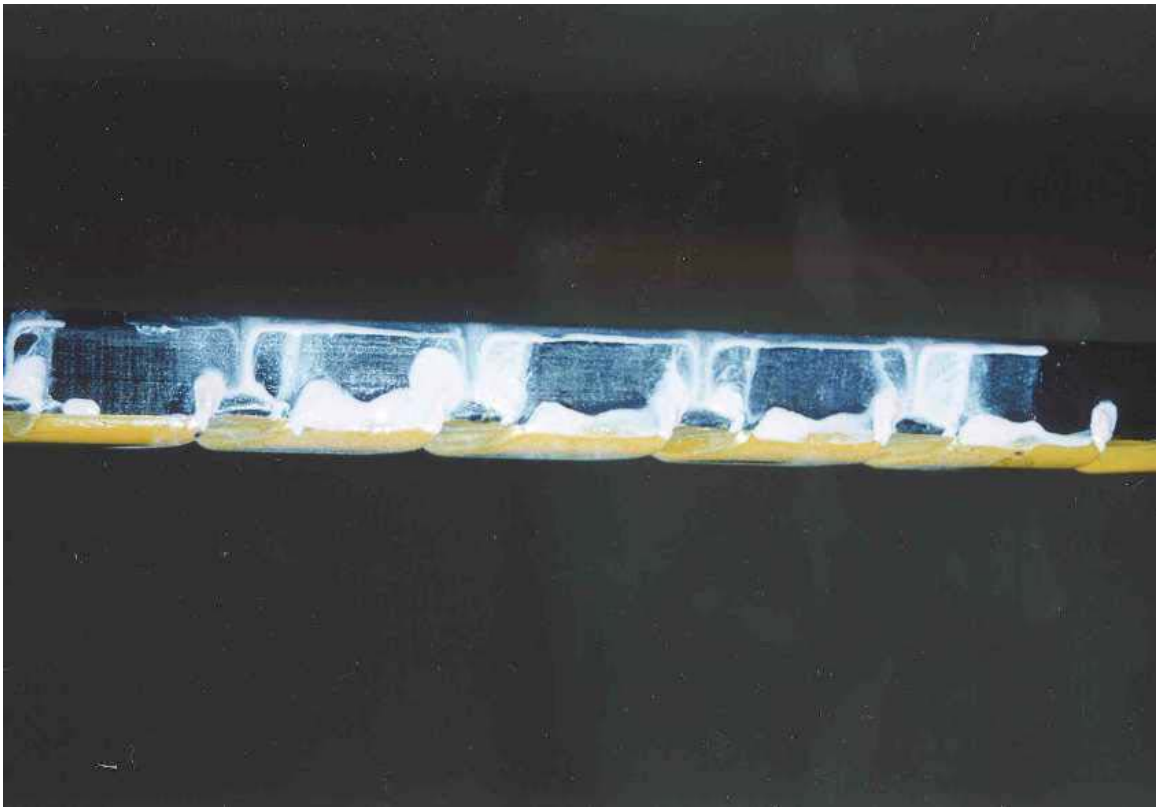

Figure K.1 Indicator paint test of Wellington roof rack.